Supplement of Clim. Past Discuss., 11, 831–872, 2015
http://www.clim-past-discuss.net/11/831/2015/
doi:10.5194/cpd-11-831-2015-supplement

Climate of the Past
Discussions
Open Access

Supplement of

Glacial–interglacial shifts in global and regional precipitation δ^{18}O

S. Jasechko et al.

Correspondence to: S. Jasechko (sjasechk@ucalgary.ca)

Supporting Online Information

This document presents groundwater age dating methods (S1), $\Delta^{18}O_{ice\ age}$ calculation details (S2), inter-model simulation details (S3) and tabulated data and sources (S4).

S1. Groundwater age dating

Mean ^{14}C-based groundwater ages (*t*, the time elapsed since recharge) were calculated for each groundwater sample by accounting for the radioactive decay of ^{14}C and for the dissolution of ^{14}C-dead aquifer materials (Clark and Fritz, 1997):

$$t = -8267 \times ln\left(\frac{A}{q \times A_o}\right) \qquad \text{Equation S1.}$$

where *t* is the time elapsed since the groundwater sample recharged (i.e., groundwater age), *A* is the measured ^{14}C activity in a groundwater sample, A_o is the initial ^{14}C activity (100 pmC) and *q* is a correction factor applied to account for the dissolution of aquifer material with zero ^{14}C (i.e., ^{14}C-dead). In cases where $\delta^{13}C$ data was available *q* was calculated as:

$$q = \frac{\delta^{13}C_{measured} - \delta^{13}C_{aquifer}}{\delta^{13}C_{recharge} - \delta^{13}C_{aquifer}} \qquad \text{Equation S2.}$$

where $\delta^{13}C_{measured}$, $\delta^{13}C_{aquifer}$ and $\delta^{13}C_{recharge}$ represent the carbon isotope composition of a groundwater sample, the aquifer and recharging groundwater. $\delta^{13}C_{aquifer}$ was set to 1.0±3.4 ‰ PDB (average ± 1 s.d.) as determined by $\delta^{13}C$ values of 16359 rock and sediment samples (Veizer et al., 1999). $\delta^{13}C_{recharge}$ was set to −12.6±4.3 ‰ PDB (average ± 1 s.d.) as determined by 120 groundwater samples having a ^{14}C activity of greater than 90 p.m.C. compiled in this study (i.e., recently recharged water bearing near-atmospheric radioactive activities; Burchuladze et al., 1989). *q* was set to 0.76±0.41 in cases where $\delta^{13}C_{measured}$ data were unavailable, as determined by the most common $\delta^{13}C$-based *q* values (q = 0.76±0.41 represents the average and

one standard deviation of all $\delta^{13}C$-based q values calculated in this compilation). Uncertainties in groundwater ages were calculated by Gaussian error propagation (calculated values of q exceeding 1 were set to a value of 1). The $\delta^{13}C_{recharge}$ and $\delta^{13}C_{aquifer}$ ranges do not encompass all possible geochemical scenarios, and likely introduce additional errors into our groundwater age dates.

Equivalent calendar year ages were estimated from ^{14}C-ages by applying a polynomial fit of compiled ^{14}C-to-calender age corrections (Fairbanks et al., 2005). Samples were then divided into two age categories: (i) the late-Holocene (^{14}C-based age of less than 5,000 calendar years before present, or having a ^{3}H activity of greater than 4 T.U., indicating modern recharge), or (ii) the last ice age (^{14}C-based age of 19,500 to less than ~50,000 calendar years before present and samples with ^{14}C activities below analytical detection). An upper ice age limit of less than ~50,000 years before present was set because of limitations with ^{14}C age calculations, even though the most recent ice age extends to ~110,000 years before present (Lisiecki and Raymo, 2005).

S2. $\Delta^{18}O_{ice\ age}$ calculation

$\Delta^{18}O_{ice\ age}$ values (defined as $\Delta^{18}O_{ice\ age} = \delta^{18}O_{ice\ age} - \delta^{18}O_{late\text{-}Holocene}$) were analyzed on an aquifer-by-aquifer basis. Only aquifers with a minimum of two samples dated to both the late-Holocene and the last glacial time periods were included in this analysis. Comparisons of isotopic data for the last ice age and the late-Holocene were made by subtracting median $\delta^{18}O$ and $\delta^{2}H$ values from each age group, with errors calculated by maximizing the 25^{th} to 75^{th} percentile distributions for the two data groups (i.e., late-Holocene and last glacial period age groups). Samples were omitted from our analysis if they exhibited an evaporative signature ($\delta^{2}H - 8\times\delta^{18}O$ of less than 0), contained a mixture of modern and ice age groundwater (^{3}H activity of

45 greater than 1 tritium unit and a ^{14}C-age of more than 19,500 calendar years before present),
46 were suspected to have mixed with intruding seawater (e.g., Geyh and Söfner, 1989; Bouchaou
47 et al., 2008) or were presumed to have been recharged by subglacial meltwaters beneath the
48 Fennoscandinavian (e.g., Karro et al., 2004) or the Laurentide (e.g., Grasby and Chen, 2005;
49 Ferguson et al., 2007; Stotler et al., 2010) ice sheets (review by McIntosh et al., 2012).

50 Ice core and speleothem $\Delta^{18}O_{ice\ age}$ values were calculated by comparing $\delta^{18}O$ values
51 from the late-Holocene (<5,000 years) and the last ice age (19,500 to less than 50,000 years). A
52 threshold of less than 50,000 years before present was selected as an upper limit for the last ice
53 age $\delta^{18}O$ value for consistency with the groundwater records. Speleothem as $\Delta^{18}O_{ice\ age}$ values
54 were corrected to account for temperatures at the last ice age from the late-Holocene that impact
55 the water-calcite isotopic fractionation factor. Temperature-based H_2O-$CaCO_3$ fractionation
56 factors were obtained from O'Neil et al. (1969) with temperatures calculated under the
57 assumption that atmospheric temperatures are indicative of temperatures in the shallow
58 subsurface. Temperatures for the late-Holocene were assumed to be equivalent to modern mean
59 annual near surface temperatures (New et al., 2002), potentially introducing <1°C of error
60 because of temperature change throughout the last 5,000 years (Marcott et al., 2013). Adding
61 1°C of added uncertainty into late-Holocene temperature equates to an added ±0.4 ‰ ($\delta^{18}O$) of
62 uncertainty in the temperature-corrected difference between ice age and late-Holocene $\delta^{18}O$
63 values (O'Neil et al., 1969). Last glacial period temperatures were calculated by applying the
64 temperature offset of the last glacial maximum (Figure S1; Annan and Hargreaves, 2013) to
65 gridded values of modern mean annual air temperatures (New et al., 2002).

66 **S3. Simulated precipitation $\delta^{18}O$**

Simulated precipitation $\Delta^{18}O_{ice\ age}$ values compiled from five general circulation models are reported in this study. Table S1 describes model-specific parameterizations, input data and boundary conditions.

S4. Groundwater, speleothem and ice core isotope records

Tabulated paleowater isotope records of groundwater (Tables S2 to S3), speleothem (Table S4), glacier ice (Table S5) and ground ice (Table S6) records presented in the following supplemental tables.

S5. Groundwater $\delta^{18}O$ over time

Figures S4 – S62 present groundwater $\delta^{18}O$ variations from the last ice age to present day for 59 globally-distributed aquifer systems (two ground ice records not included in this series of plots). Figures are sorted by country alphabetically. Exact ages for Germany's Benker-sandstein aquifer are not available, however, the stable isotope data two data clusters are interpreted to be representative of late-Holocene and Pleistocene climate states (Figure S24, van Geldern et al., 2014). The most recent age end member for the "last ice age" time period—usually set to 19,500 years before present—was set to 22,000 years before present for the Pannonian Basin to avoid samples with ^{14}C-ages between 19,500 and 22,000 years before present showing evidence of groundwater mixing (Figure S26; Varsanyi et al., 2011). Syrian Aleppo Basin groundwaters having a $\delta^{13}C$-based q value of less than 0.3 were not included in our analysis on the basis of highly uncertain groundwater ages at low values of q (Figure S49; Al-Charideh, 2012; Stadler et al., 2012).

88 **Table S1.** Information for isotope enabled general circulation models compiled in this study

Model name:	**CAM3iso**	**ECHAM5-wiso**	**GISSE2-R, NINT**	**IsoGSM**	**LMDZ4**
Reference for model:	Collins et al., 2006	Roeckner et al., 2006	Schmidt et al., 2014	Kanamitsu et al., 2002	Hourdin et al., 2006
Reference for isotopic version:	Noone and Sturm, 2009; Sturm et al., 2010	Werner et al., 2011	LeGrande and Schmidt, 2009 *	Yoshimura et al., 2008	Risi et al., 2010
Forced or coupled simulation:	Forced	Forced	Coupled	Forced	Forced
Sea surface temperature forcing (if forced):	Monthly-mean anomalies from a LGM simulation by the CCSM3 coupled model (Otto-Bliesner et al., 2006)	Monthly-mean anomalies from GLAMAP reconstruction (footnote: LGM anomalies were calculated with respect to a pre-industrial simulation, and added to present-day observed SSTs from AMIP)	N/A	Monthly-mean anomalies from a LGM simulation by the IPSL coupled model (footnote: LGM anomalies were calculated with respect to a pre-industrial simulation, and added to present-day observed SSTs from AMIP)	Monthly-mean anomalies from a LGM simulation by the IPSL coupled model (footnote: LGM anomalies were calculated with respect to a pre-industrial simulation, and added to present-day observed SSTs from AMIP)
Sea ice forcing (if forced):	Same as SSTs	Same as SSTs	N/A	Same as SSTs	Same as SSTs
Climatological or inter-annual forcing:	Climatological (average over 100 years)	Climatological	N/A	Climatological (average over 30 years)	Climatological (average over 30 years)
Topography/ land ice:	Ice 5G (Peltier, 1994)	As advised by PMIP3 (Braconnot et al., 2012)	Ice 5.2G, with LIS of Licciardi et al. (1998)	Ice 5G (Peltier, 1994)	Ice 5G (Peltier, 1994)

Model name:	**CAM3iso**	**ECHAM5-wiso**	**GISSE2-R, NINT**	**IsoGSM**	**LMDZ4**
Aerosol:	Pre-industrial	None	NINT physics (Koch et al., 2011; Shindell et al., 2006) and includes a tuned aerosol indirect effect (AIE) following (Hansen et al., 2005)	None	None
Solar/orbital forcing:	PMIP2 protocol	PMIP3 protocol	PMIP3 protocol	PMIP2 protocol	PMIP2 protocol
Number of years:	15	12 years and last 10 years average	1500	30 years and last 20 years average	3
Horizontal resolution:	2.8° x 2.8°	1.1° x 1.1° (T106 spectral resolution)	Atmosphere: 2.0° x 2.5°; Ocean: 1.0° x 1.25°	1.8° x 1.8° (T62 spectral resolution)	2.5° latitude x 3.75° longitude
Vertical resolution:	26 levels	31 levels	Ocean: 26 levels; atmosphere: 40 levels, top at 0.1 mb	28 levels	19 levels
Seawater $\delta^{18}O$ (modern):	0 ‰, globally constant	LeGrande and Schmidt, 2006	0 ‰ mean, but coupled	0 ‰, globally constant	0.5 ‰, globally constant
Seawater $\delta^{18}O$ (LGM):	+1.1‰ with respect to present	+1‰ with respect to present	+1‰ with respect to present, but coupled	0 permil, globally constant; +1 per mille added after to account for seawater change	+1.2 ‰ with respect to present

89 * Last Glacial Maximum simulation cited as Ullman et al. (2014)

90

91 **Table S2.** Groundwater datasets compiled in this study

Country	Aquifer	Citation(s)
Algeria	Great Oriental Erg: CI	Edmunds et al., 2003
Botswana	Kalahari: Ntane	Kulongoski et al., 2004
Botswana	Lokalane-Nakojane	Rahube, 2003
Burkina Faso	Taoudeni basin	Huneau et al., 2011
Chad	Chad aquifer	Edmunds, 2009
Egypt	Nubian aquifer	Shehata and Al-Ruwaih, 1999; Patterson et al., 2005; Edmunds, 2009
Mali	Mali aquifer	Edmunds, 2009
Morocco	Tadla basin	Bouchaou et al., 2009
Morocco	Nappe des sables	Castany et al., 1974
Namibia	Omatako basin	Külls, 2000
Niger	Djardo-Bilma	Dodo and Zuppi, 1997; 1999
Niger	Irhazer: CI	Andrews et al., 1994; Edmunds, 2005
Niger	Illumeden: CT	Le Gal La Salle et al., 2001; Beyerle et al., 2003
Nigeria	Chad basin	Maduabuchi et al., 2006
Senegal	Senegalese CT	Castany et al., 1974; Edmunds, 2009
South Africa	Uitenhage aquifer	Heaton et al., 1986
Tunisia	Kairouan Plain	Derwich et al., 2012
Zimbabwe	Zimbabwe aquifer	Larsen et al., 2002
Australia	Canning basin	Harrington et al., 2011
Australia	Murray aquifer	Leaney and Allison, 1986
Bangladesh	Bengal basin	Aggarwal et al., 2000; Sikdar and Sahu, 2009; Majumder et al., 2011; Hoque and Burgess, 2012
China	Songnen Plain	Chen et al., 2011
China	North China Plain	Zongyu et al., 2003; Kreuzer et al., 2009
China	Yuncheng basin	Currell et al., 2010
India	Cuddalore sandstone	Sukhija et al., 1998
India	Tiruvadanai aquifer	Kumar et al., 2009
Indonesia	Jakarta basin	Geyh and Söfner, 1989
Israel	Israel coastal aquifer	Yechieli et al., 2008
Israel	Dead Sea rift valley	Gat and Galai, 1982; Mazor et al., 1995
Kuwait	Al-Raudhatain and Damman aquifers	Al-Ruwaih and Shehata, 2004; Fadlelmawla et al., 2008
Oman	Batinah coastal plain	Weyhenmeyer et al., 2000; 2002
Oman	Najd aquifer	Clark et al., 1987; Al-Mashaikhi et al., 2012
Syria	Aleppo basin	Al-Charideh, 2012; Stadler et al., 2012
Belgium	Ledo-Paniselian	Walraevens, 1990; Walraevens et al., 2001
Czech Rep.	Sokolov aquifer	Noseck et al., 2009
Denmark	Ribe Formation	Hinsby et al., 2001
France	Bathonian coast	Barbecot et al., 2000
France	Lorraine sandstone	Celle-Jeanton et al., 2009

Country	Aquifer	Citation(s)
France	Aquitaine basin	La Salle et al., 1995
Germany	Benker-Sandstein	van Geldern et al., 2014
Hungary	Great Hungarian Plain	Stute and Deak, 1989
Hungary	Pannonian basin	Varsanyi et al., 2011
Italy	Emilia-Romagna Plain	Martinelli et al., 2011
Poland	S. Poland carbonates	Samborska et al., 2012
Poland	Malm limestone	Zuber et al., 2004
Portugal	Sado basin	Galego Fernandes and Carreira, 2008
Turkey	Kazan Trona Ore Field	Arslan et al., 2014
United Kingdom	Lincolnshire limestone	Darling et al., 1997
United Kingdom	Chalk aquifer	Darling and Bath, 1988; Dennis et al., 1997; Elliot et al., 1999
U.S.A.	Columbia Flood Bslts.*	Douglas et al., 2007; Brown et al., 2010
U.S.A.	Idaho Batholith	Schlegel et al., 2009
U.S.A.	Mahomet aquifer	Hackley et al., 2010
U.S.A.	Aquia aquifer	Aeschbach-Hertig et al., 2002
U.S.A.	High Plains: Central	Dutton, 1995; Clark et al. 1998
U.S.A.	High Plains: South	Dutton, 1995; Mehta et al., 2000
U.S.A.	San Juan Basin	Phillips et al., 1986
U.S.A.	Floridan aquifer	Clark et al., 1997
Brazil	Portigar basin: Acu	Salati et al., 1974
Brazil	Botacatu: central	Gouvea da Silva, 1983
Russia	Bykovsky Peninsula**	Meyer et al., 2002
Canada	Near Dawson City***	Kotzer and Burn, 2000

92 * Columbia Flood Basalt ice age groundwater may be glacial Lake Missoula floodwaters rather
93 than regional precipitation (Brown et al., 2010).

94 ** Ground ice record – comparison of ice wedge $\delta^{18}O$ values <1m from edge (Holocene) and
95 inner-most (2.5m – 5m; Pleistocene) samples (horizontal ice wedge sample transect MKh-3).

96 *** Ground ice record – comparison of ground ice $\delta^{18}O$ values from the Dago Hill (Holocene)
97 and Quartz Creek (Pleistocene) formations.

Table S3. Groundwater $\delta^{18}O_{ice\ age}$ and $\delta^{18}O_{late\text{-}Holocene}$ ($\Delta^{18}O_{ice\ age} = \delta^{18}O_{ice\ age} - \delta^{18}O_{late\text{-}Holocene}$)

Country	**Aquifer**	**Lon.**	**Lat.**	**$\delta^{18}O_{late-Holo.}$**	**$\delta^{18}O_{ice\ age}$**	**$\Delta^{18}O_{ice\ age}$**
Australia	Canning basin	125.1	−17.5	−6.8±1.6	−7.7±0.3	−0.9±1.7
Australia	Murray aquifer	140.2	−34.2	−4.5	−4.8±0.6	−0.3±0.6
Indonesia	Jakarta basin	106.8	−6.3	−6.1±0.1	−5.9±0.5	+0.1±0.5
Bangladesh	Bengal basin	90.1	23.6	−4.8±1.1	−3.3±0.5	+1.5±1.2
China	Songnen plain	124.5	45.9	−10.3±1.4	−10.2±0.4	+0.2±1.4
China	North China Plain	115.4	38.0	−8.4±0.5	−10.8±0.4	−2.4±0.6
China	Yuncheng basin	110.6	35.0	−8.7±1.3	−9.7±1.3	−0.9±1.9
India	Cuddalore sandstone	79.5	11.4	−5.6±0.3	−4.9±0.6	+0.7±0.7
India	Tiruvadanai aquifer	78.9	9.9	−3.9±0.5	−5.6±0.3	−1.7±0.6
Algeria	Great Oriental Erg: CI	5.9	32.4	−7.1±1.0	−8.3±0.7	−1.2±1.3
Botswana	Kalahari: Ntane	25.2	−24.0	−4.8	−5.6±0.1	−0.8±0.1
Botswana	Lokalane-Nakojane	22.0	−22.3	−6.1±0.1	−7.2±0.1	−1.2±0.2
Burkina Faso	Taoudeni basin	−4.7	12.8	−5.1±0.6	−5.9±0.3	−0.8±0.7
Chad	Chad aquifer	18.3	11.2	−3.9±1.2	−5.6±0.6	−1.7±1.3
Egypt	Nubian aquifer	28.7	25.9	−7.9±2.0	−10.4±0.3	−2.5±2.0
Mali	Mali aquifer	−7.2	15.2	−5.2±0.7	−6.5±0.5	−1.4±0.9
Morocco	Tadla basin	−6.7	32.6	−6.2±0.9	−6.2±0.6	−0.1±1.1
Morocco	Nappe des sables	−14.5	15.4	−6.4±0.6	−6.0±0.5	+0.4±0.8
Namibia	Omatako basin	17.9	−20.1	−8.6±0.7	−9.0±0.1	−0.4±0.7
Niger	Djardo-Bilma	12.9	18.9	−8.1±3.6	−8.1±0.3	+0.0±3.6
Niger	Irhazer: CI	7.5	17.3	−5.3±1.8	−7.3±0.9	−2.0±2.0
Niger	Illumeden: CT	2.7	13.6	−4.5±0.9	−7.3±0.3	−2.9±0.9
Nigeria	Chad basin	12.8	12.0	−4.2±1.0	−6.2±0.5	−2.0±1.1
Senegal	Senegalese CT	−16.4	15.2	−6.1±0.7	−5.9±0.5	+0.1±0.8
S. Africa	Uitenhage aquifer	25.5	−33.7	−4.7±0.2	−5.4±0.1	−0.8±0.2
Tunisia	Kairouan Plain	10.0	35.5	−4.9±1.6	−5.7±0.5	−0.8±1.7
Zimbabwe	Zimbabwe aquifer	28.1	−19.5	−5.9±0.4	−6.9±0.3	−1.0±0.5
Kuwait	Al-Raudhatain and Damman aquifers	47.7	29.9	−2.7±0.4	−4.5±0.4	−1.8±0.6
Oman	Batinah coastal plain	57.7	23.6	−2.4±1.2	−1.6±0.6	+0.9±1.3
Oman	Najd aquifer	53.9	18.1	−1.8±2.6	−4.7±0.8	−2.8±2.7
Syria	Aleppo basin	37.3	35.9	−6.8±1.1	−7.4±0.7	−0.7±1.3
Belgium	Ledo-Paniselian	3.7	51.2	−6.5±1.6	−7.0±0.3	−0.5±1.6
Czech Rep.	Sokolov aquifer	12.7	50.2	−9.1±0.1	−9.5±0.5	−0.4±0.5
Denmark	Ribe Formation	8.6	56.1	−7.9±0.1	−8.8±0.5	−0.8±0.5
France	Bathonian coast	−0.2	49.2	−6.6±0.1	−7.1±0.1	−0.5±0.2
France	Lorraine sandstone	6.6	48.9	−8.9	−10.0±0.4	−1.0±0.4
France	Aquitaine basin	−0.3	46.2	−5.7±0.2	−6.7±0.5	−1.0±0.6
Germany	Benkerstein	11.1	49.5	−9.3±0.2	−10.5±0.1	−1.3±0.2
Hungary	Great Hungarian Plain	20.8	47.6	−9.6	−11.3±0.5	−1.7±0.5
Hungary	Pannonian basin	20.1	46.3	−9.3±0.4	−13.0±0.3	−3.7±0.5

Country	Aquifer	Lon.	Lat.	$\delta^{18}O_{late-Holo.}$	$\delta^{18}O_{ice\ age}$	$\Delta^{18}O_{ice\ age}$
Italy	Emilia Romagna plain	11.0	44.7	−8.4±0.5	−10.3±0.6	−1.9±0.8
Israel	Israel coastal aquifer	34.8	32.0	−4.3±1.7	−4.6±0.1	−0.3±1.7
Israel	Dead Sea rift valley	35.2	30.7	−4.8±0.3	−6.6±0.5	−1.7±0.6
Poland	S. Poland carbonates	19.2	50.6	−10.2±0.4	−11.4±0.8	−1.3±0.9
Poland	Malm limestone	19.8	50.0	−10.2±0.4	−11.2±0.8	−1.0±0.9
Portugal	Sado basin	−8.5	38.3	−4.7±0.3	−4.7±0.1	+0.0±0.3
Turkey	Kazan Trona Ore Field	40.1	32.5	−9.2±0.7	−12.1±0.6	−2.9±0.9
U.K.	Lincolnshire limestone	−0.3	52.8	−7.8±0.1	−8.1±0.3	−0.3±0.3
U.K.	Chalk aquifer	−1.2	51.4	−7.4	−7.6±0.2	−0.2±0.2
Brazil	Portigar basin: Acu	−37.0	−6.1	−1.8±1.2	−4.5±0.3	−2.7±1.3
Brazil	Botacatu: central	−48.7	−22.3	−8.5±1.4	−8.3±1.0	+0.3±1.7
U.S.A.	Columbia Flood Bslts	−119.0	46.6	−14.8±0.9	−18.0±0.6	−3.2±1.1
U.S.A.	Idaho Batholith	−116.1	43.7	−16.5±0.7	−17.2±0.4	−0.7±0.8
U.S.A.	San Juan Basin	−107.7	36.4	−12.0±0.6	−14.4±0.9	−2.5±1.1
U.S.A.	Mahomet aquifer	−88.8	39.9	−6.8±0.3	−7.2±0.6	−0.4±0.6
U.S.A.	High Plains: Central	−101.0	37.5	−9.3±1.6	−12.0±1.0	−2.7±1.9
U.S.A.	High Plains: South	−101.8	35.2	−6.7±1.0	−8.7±1.2	−2.0±1.6
U.S.A.	Aquia aquifer	−76.6	38.7	−7.0±0.2	−7.1±0.3	−0.1±0.4
U.S.A.	Floridan aquifer	−82.1	32.0	−4.7±0.2	−3.7±0.4	+1.0±0.4
Russia	Bykovsky Peninsula	129.4	71.8	−25.4	−30.8±1.3	−5.4±1.3
Canada	Near Dawson City	−139.0	63.9	−26.1±0.8	−31.5±0.4	−5.5±0.9

99 * average ± 1 standard deviation shown

Table S4. Speleothem $\delta^{18}O$ change from the last ice age to the late-Holocene

Cave	Cntry.	Reference	Lon.	Lat.	$\Delta^{18}O_{ice\ age}$	Corr.[x]
Gunung Buda	Borneo	Partin et al., 2007	114.8	4.0	+2.0±0.3	−0.9±0.2
Botuverá Cave	Brazil	Cruz et al., 2005; Wang et al., 2007	−49.2	−27.2	−0.7±0.4	−0.9±0.2
Dongge [t]	China	Dykoski et al., 2005; Yuan et al., 2004	108.1	25.3	+2.6±0.5	−0.9±0.2
Hulu *	China	Wang et al., 2001	119.2	32.5	+1.6±0.3	−1.0±0.2
Jiuxian [t]	China	Cai et al., 2010	109.1	33.6	+1.3±1.9	−1.0±0.2
Yaman [t]	China	Yang et al., 2010	107.9	24.5	+2.7±0.5	−0.9±0.2
Soreq	Israel	Bar-Matthews et al., 2003	35.0	31.5	+2.3±0.2	−1.0±0.1
Peqin*	Israel	Bar-Matthews et al., 2003	35.2	32.6	+2.0±0.5	−0.9±0.2
Jerusalem W	Israel	Frumkin et al., 1999	35.2	31.7	+1.8±0.6	−1.0±0.2
NW South Island	New Zealand	Williams et al., 2010	172.0	−42.0	+0.4±0.2	−1.0±0.3
Cold Air Cave	South Africa	Holmgren et al., 2003	29.1	−24.0	+1.2±0.5	−1.0±0.1
Sofular	Turkey	Fleitmann et al., 2009	31.9	41.4	−4.7±0.2	−1.0±0.2
Fort Stanton*	U.S.A.	Asmerom et al., 2010	−105.3	33.3	−2.0±1.0	−1.0±0.2
Cave of the bells*	U.S.A.	Wagner et al., 2010	−110.8	31.8	−2.4±0.2	−1.0±0.2
Moomi*	Yemen	Shakun et al., 2007	54.0	12.5	+2.2±0.6	−0.9±0.2

* early Holocene value used (i.e., shift likely larger than shown)

[t] values from 15.0 ka used

[x] Calcite-water fractionation correction subtracted from raw observed $\Delta^{18}O_{ice\ age}$ to correct for the 4.0±0.8 °C colder climate (Annan and Hargreaves, 2013) at the last glacial stage (from O'Neil et al., 1969; modern temperatures from New et al., 2002; $\Delta^{18}O_{ice\ age}$ values in preceding column are shown in raw (i.e, uncorrected) form.

Table S5. Ice core $\delta^{18}O$ change from the last ice age to the late-Holocene

Ice core	**Country**	**Reference**	**Lon.**	**Lat.**	**$\Delta^{18}O_{ice\ age}$**
Sajama	Bolivia	Thompson et al., 1998	−68.8	−18.1	−4.6±1.0
Huascaran	Peru	Thompson et al., 1995	−77.6	−9.1	−6.3±1.3
Qinghai-Tibetan	Tibet	Thompson et al., 1997	81.5	35.3	−0.6±2.8
Devon Island	Canada	Patterson et al., 1977	-82.3	75.3	−4.7±2.4
TALD Ice	Antarctica	Buiron et al., 2011	159.2	−72.8	−4.0±0.7
Byrd Glacier	Antarctica	Blunier and Brook, 2001	−119.5	−80.0	−5.9±0.9
Dome Fuji	Antarctica	Kawamura et al. 2007	39.7	−77.3	−3.6±0.9
Dronning Maud	Antarctica	EPICA Community, 2006	2.0	−75.0	−5.2±1.0
Law Dome	Antarctica	Pedro et al. 2011	112.8	−66.8	−6.7±0.7
Siple Dome	Antarctica	Pedro et al. 2011	−148.8	−81.7	−7.1±1.0
Renland ice core	Greenland	Vinther et al., 2008	−27.0	71.0	−3.9±1.0
NGRIP1	Greenland	Vinther et al., 2006	−42.3	75.1	−7.0±1.9

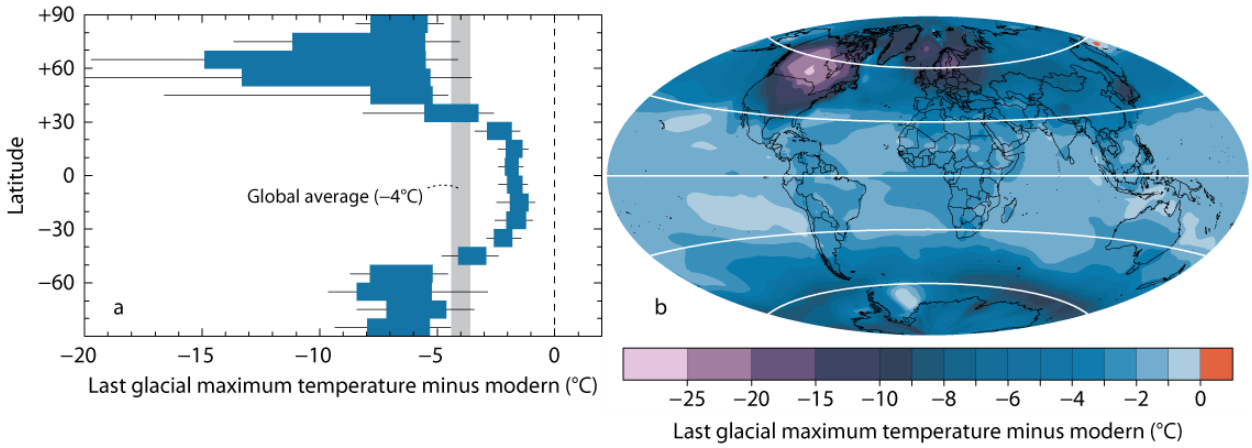

110

111 **Figure S1.** The change in surface air temperatures from the last glacial maximum to the
112 preindustrial era (gridded data from Annan and Hargreaves, 2013). (a) Percentile ranges of
113 temperature changes since the last glacial maximum for 10 degree latitudinal bands. Blue
114 shading marks the 25th-75th percentile range; thin horizontal lines mark the 10th-90th percentile
115 range. The grey band shows the globally-averaged estimate of temperature change since the last
116 glacial maximum of −4.0±0.8 °C. (b) Gridded surface air temperature anomaly from the last
117 glacial maximum to the preindustrial era (data from Annan and Hargreaves, 2013).

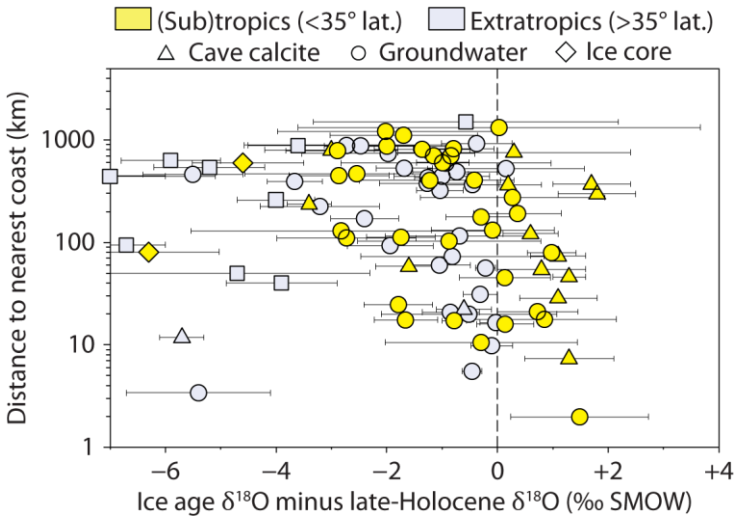

Figure S2. Variations of proxy record $\Delta^{18}O_{ice\ age}$ with distance to the nearest coast. Subtropical and (sub)tropical locations are shown in yellow (<35° absolute latitude), extra-tropical sites are shown in grey (>35° absolute latitude). The shape of each point corresponds to groundwater and ground ice (circles), ice cores (squares) and cave calcite (i.e., speleothems; triangles).

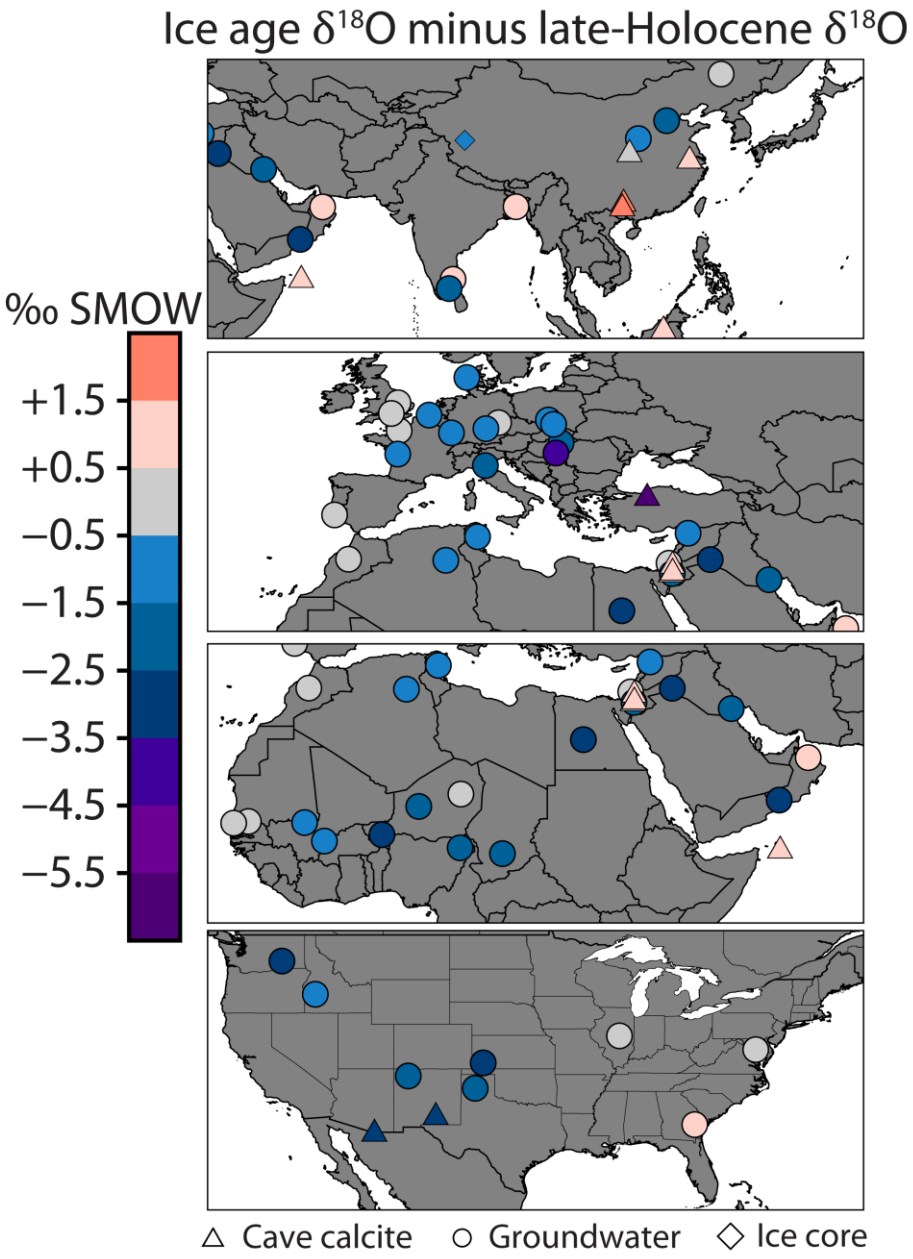

Figure S3. Regional proxy record $\Delta^{18}O_{ice\ age}$ values for (a) southeastern Asia, (b) Europe, northern Africa and the Middle-East, (c) northern and central Africa, and (d) the contiguous United States of America.

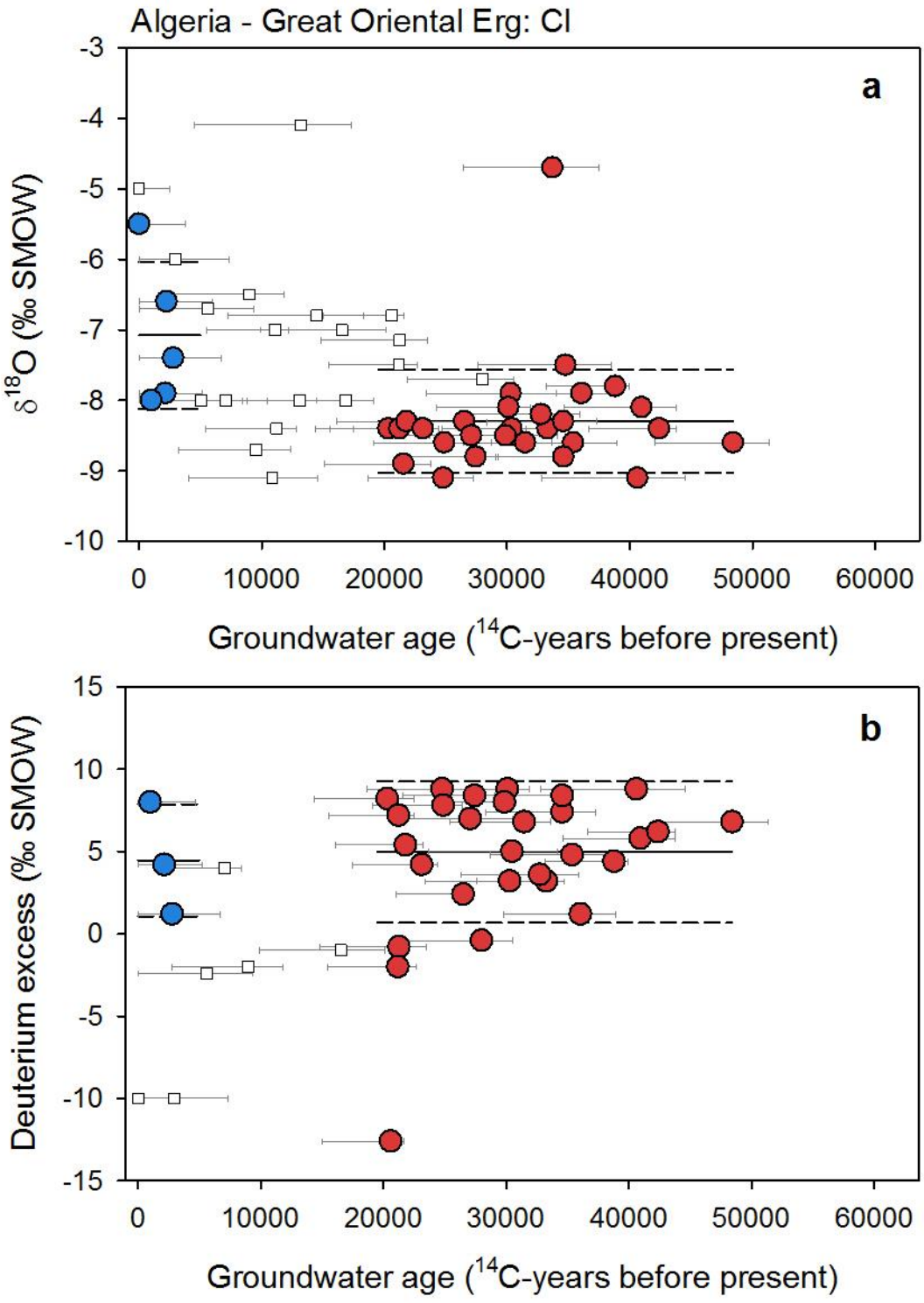

Figure S4. Groundwater isotope composition of the Great Oriental Erg (Continental Intercalaire) aquifer. Groundwater $\delta^{18}O$ (a) and deuterium excess (b) plotted against corrected ^{14}C ages for late-Holocene (blue circles) and ice age (red circles) groundwaters. Lines mark the average (solid line) and one standard deviation (dashed lines) for each age group (Edmunds et al., 2003).

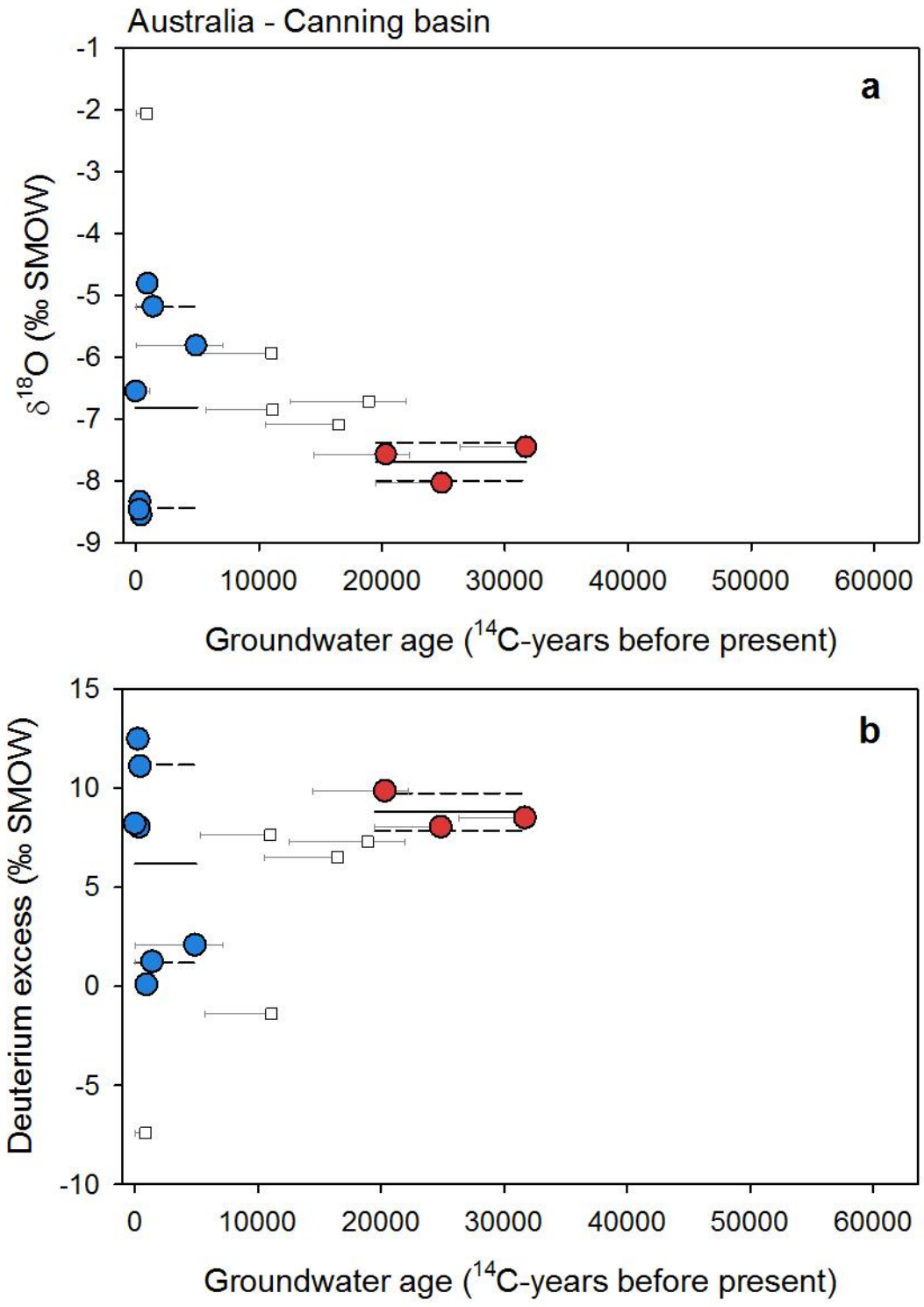

Figure S5. Groundwater isotope composition of the Canning basin. Groundwater $\delta^{18}O$ (a) and deuterium excess (b) plotted against corrected ^{14}C ages for late-Holocene (blue circles) and ice age (red circles) groundwaters. Lines mark the average (solid line) and one standard deviation (dashed lines) for each age group (Harrington et al., 2011).

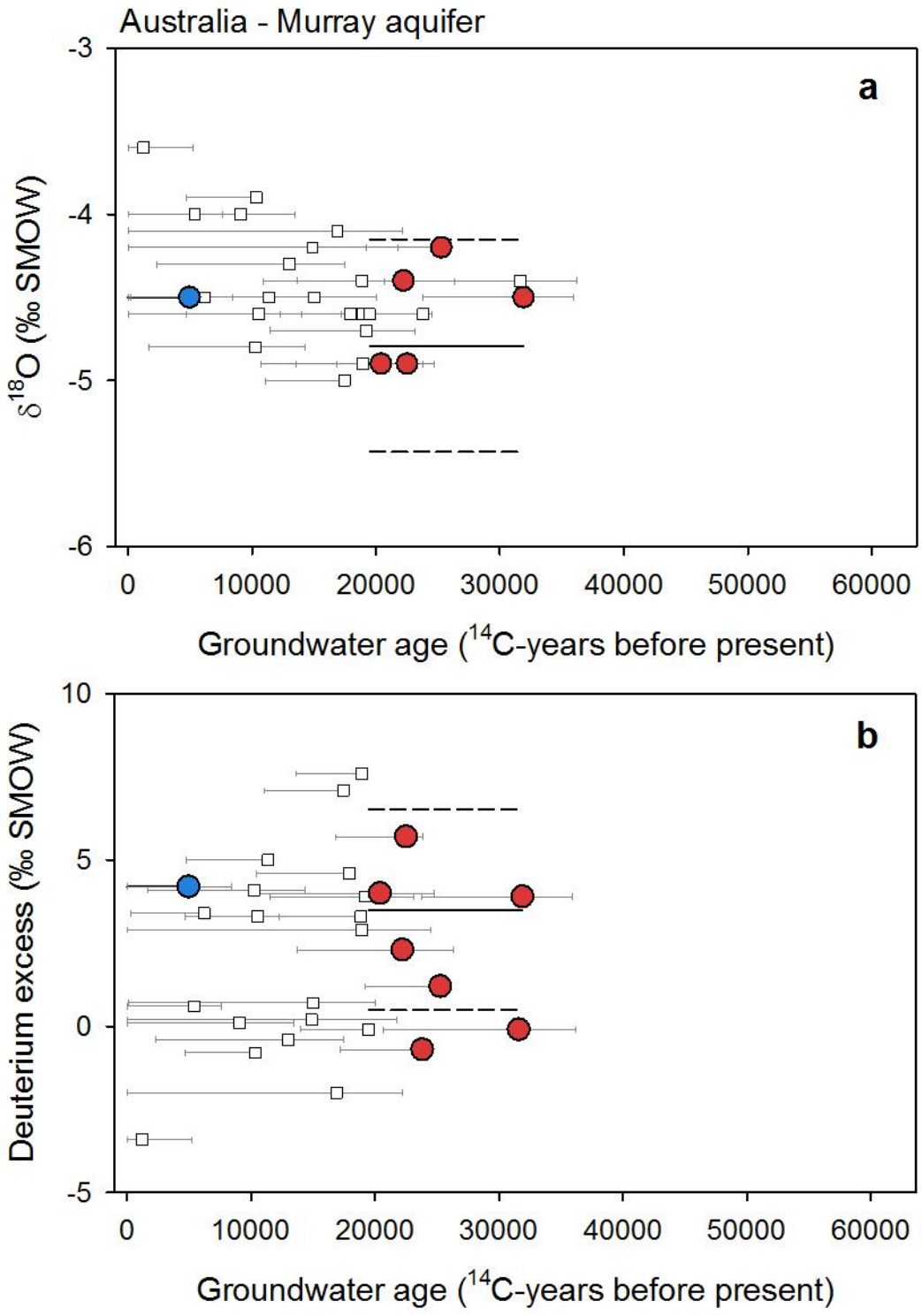

Figure S6. Groundwater isotope composition of the Murray aquifer. Groundwater $\delta^{18}O$ (a) and deuterium excess (b) plotted against corrected ^{14}C ages for late-Holocene (blue circles) and ice age (red circles) groundwaters. Lines mark the average (solid line) and one standard deviation (dashed lines) for each age group (Leaney and Allison, 1986).

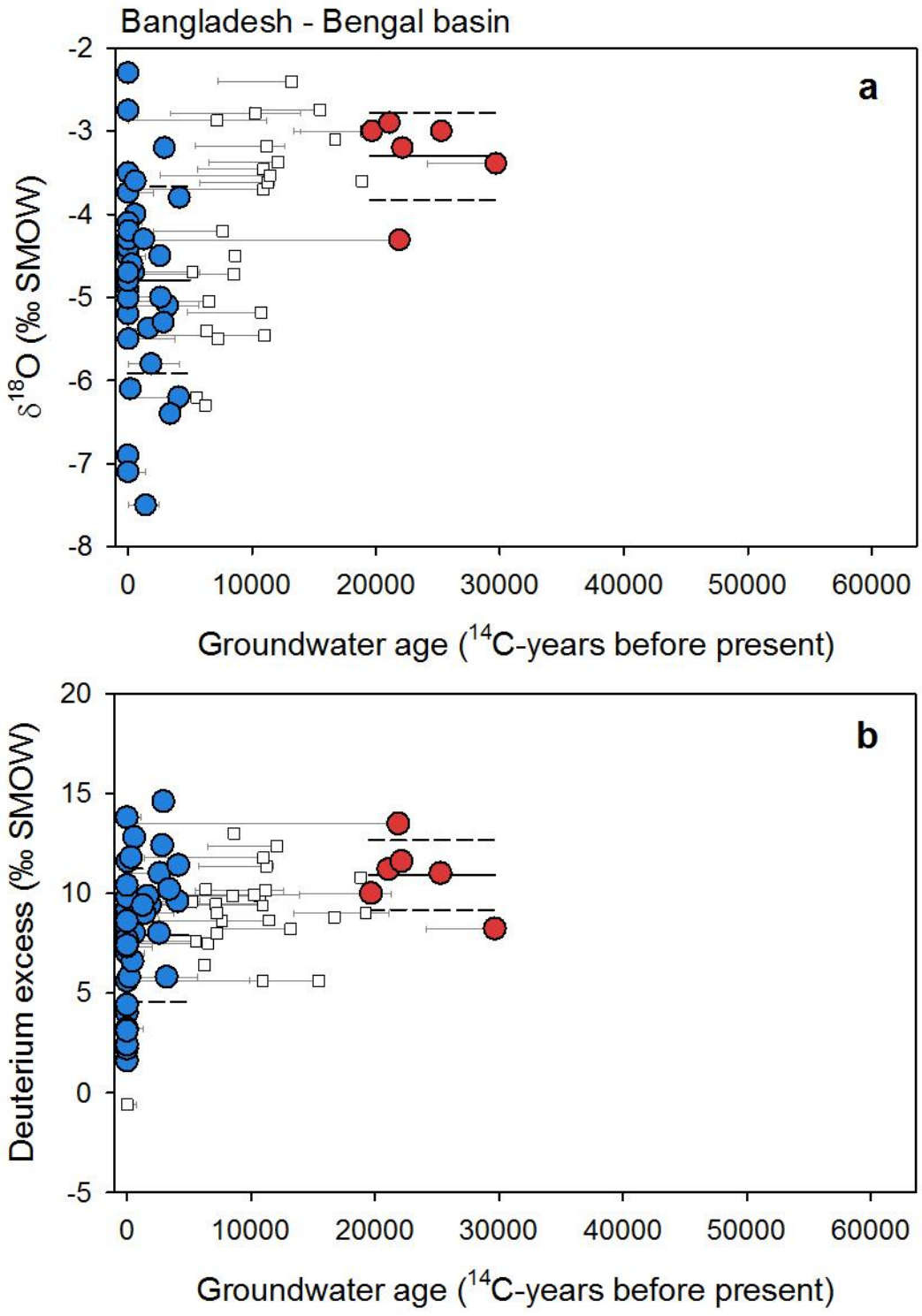

Figure S7. Groundwater isotope composition of the Bengal basin. Groundwater $\delta^{18}O$ (a) and deuterium excess (b) against corrected ^{14}C ages for late-Holocene (blue circles) and ice age (red circles) groundwaters. Lines mark average (solid line) and 1 s.d. (dashed lines) for each group (Aggarwal et al., 2000; Sikdar and Sahu, 2009; Majumder et al., 2011; Hoque and Burgess, 2012).

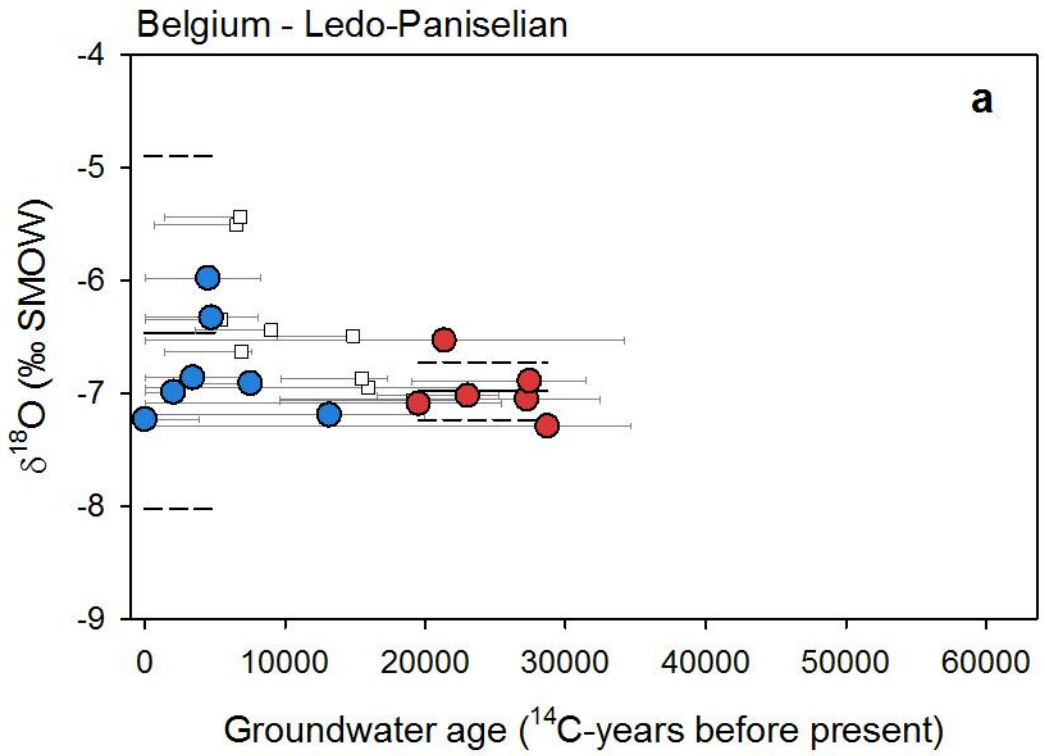

Figure S8. Groundwater isotope composition of the Ledo-Paniselian aquifer. Groundwater $\delta^{18}O$ plotted against corrected ^{14}C ages for late-Holocene (blue circles) and ice age (red circles) groundwaters. Lines mark the average (solid line) and one standard deviation (dashed lines) for each age group (Walraevens, 1990; Walraevens et al., 2001).

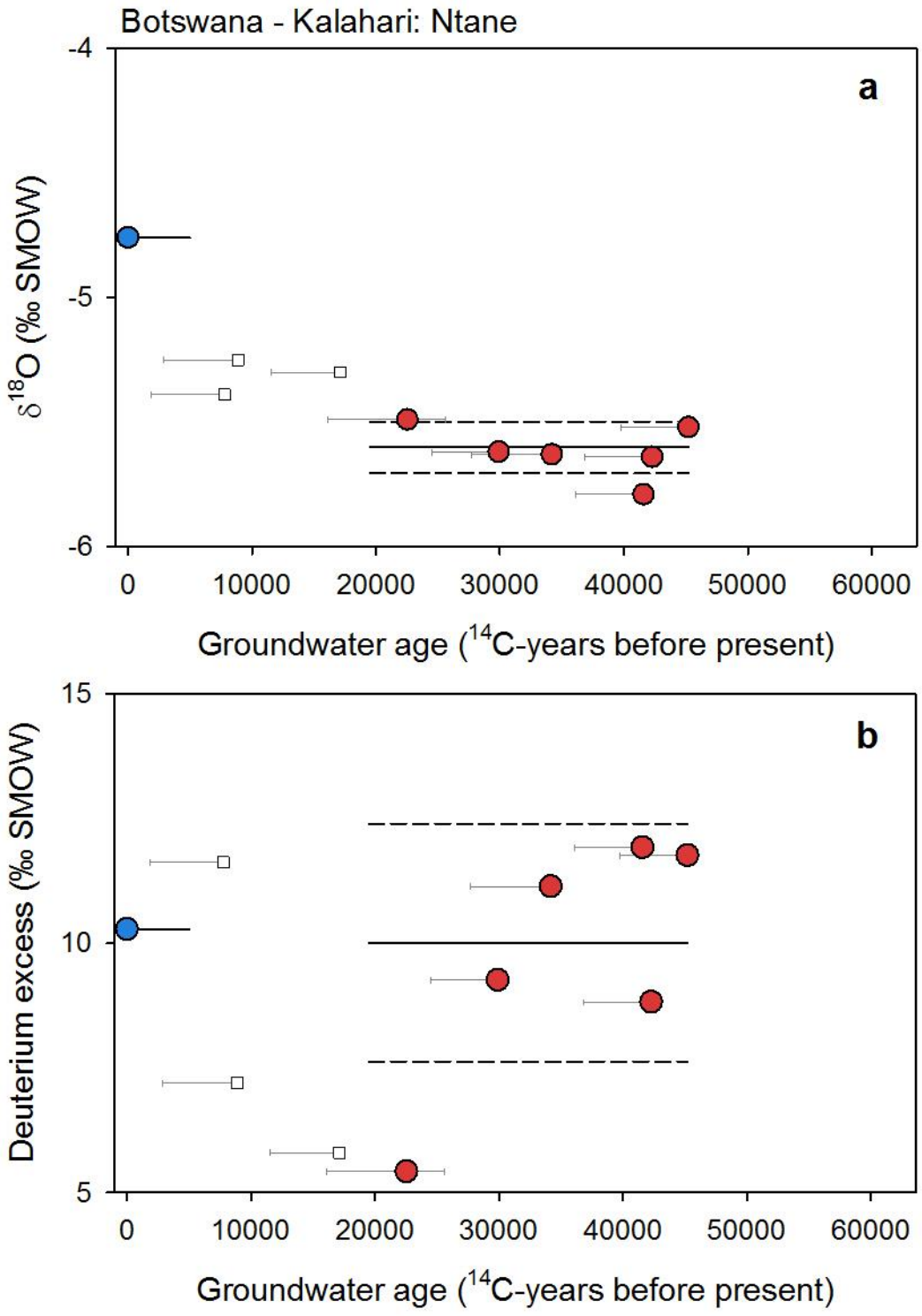

Figure S9. Groundwater isotope composition of the Ntane Sandstone aquifer. Groundwater $\delta^{18}O$ (a) and deuterium excess (b) plotted against corrected ^{14}C ages for late-Holocene (blue circles) and ice age (red circles) groundwaters. Lines mark the average (solid line) and one standard deviation (dashed lines) for each age group (Kulongoski et al., 2004).

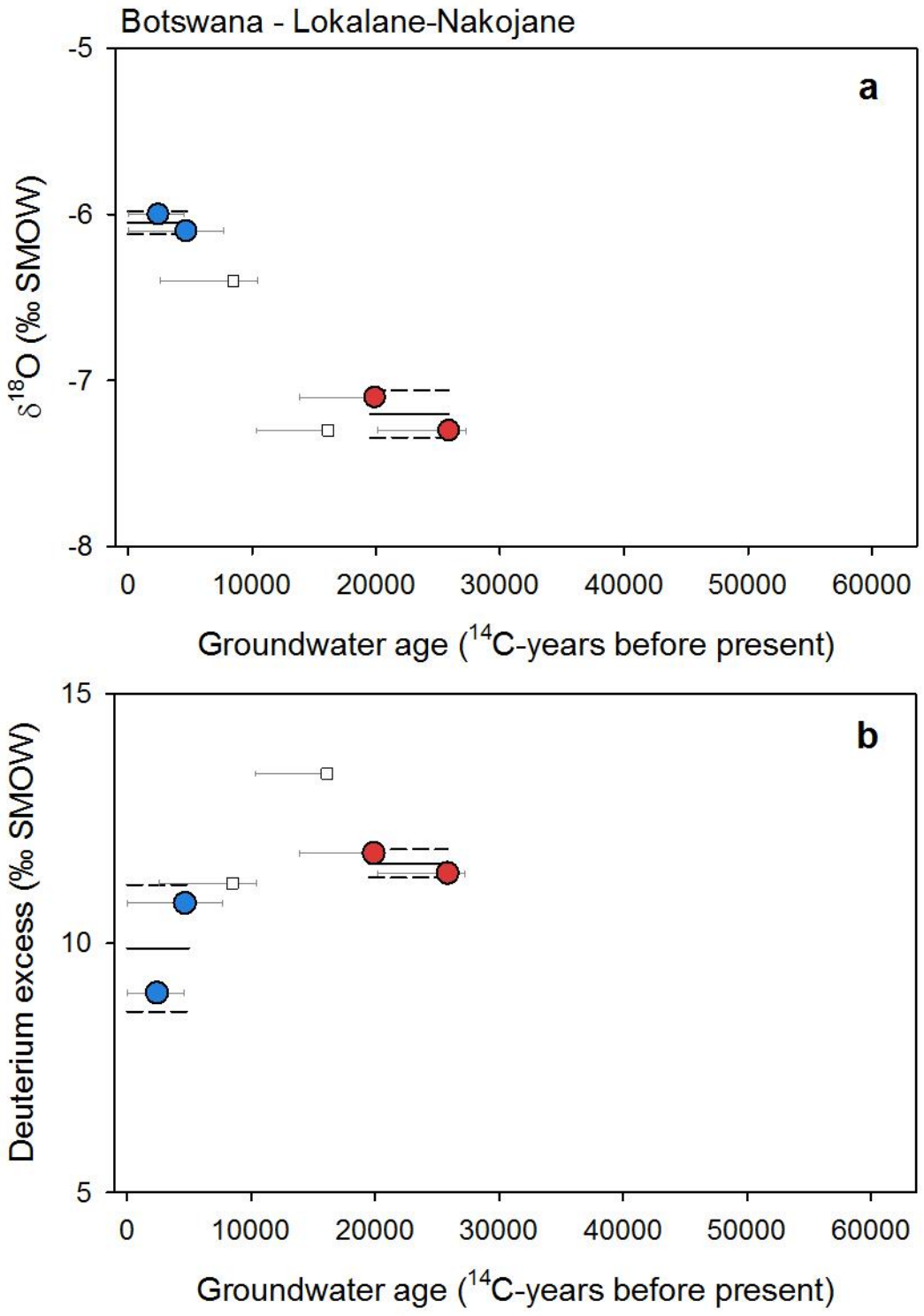

Figure S10. Groundwater isotope composition of the Lokelane-Nakojane aquifer. Groundwater $\delta^{18}O$ (a) and deuterium excess (b) plotted against corrected ^{14}C ages for late-Holocene (blue circles) and ice age (red circles) groundwaters. Lines mark the average (solid line) and one standard deviation (dashed lines) for each age group (Rahube, 2003).

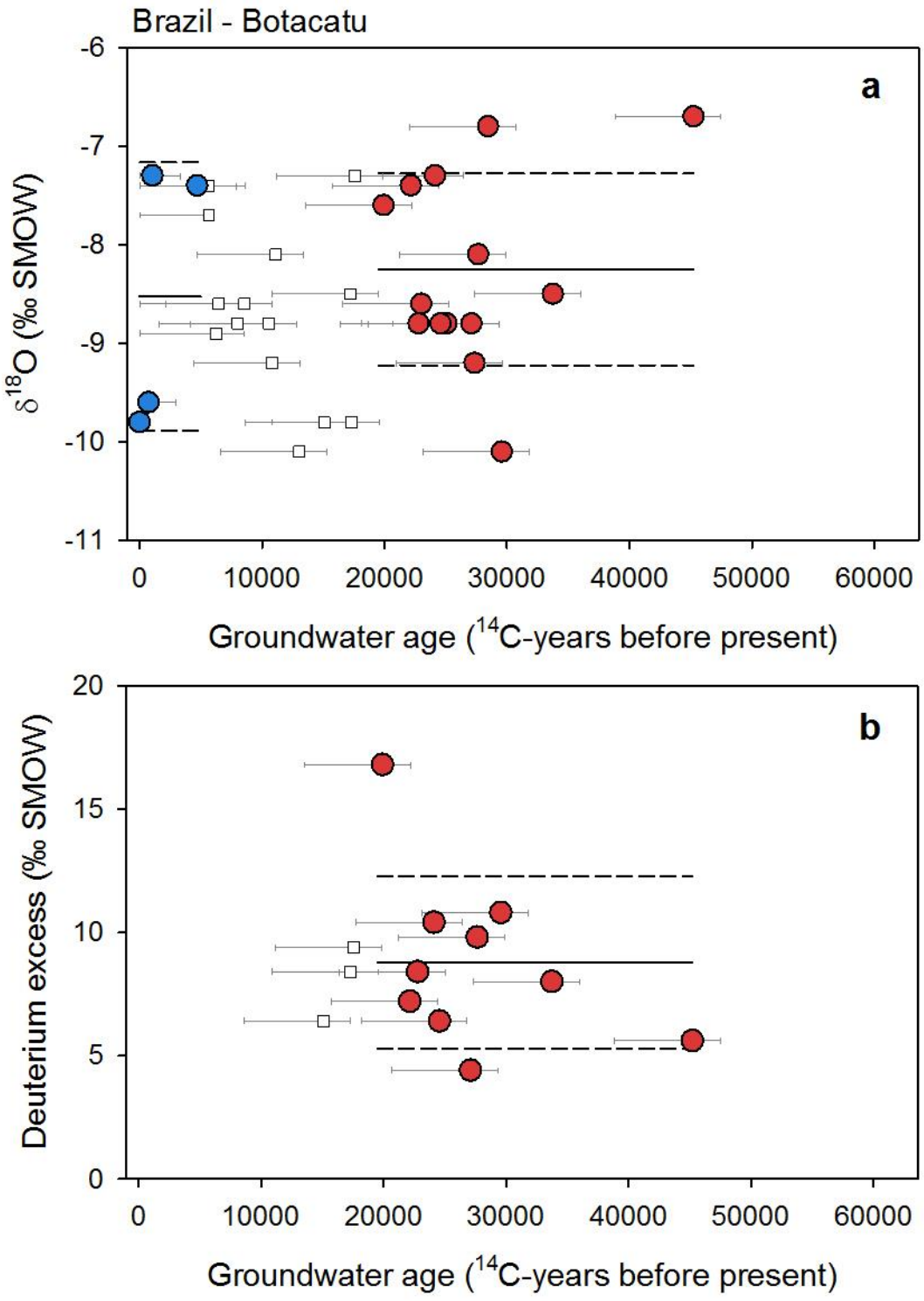

Figure S11. Groundwater isotope composition of the Botacatu aquifer system. Groundwater $\delta^{18}O$ (a) and deuterium excess (b) plotted against corrected ^{14}C ages for late-Holocene (blue circles) and ice age (red circles) groundwaters. Lines mark the average (solid line) and one standard deviation (dashed lines) for each age group (Gouvea da Silva, 1983).

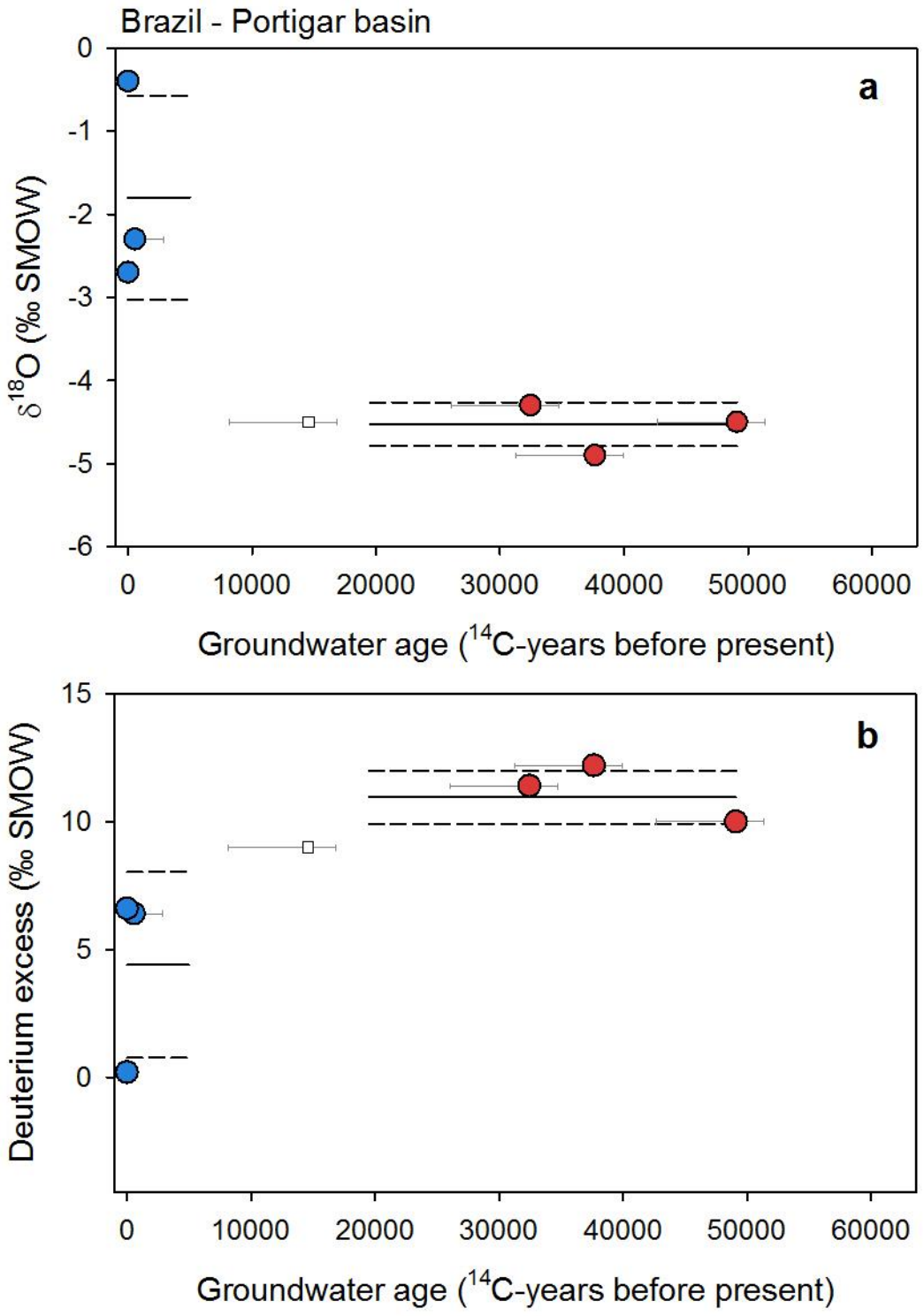

Figure S12. Groundwater isotope composition of the Portigar basin. Groundwater $\delta^{18}O$ (a) and deuterium excess (b) plotted against corrected ^{14}C ages for late-Holocene (blue circles) and ice age (red circles) groundwaters. Lines mark the average (solid line) and one standard deviation (dashed lines) for each age group (Salati et al., 1974).

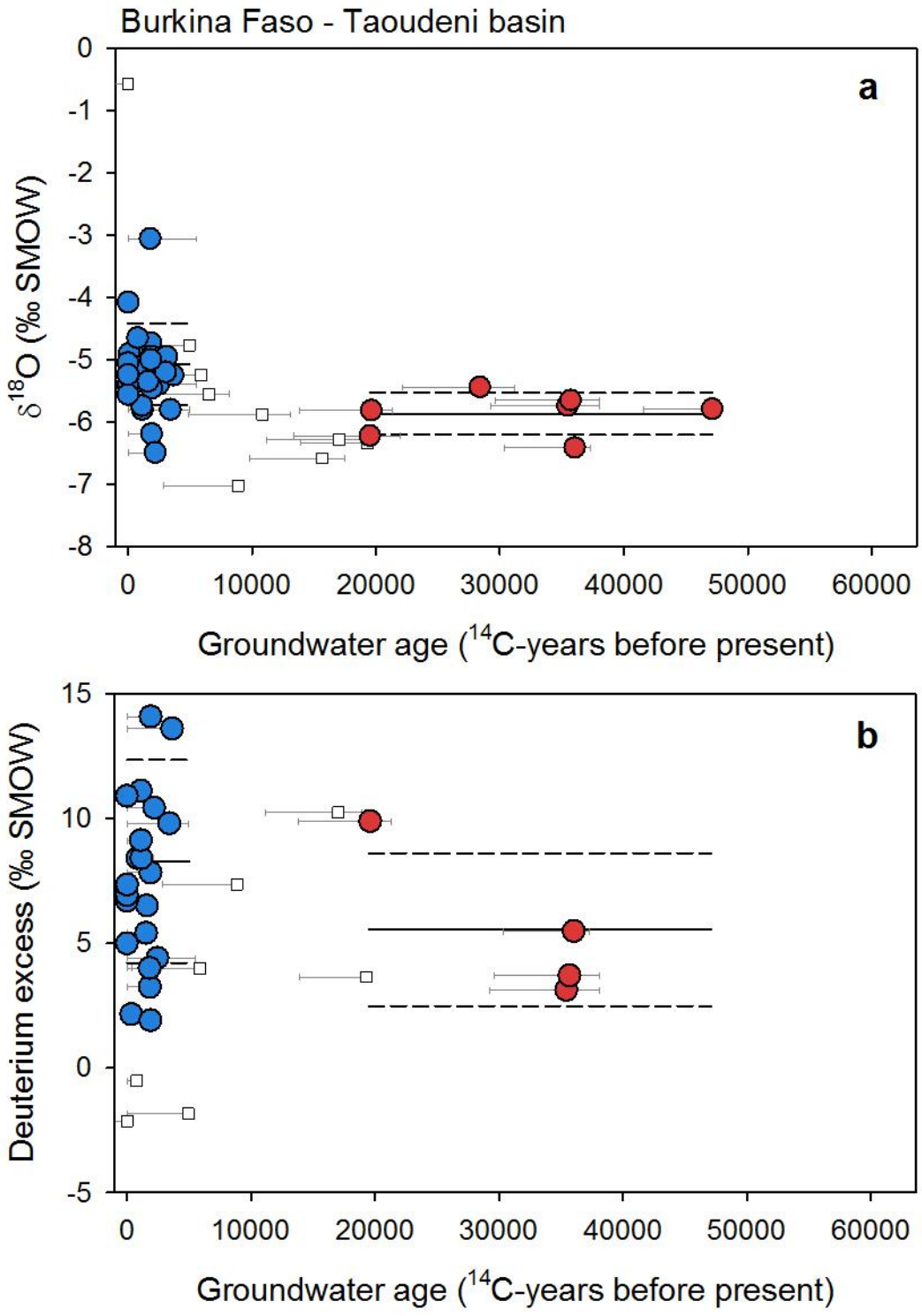

Figure S13. Groundwater isotope composition of the Taoudeni basin. Groundwater $\delta^{18}O$ (a) and deuterium excess (b) plotted against corrected ^{14}C ages for late-Holocene (blue circles) and ice age (red circles) groundwaters. Lines mark the average (solid line) and one standard deviation (dashed lines) for each age group (Huneau et al., 2011).

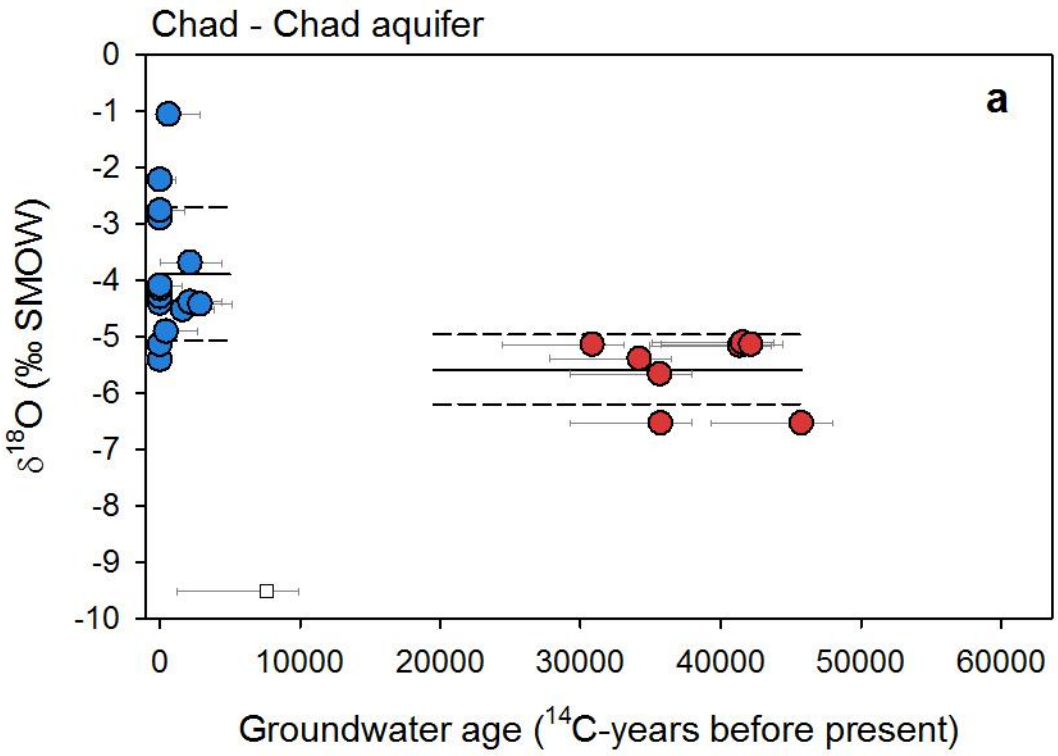

Figure S14. Groundwater isotope composition of the Chad aquifer (in Chad). Groundwater $\delta^{18}O$ plotted against corrected ^{14}C ages for late-Holocene (blue circles) and ice age (red circles) groundwaters. Lines mark the average (solid line) and one standard deviation (dashed lines) for each age group (Edmunds, 2009).

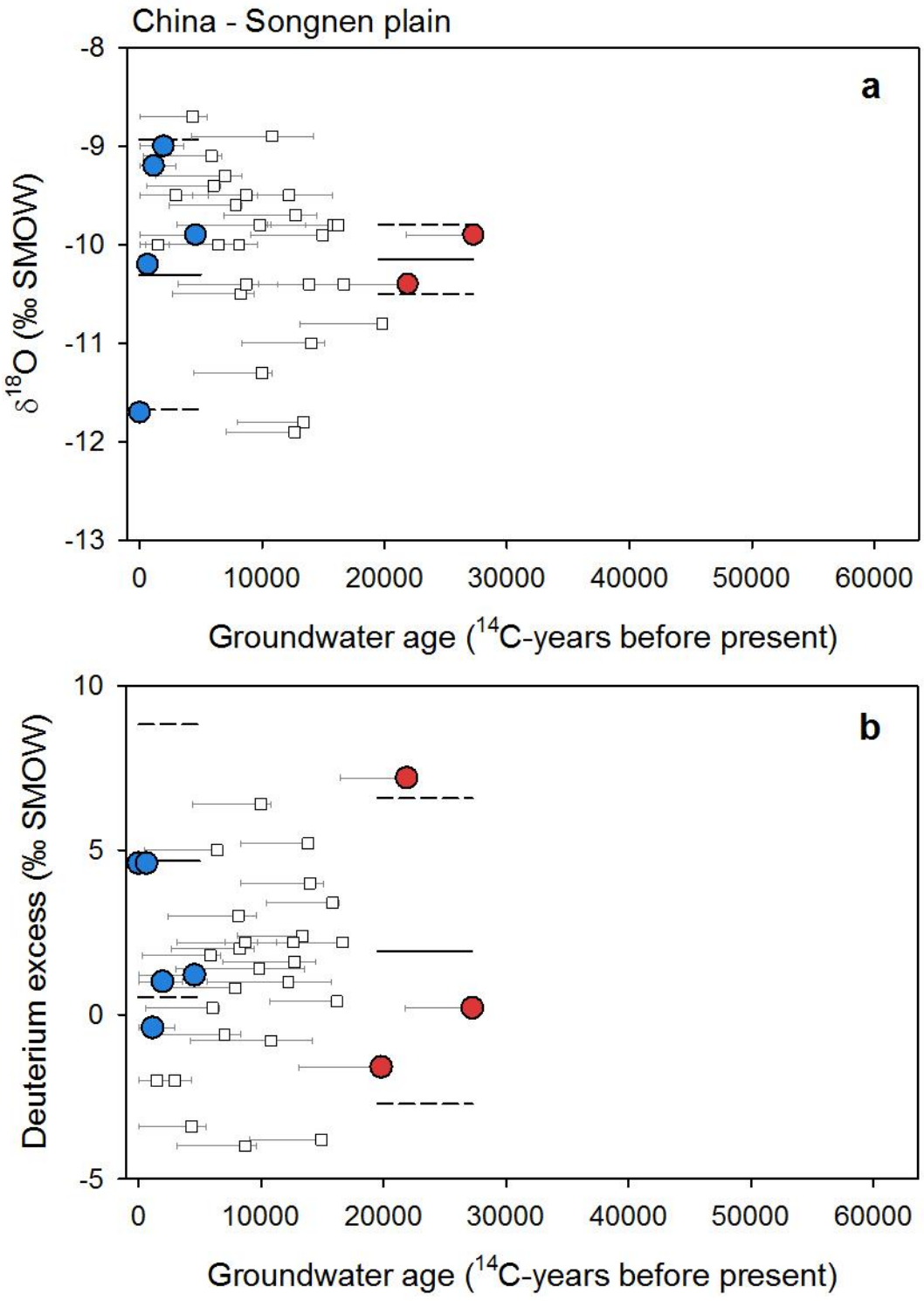

Figure S15. Groundwater isotope composition of the Songnen Plain. Groundwater $\delta^{18}O$ (a) and deuterium excess (b) plotted against corrected ^{14}C ages for late-Holocene (blue circles) and ice age (red circles) groundwaters. Lines mark the average (solid line) and one standard deviation (dashed lines) for each age group (Chen et al., 2011).

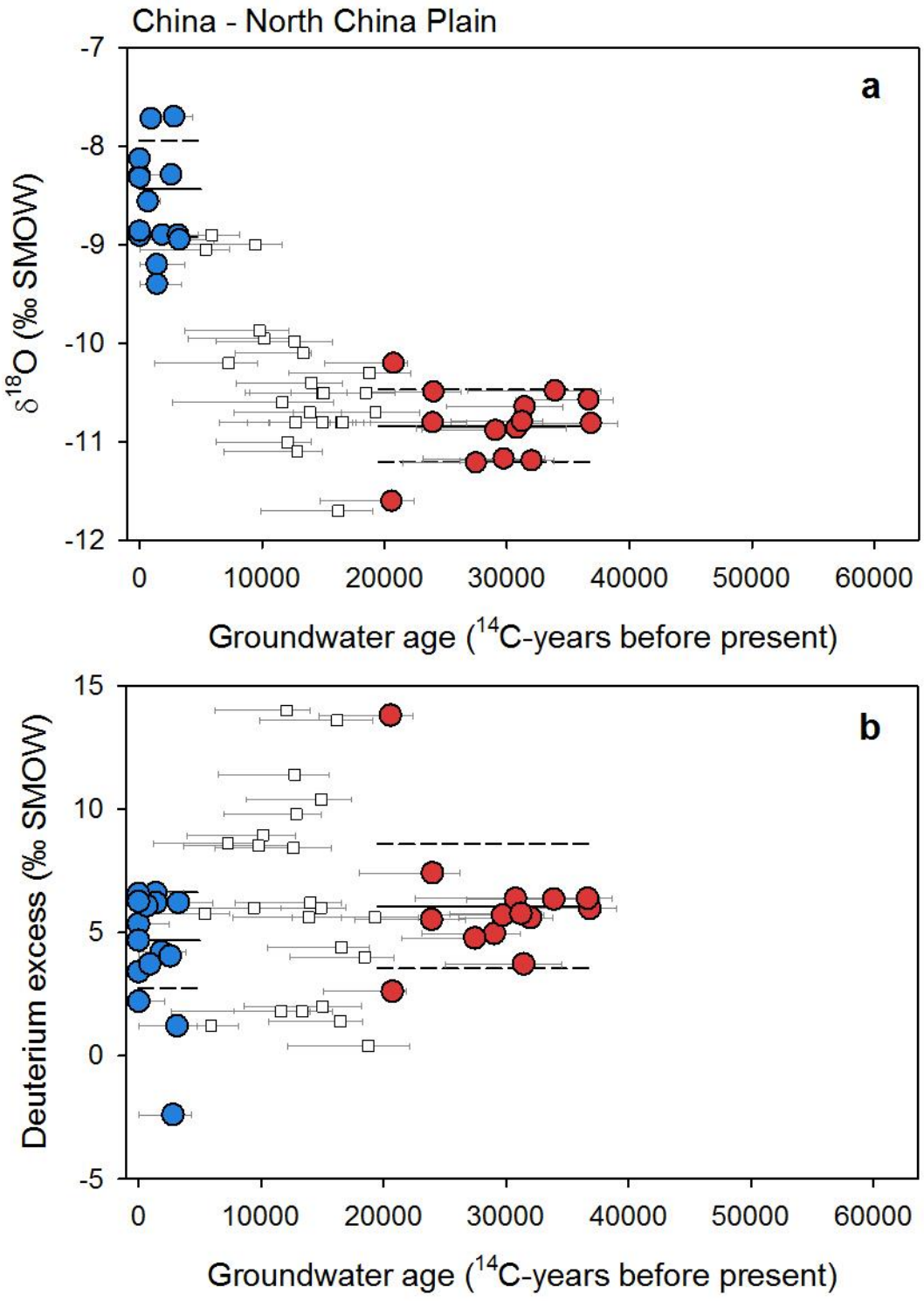

Figure S16. Groundwater isotope composition of the North China Plain. Groundwater $\delta^{18}O$ (a) and deuterium excess (b) plotted against corrected ^{14}C ages for late-Holocene (blue circles) and ice age (red circles) groundwaters. Lines mark the average (solid line) and one standard deviation (dashed lines) for each age group (Zongyu et al., 2003; Kreuzer et al., 2009).

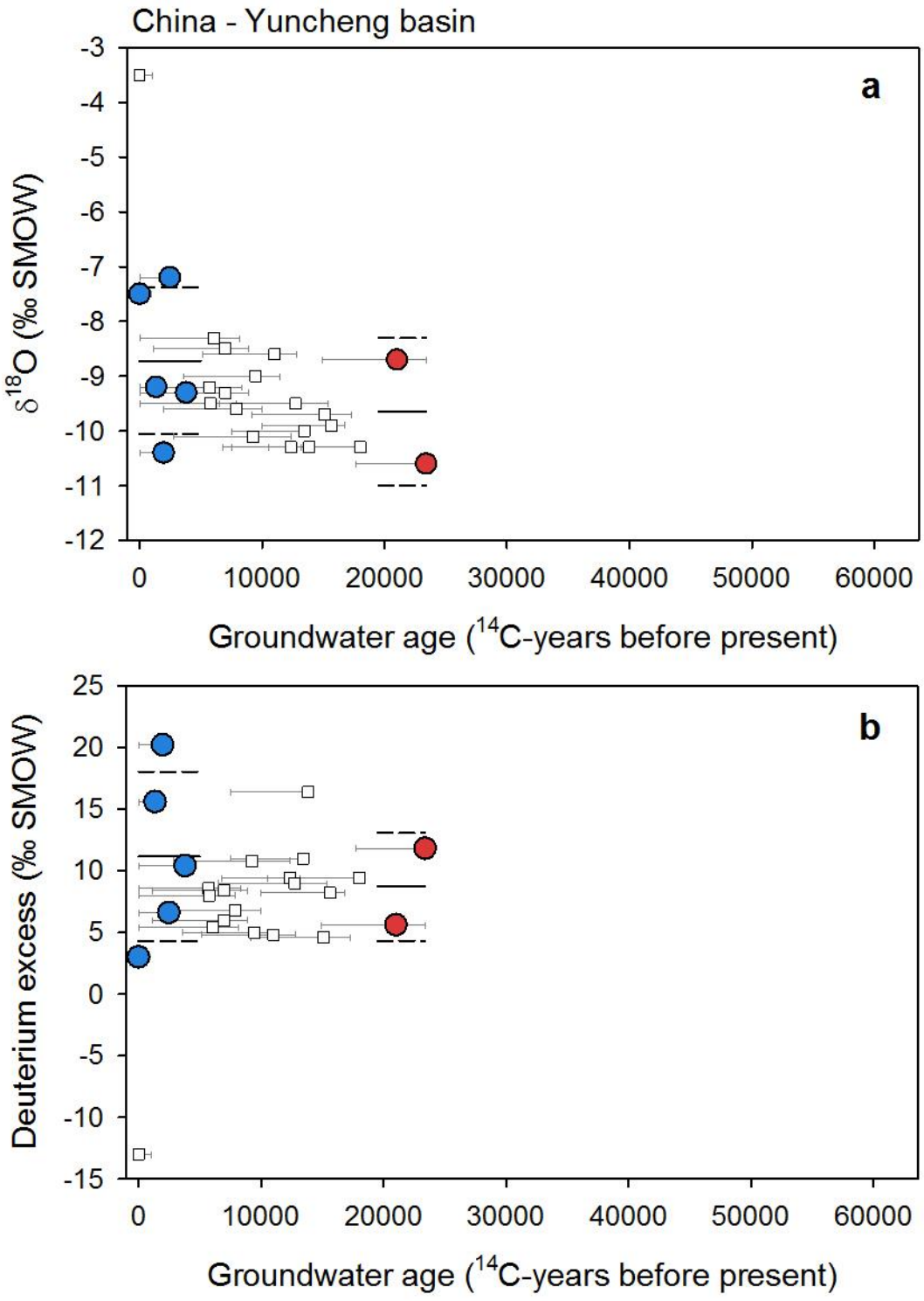

Figure S17. Groundwater isotope composition of the Yuncheng basin. Groundwater $\delta^{18}O$ (a) and deuterium excess (b) plotted against corrected ^{14}C ages for late-Holocene (blue circles) and ice age (red circles) groundwaters. Lines mark the average (solid line) and one standard deviation (dashed lines) for each age group (Currell et al., 2010).

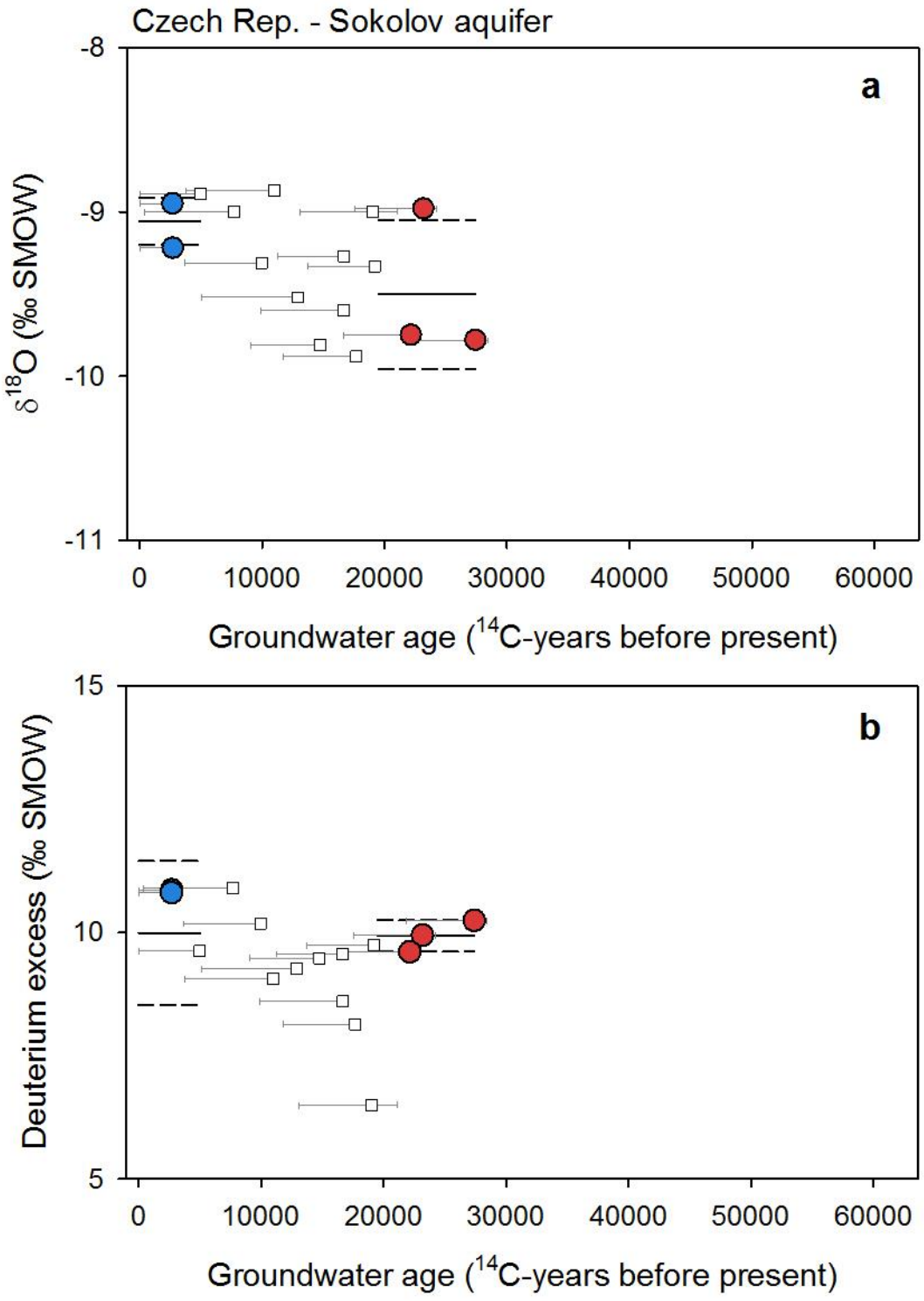

200

201 **Figure S18.** Groundwater isotope composition of the Sokolov aquifer. Groundwater $\delta^{18}O$ (a) and
202 deuterium excess (b) plotted against corrected ^{14}C ages for late-Holocene (blue circles) and ice
203 age (red circles) groundwaters. Lines mark the average (solid line) and one standard deviation
204 (dashed lines) for each age group (Noseck et al., 2009).

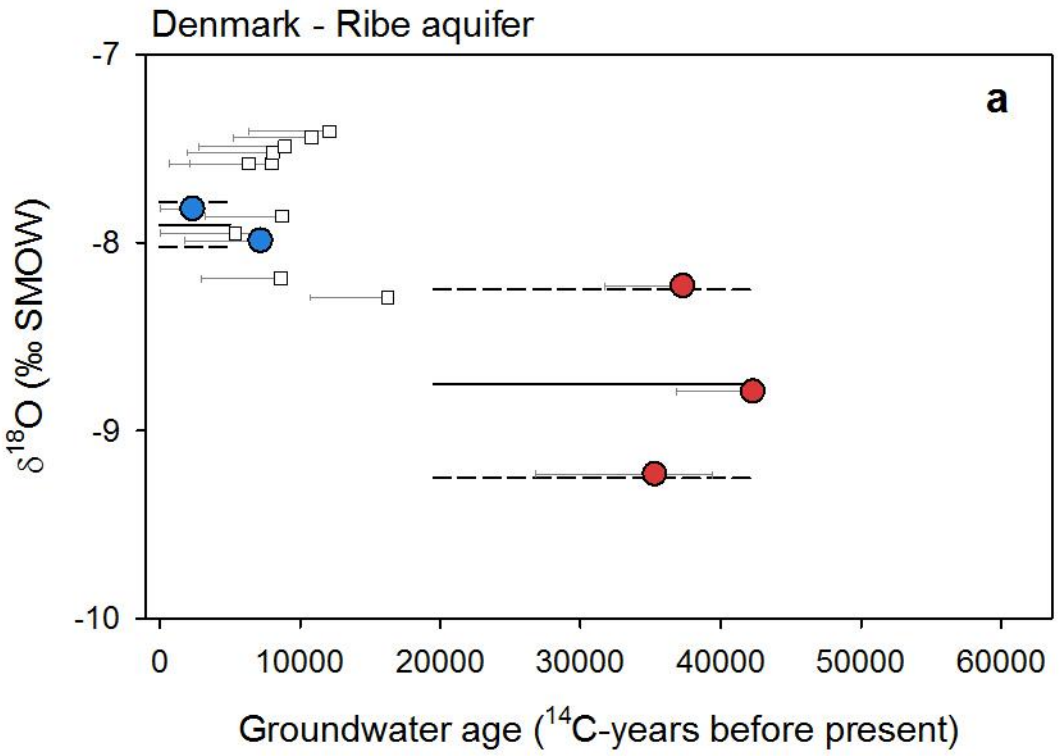

Figure S19. Groundwater isotope composition of the Ribe aquifer. Groundwater $\delta^{18}O$ plotted against corrected ^{14}C ages for late-Holocene (blue circles) and ice age (red circles) groundwaters. Lines mark the average (solid line) and one standard deviation (dashed lines) for each age group (Hinsby et al., 2001).

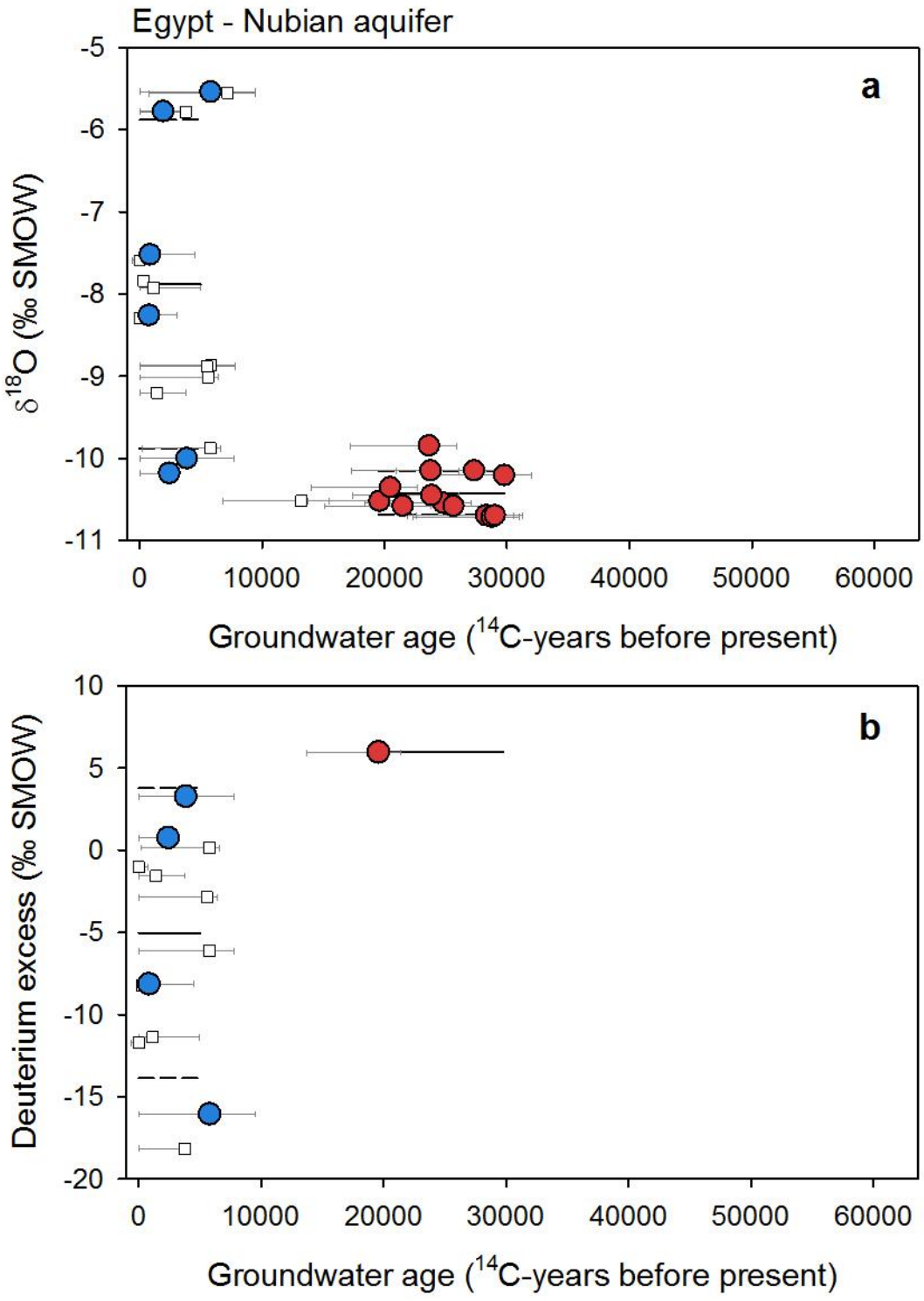

Figure S20. Groundwater isotope composition of the Nubian aquifer. Groundwater $\delta^{18}O$ (a) and deuterium excess (b) plotted against corrected ^{14}C ages for late-Holocene (blue circles) and ice age (red circles) groundwaters. Lines mark the average (solid line) and one standard deviation (dashed lines) for each age group (Shehata and Al-Ruwaih, 1999; Patterson et al., 2005; Edmunds, 2009).

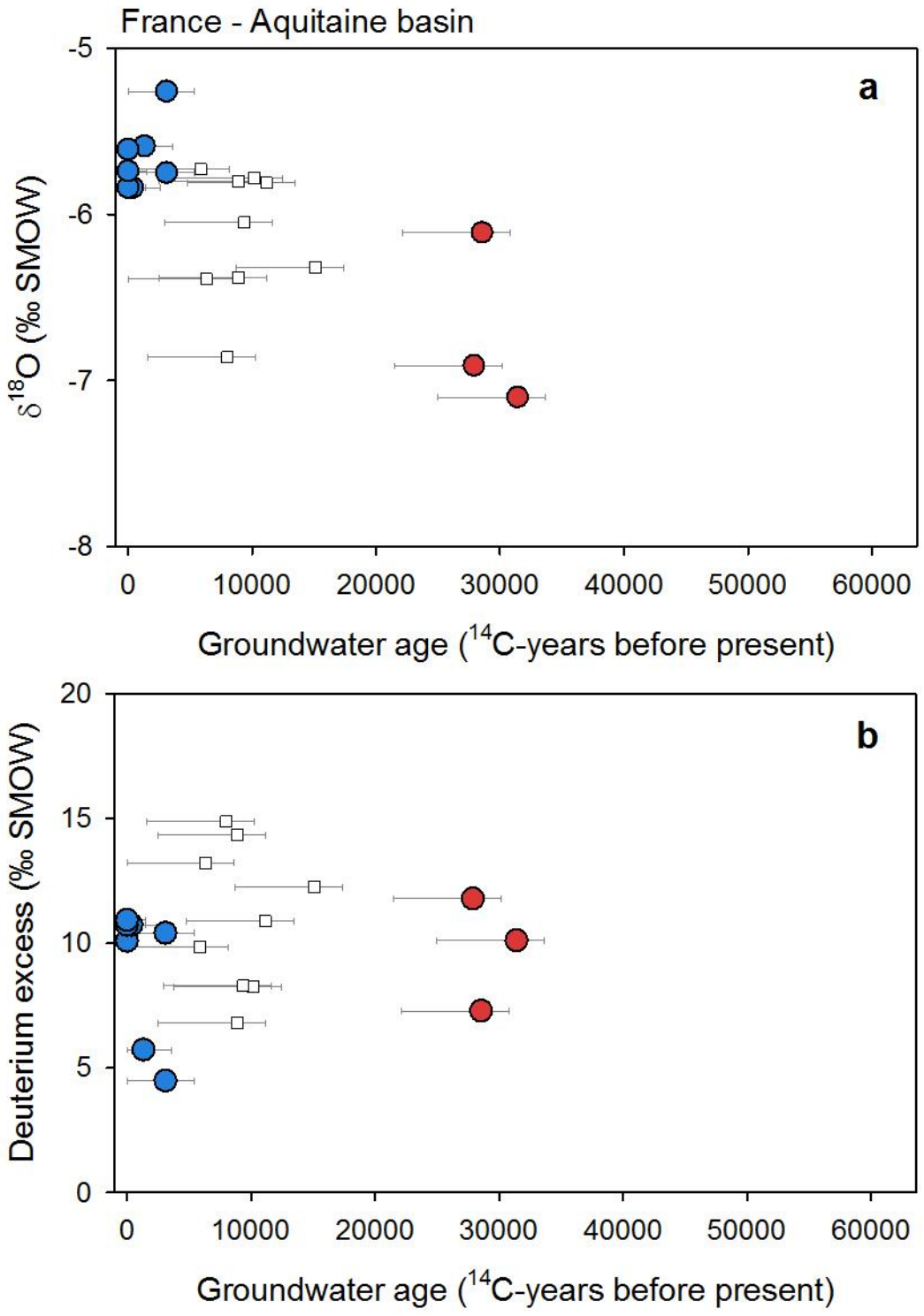

Figure S21. Groundwater isotope composition of the Aquitaine basin. Groundwater $\delta^{18}O$ (a) and deuterium excess (b) plotted against corrected ^{14}C ages for late-Holocene (blue circles) and ice age (red circles) groundwaters. Lines mark the average (solid line) and one standard deviation (dashed lines) for each age group (La Salle et al., 1995).

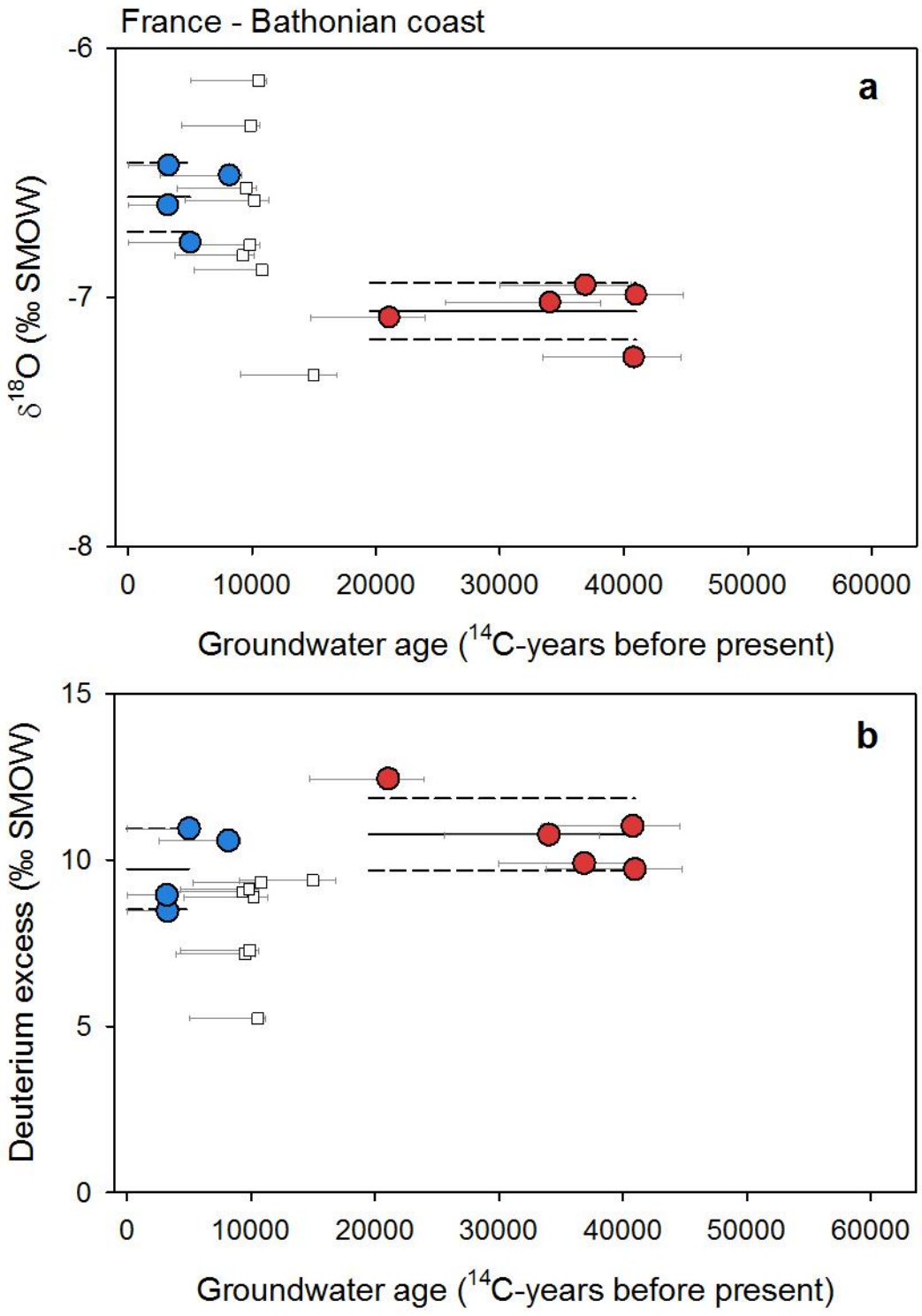

Figure S22. Groundwater isotope composition of the Bathonian coastal aquifer. Groundwater $\delta^{18}O$ (a) and deuterium excess (b) plotted against corrected ^{14}C ages for late-Holocene (blue circles) and ice age (red circles) groundwaters. Lines mark the average (solid line) and one standard deviation (dashed lines) for each age group (Barbecot et al., 2000).

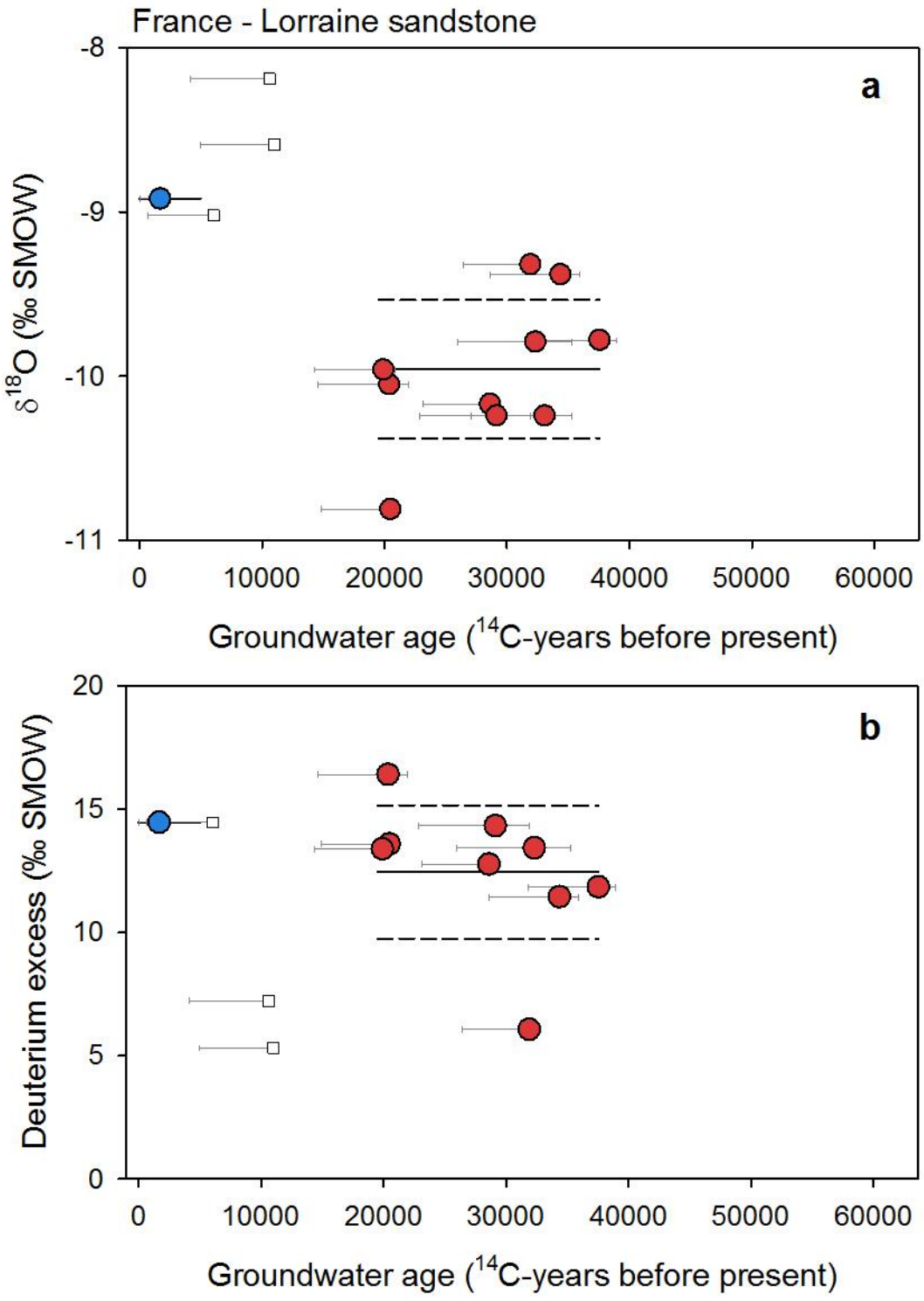

Figure S23. Groundwater isotope composition of the Lorraine sandstone aquifer. Groundwater $\delta^{18}O$ (a) and deuterium excess (b) plotted against corrected ^{14}C ages for late-Holocene (blue circles) and ice age (red circles) groundwaters. Lines mark the average (solid line) and one standard deviation (dashed lines) for each age group (Celle-Jeanton et al., 2009).

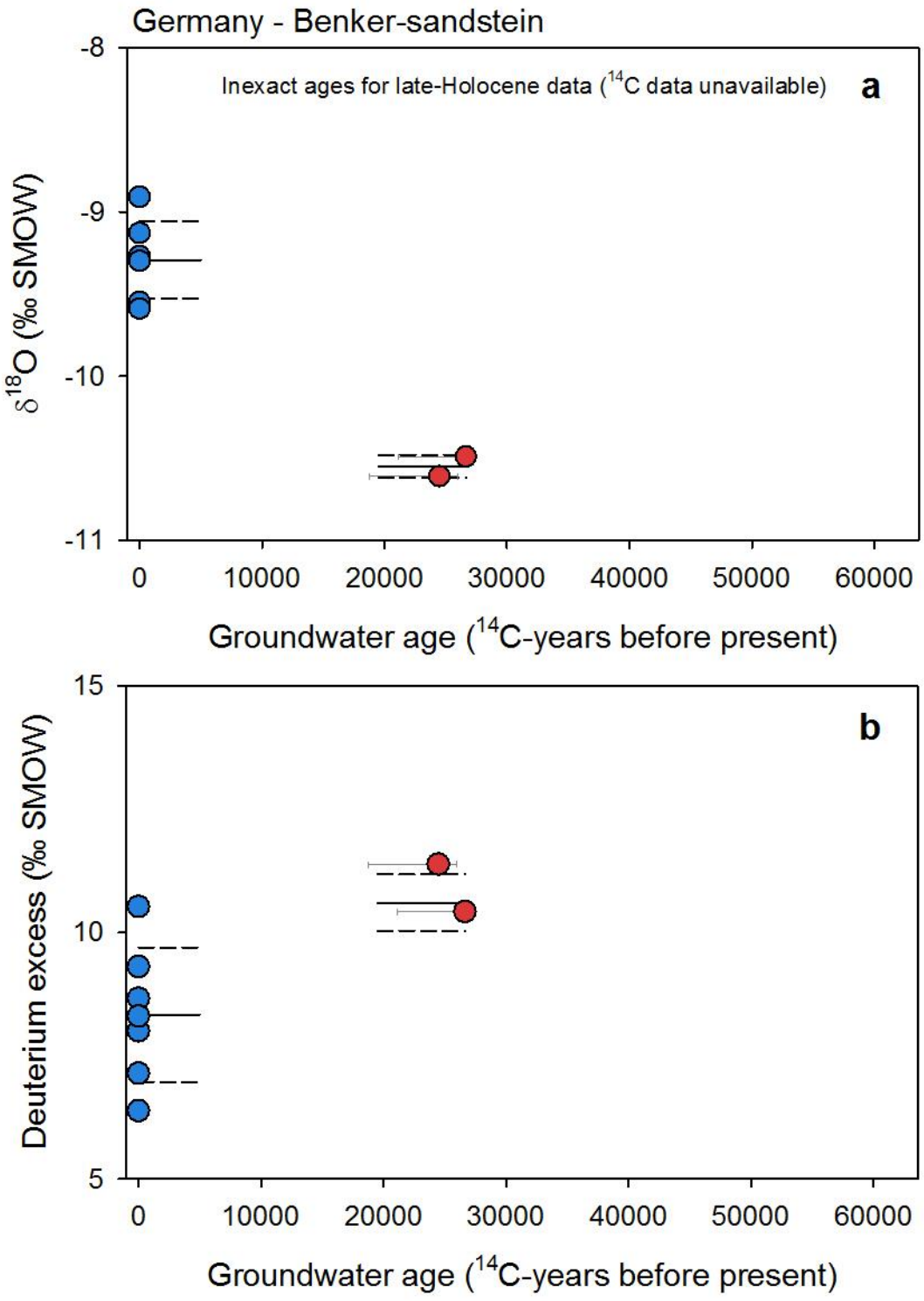

Figure S24. Groundwater isotope composition of the Benker-sandstein aquifer. Groundwater $\delta^{18}O$ (a) and deuterium excess (b) plotted against corrected ^{14}C ages for late-Holocene (blue circles) and ice age (red circles) groundwaters. Lines mark the average (solid line) and one standard deviation (dashed lines) for each age group (van Geldern et al., 2014).

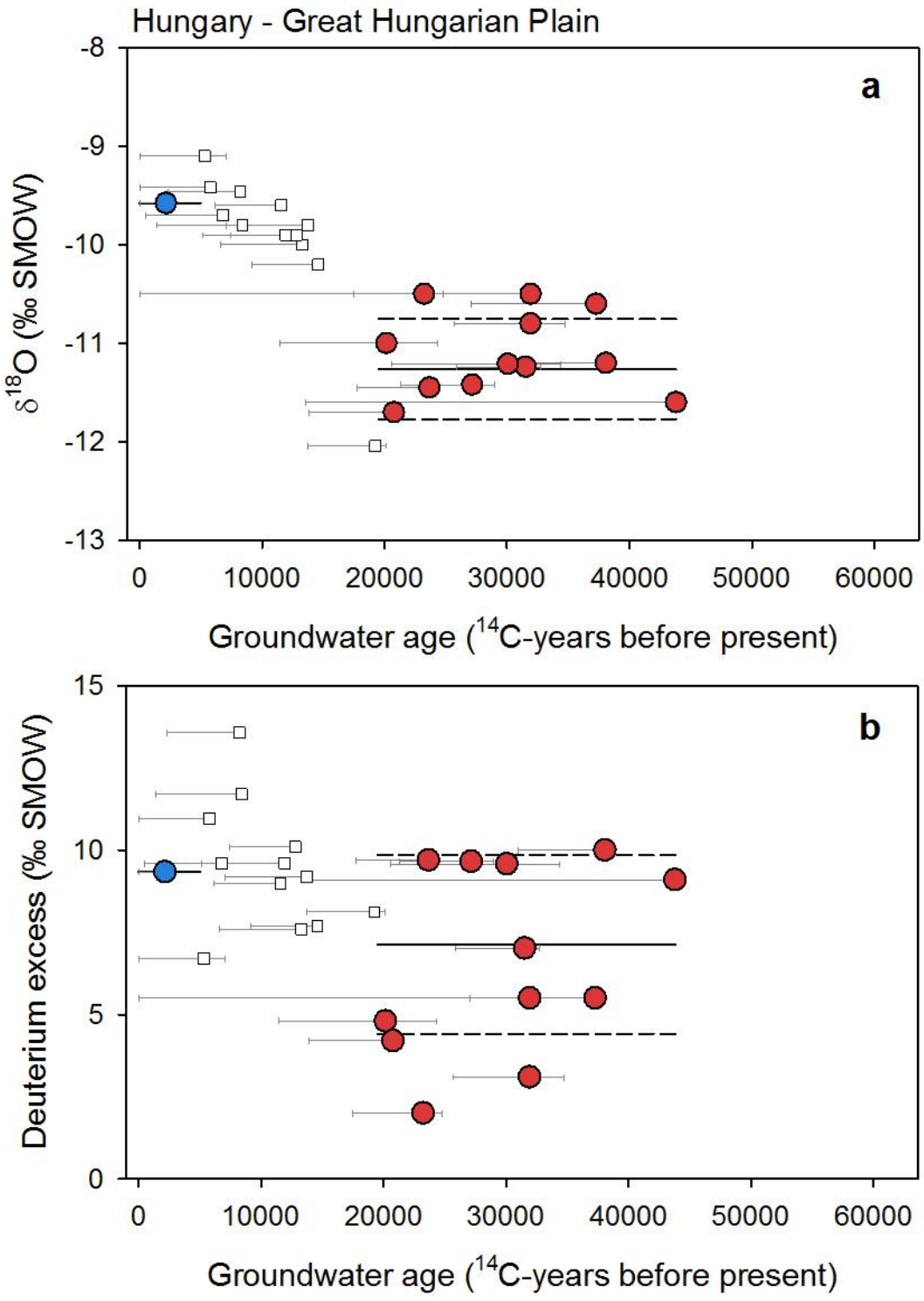

Figure S25. Groundwater isotope composition of the Great Hungarian Plain. Groundwater $\delta^{18}O$ (a) and deuterium excess (b) plotted against corrected ^{14}C ages for late-Holocene (blue circles) and ice age (red circles) groundwaters. Lines mark the average (solid line) and one standard deviation (dashed lines) for each age group (Stute and Deak, 1989).

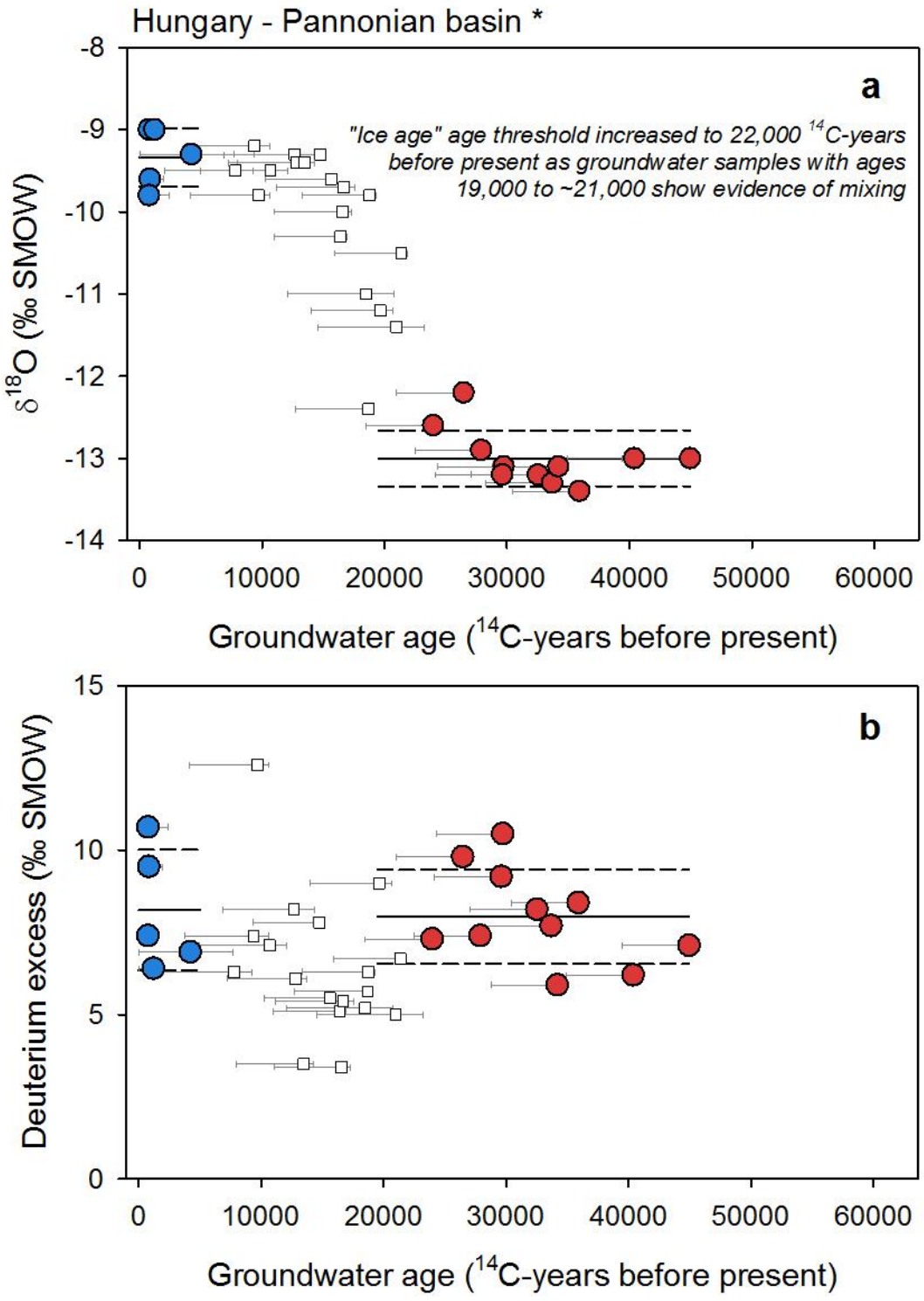

Figure S26. Groundwater isotope composition of the Pannonian basin. Groundwater $\delta^{18}O$ (a) and deuterium excess (b) plotted against corrected ^{14}C ages for late-Holocene (blue circles) and ice age (red circles) groundwaters. Lines mark the average (solid line) and one standard deviation (dashed lines) for each age group (Varsanyi et al., 2011).

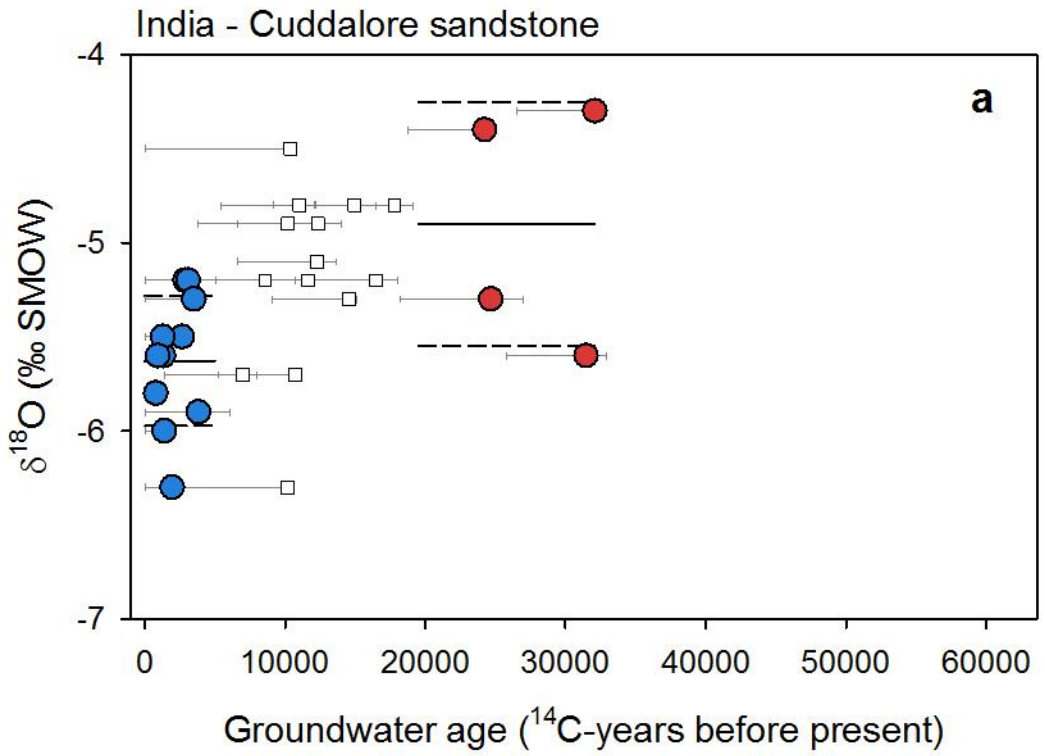

Figure S27. Groundwater isotope composition of the Cuddalore sandstone aquifer. Groundwater $\delta^{18}O$ plotted against corrected ^{14}C ages for late-Holocene (blue circles) and ice age (red circles) groundwaters. Lines mark the average (solid line) and one standard deviation (dashed lines) for each age group (Sukhija et al., 1998).

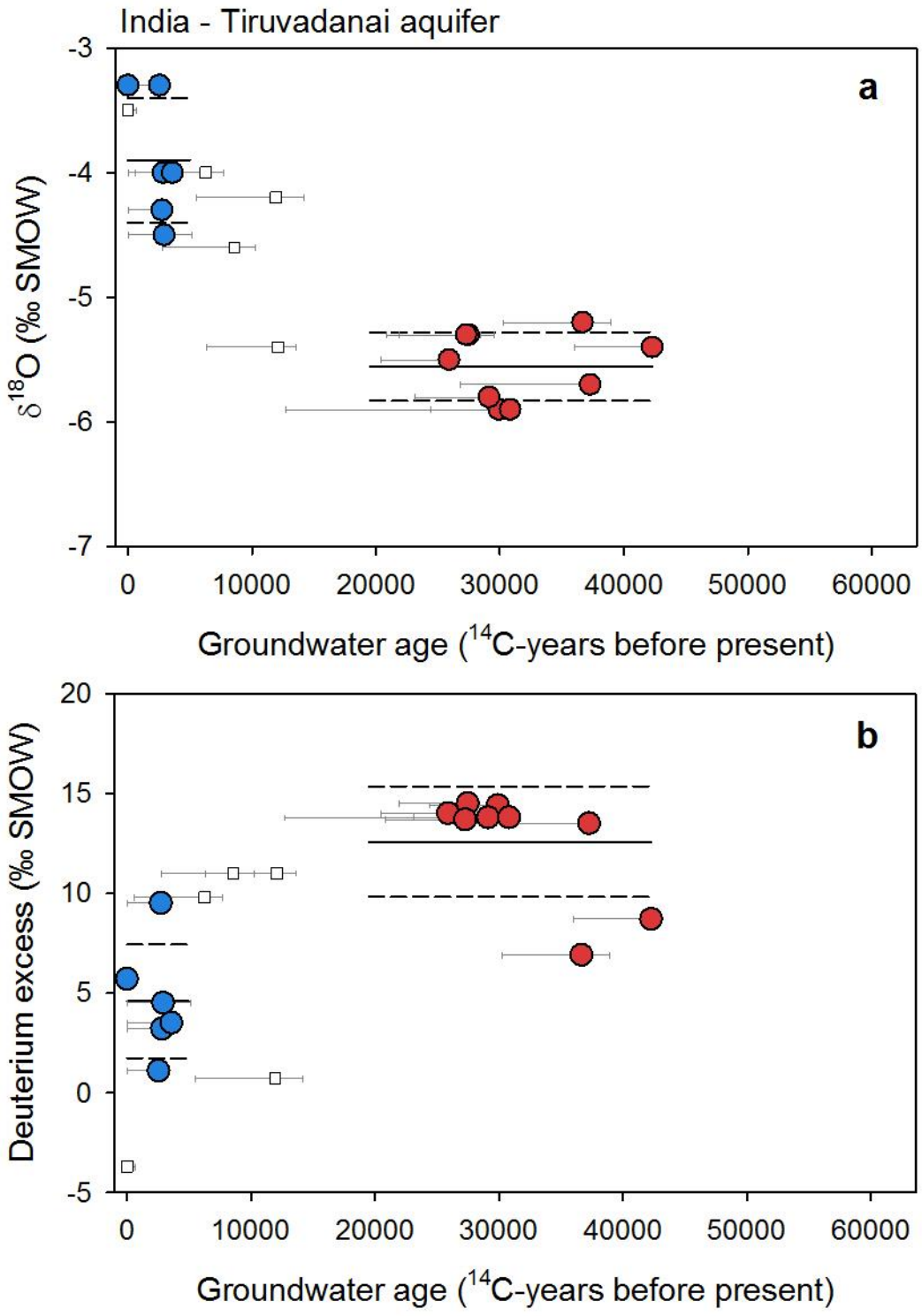

Figure S28. Groundwater isotope composition of the Tiruvadanai aquifer. Groundwater $\delta^{18}O$ (a) and deuterium excess (b) plotted against corrected ^{14}C ages for late-Holocene (blue circles) and ice age (red circles) groundwaters. Lines mark the average (solid line) and one standard deviation (dashed lines) for each age group (Kumar et al., 2009).

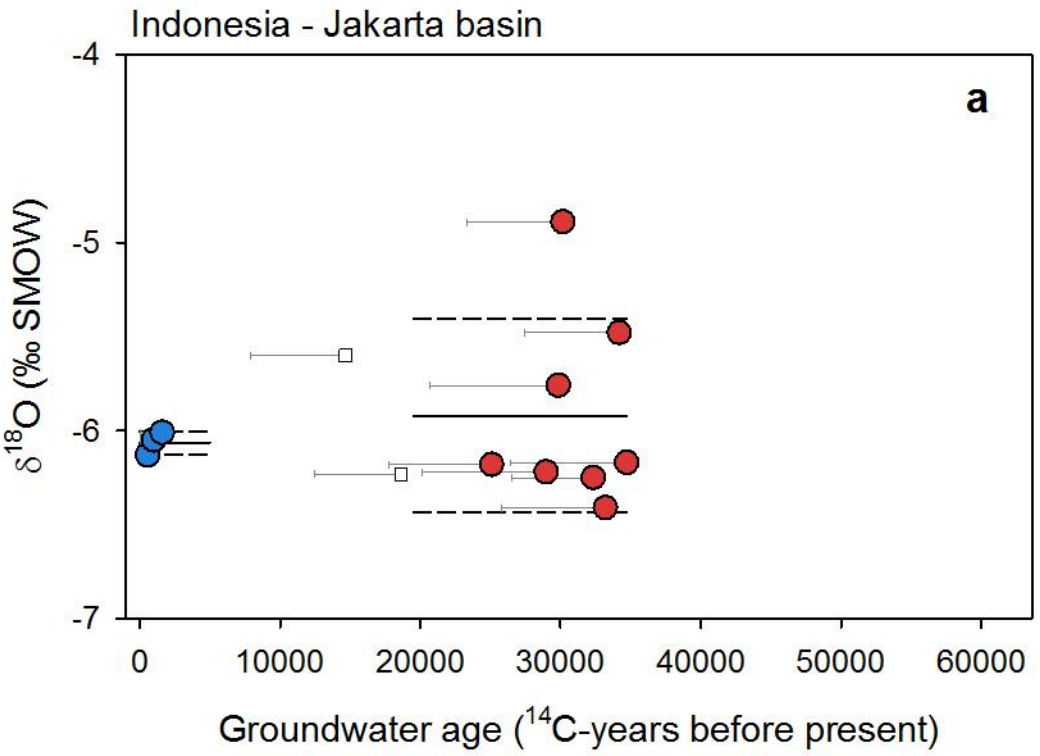

Figure S29. Groundwater isotope composition of the Jakarta aquifer. Groundwater $\delta^{18}O$ plotted against corrected ^{14}C ages for late-Holocene (blue circles) and ice age (red circles) groundwaters. Lines mark the average (solid line) and one standard deviation (dashed lines) for each age group (Geyh and Söfner, 1989).

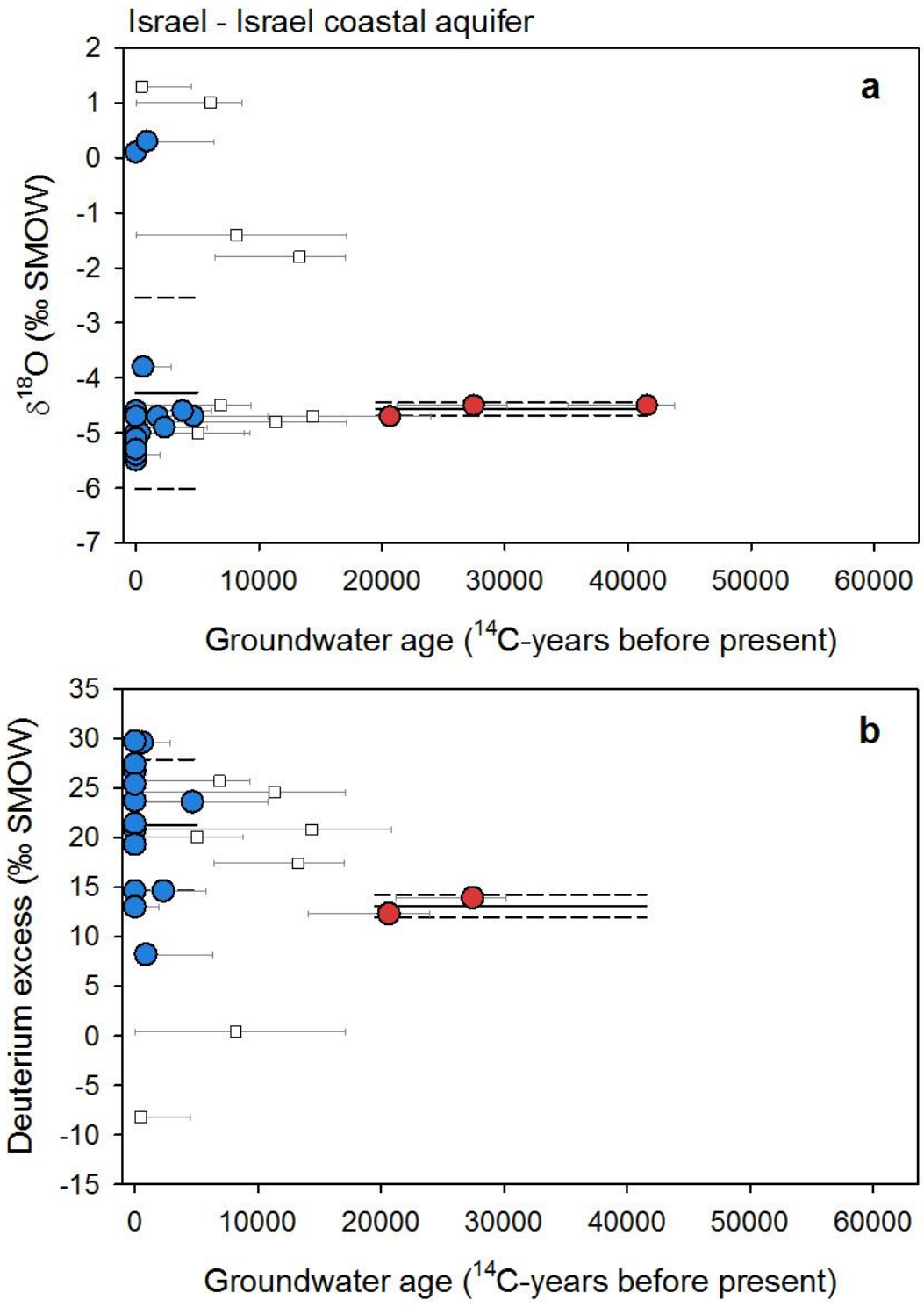

Figure S30. Groundwater isotope composition of the Israel coastal aquifer. Groundwater $\delta^{18}O$ (a) and deuterium excess (b) plotted against corrected ^{14}C ages for late-Holocene (blue circles) and ice age (red circles) groundwaters. Lines mark the average (solid line) and one standard deviation (dashed lines) for each age group (Yechieli et al., 2008).

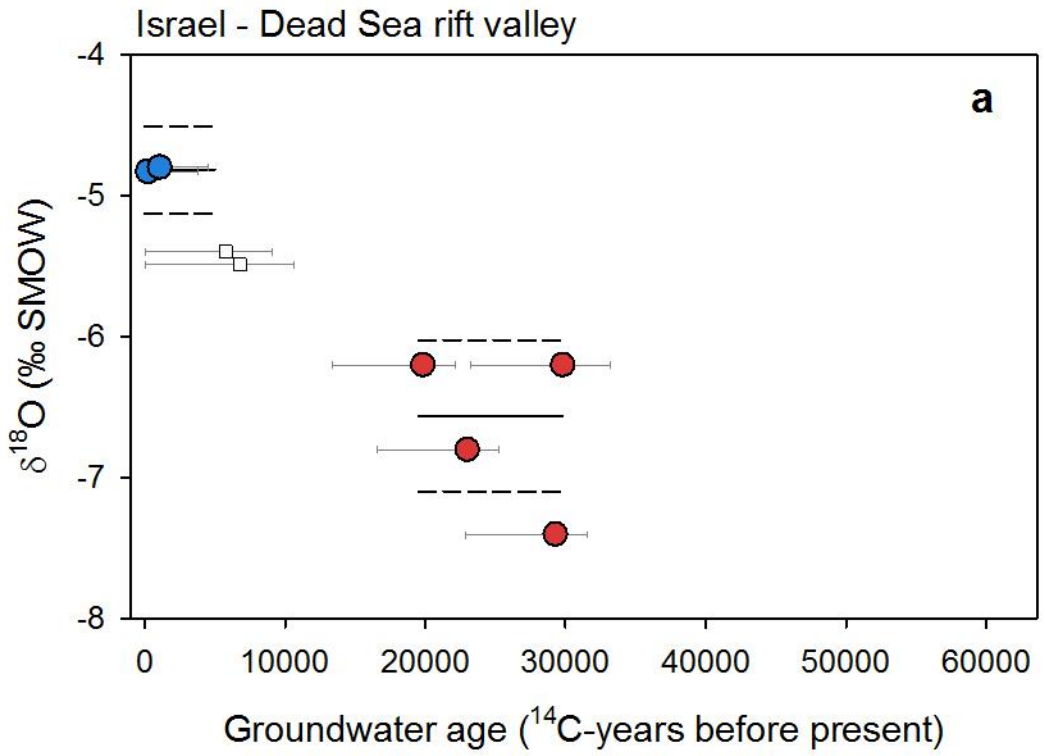

Figure S31. Groundwater isotope composition of the Dead Sea Rift aquifer. Groundwater $\delta^{18}O$ plotted against corrected ^{14}C ages for late-Holocene (blue circles) and ice age (red circles) groundwaters. Lines mark the average (solid line) and one standard deviation (dashed lines) for each age group (Gat and Galai, 1982; Mazor et al., 1995).

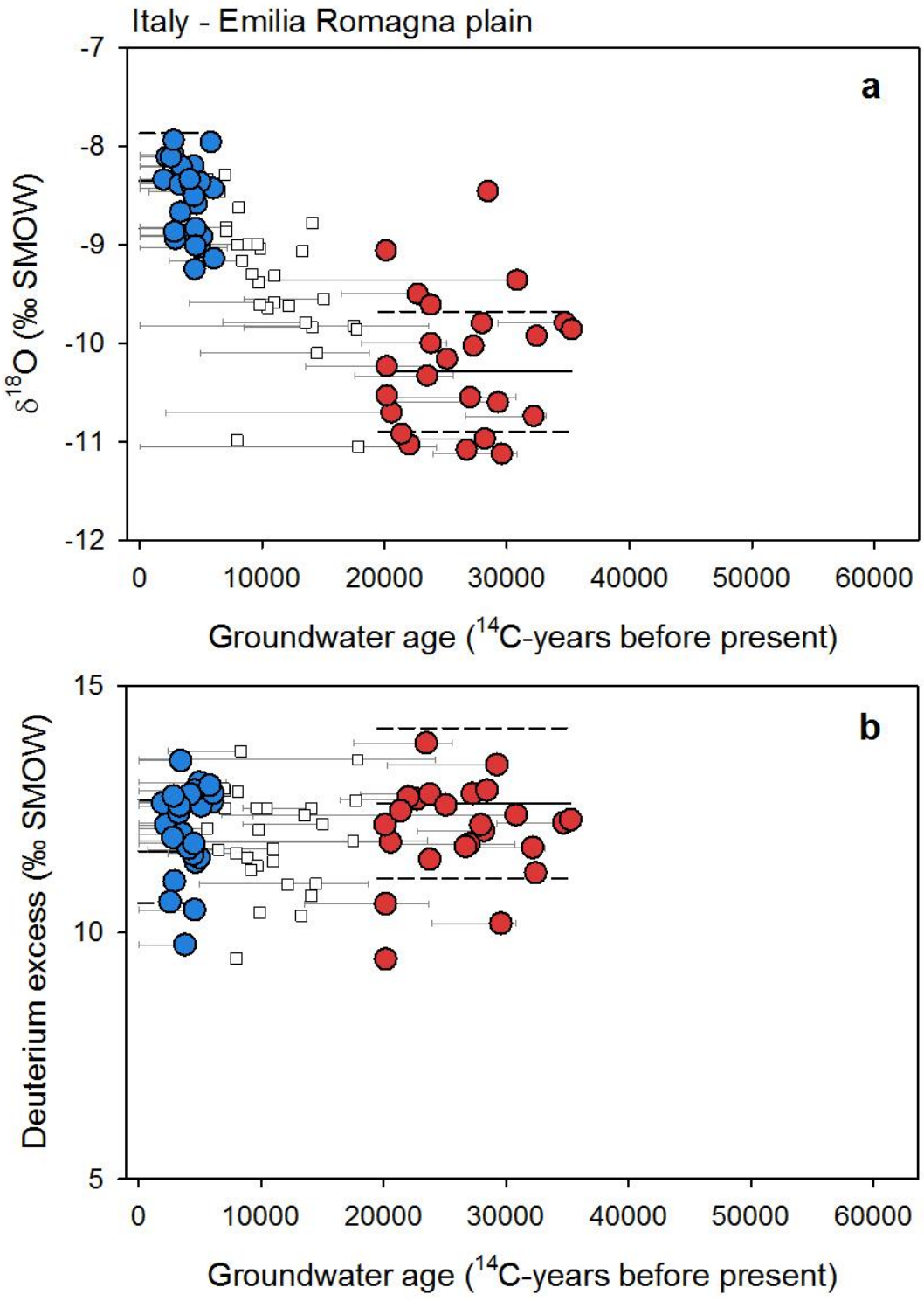

Figure S32. Groundwater isotope composition of the Emilia Romagna Plain. Groundwater $\delta^{18}O$ (a) and deuterium excess (b) plotted against corrected ^{14}C ages for late-Holocene (blue circles) and ice age (red circles) groundwaters. Lines mark the average (solid line) and one standard deviation (dashed lines) for each age group (Martinelli et al., 2011).

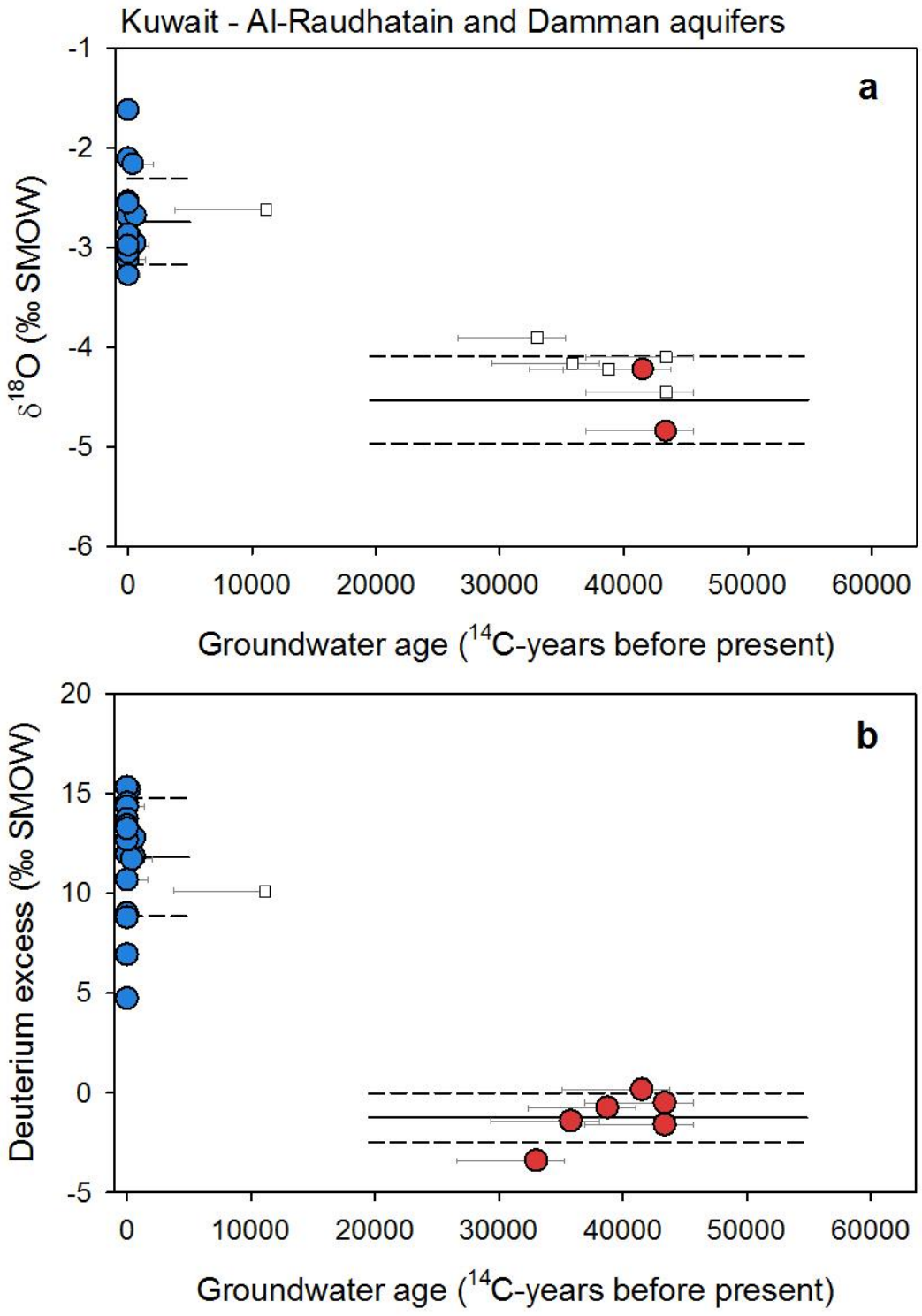

Figure S33. Groundwater isotope composition of the Al-Raudhatain and Damman aquifer. Groundwater $\delta^{18}O$ (a) and deuterium excess (b) plotted against corrected ^{14}C ages for late-Holocene (blue circles) and ice age (red circles) groundwaters. The average (solid line) and 1 s.d. (dashed lines) are shown for each group (Al-Ruwaih and Shehata, 2004; Fadlelmawla et al., 2008).

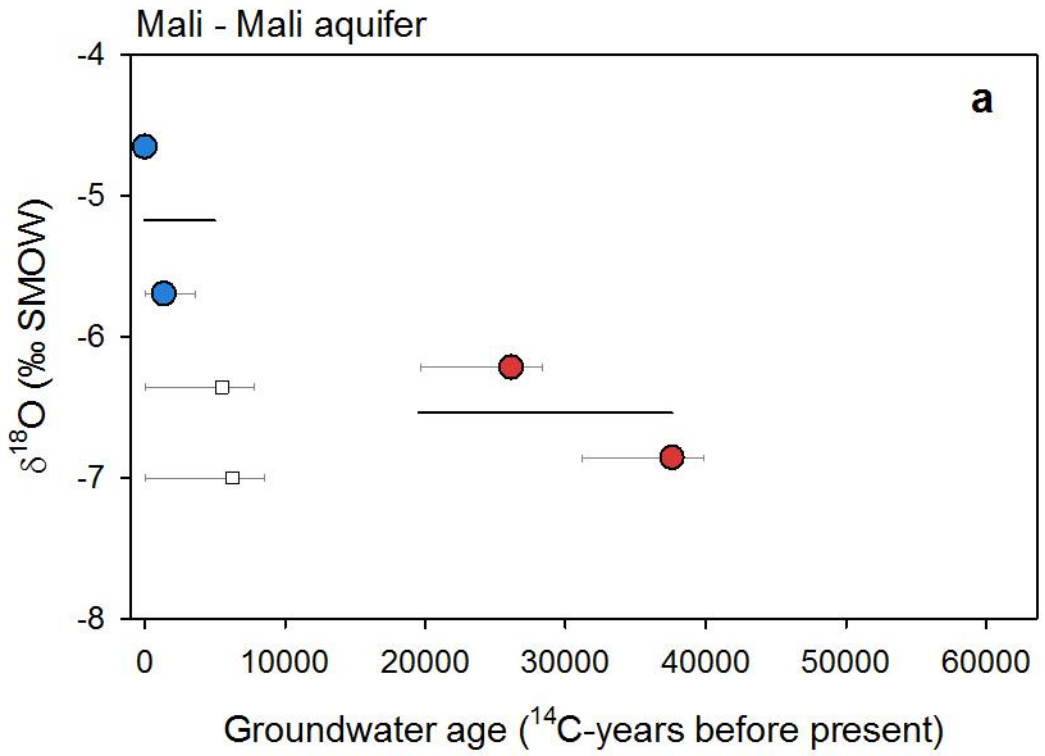

Figure S34. Groundwater isotope composition of the Mali aquifer. Groundwater $\delta^{18}O$ plotted against corrected ^{14}C ages for late-Holocene (blue circles) and ice age (red circles) groundwaters. Lines mark the average (solid line) and one standard deviation (dashed lines) for each age group (Edmunds, 2009).

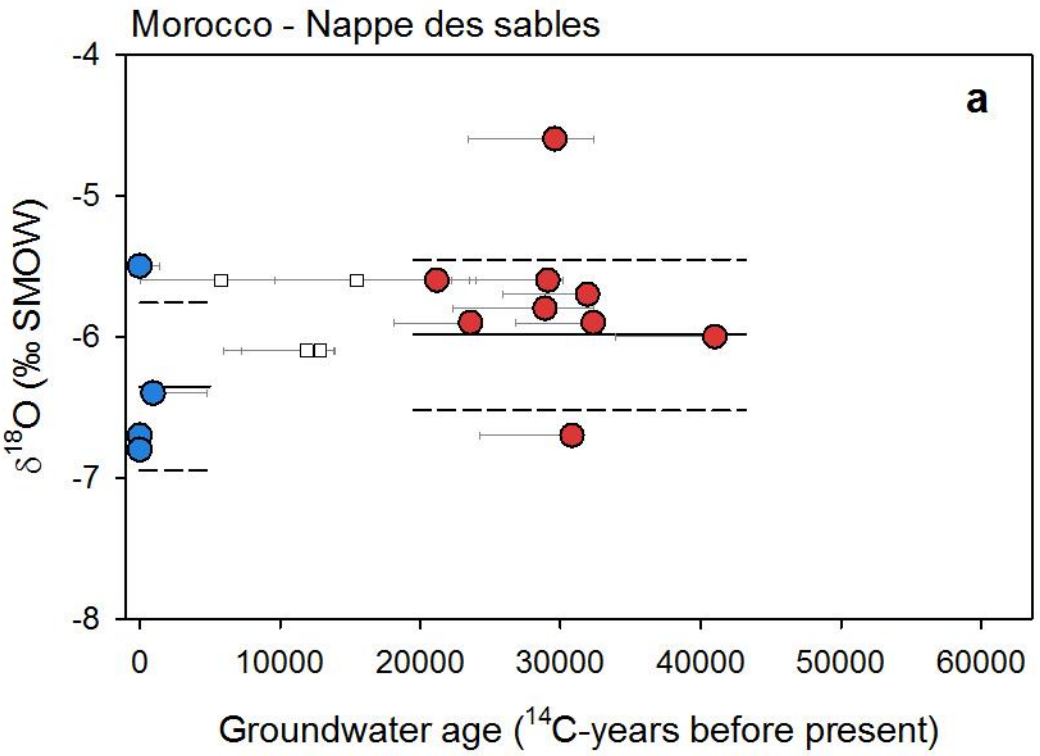

Figure S35. Groundwater isotope composition of the Nappe des sables. Groundwater $\delta^{18}O$ plotted against corrected ^{14}C ages for late-Holocene (blue circles) and ice age (red circles) groundwaters. Lines mark the average (solid line) and one standard deviation (dashed lines) for each age group (Bouchaou et al., 2009).

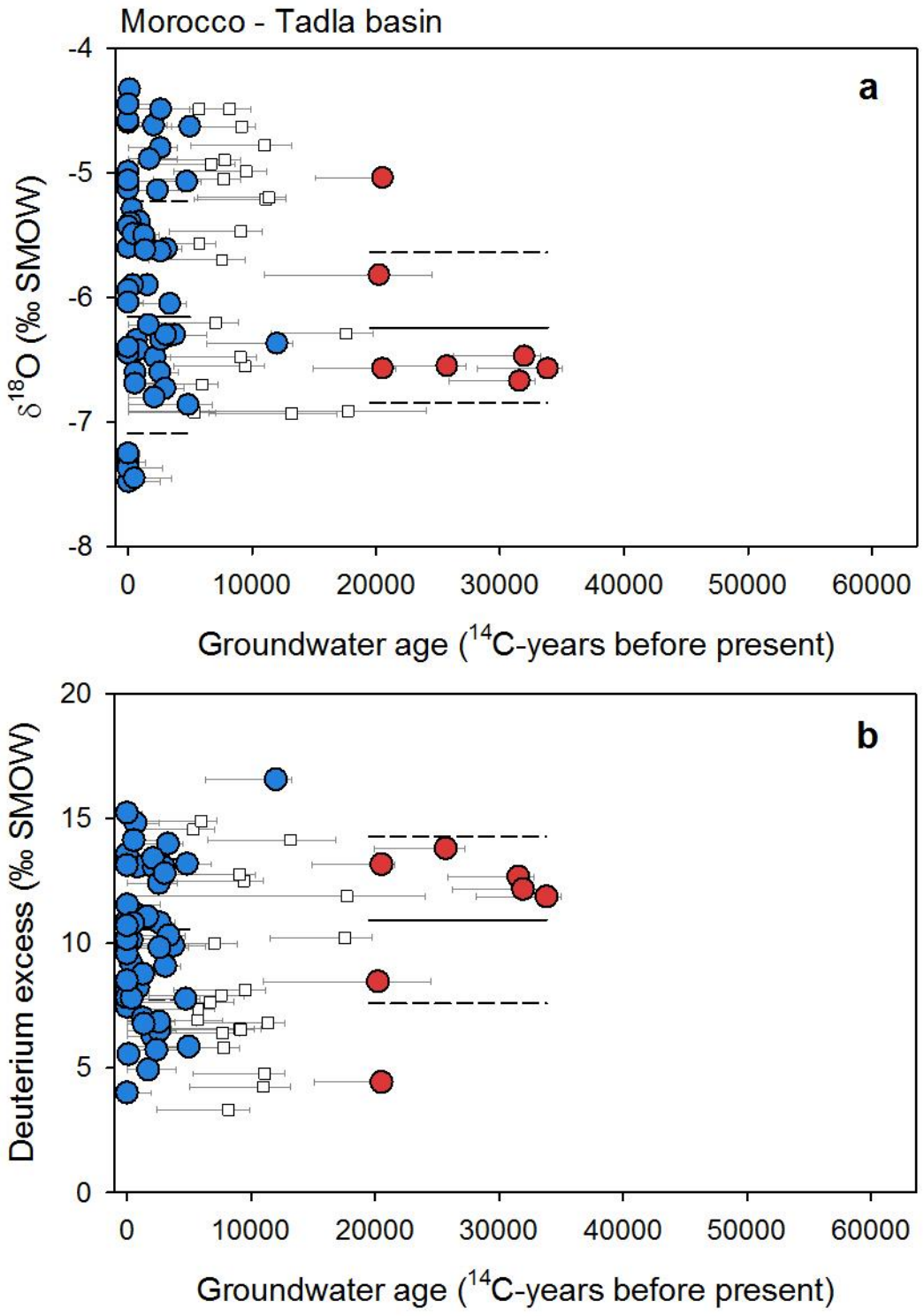

Figure S36. Groundwater isotope composition of the Tadla basin. Groundwater $\delta^{18}O$ (a) and deuterium excess (b) plotted against corrected ^{14}C ages for late-Holocene (blue circles) and ice age (red circles) groundwaters. Lines mark the average (solid line) and one standard deviation (dashed lines) for each age group (Castany et al., 1974).

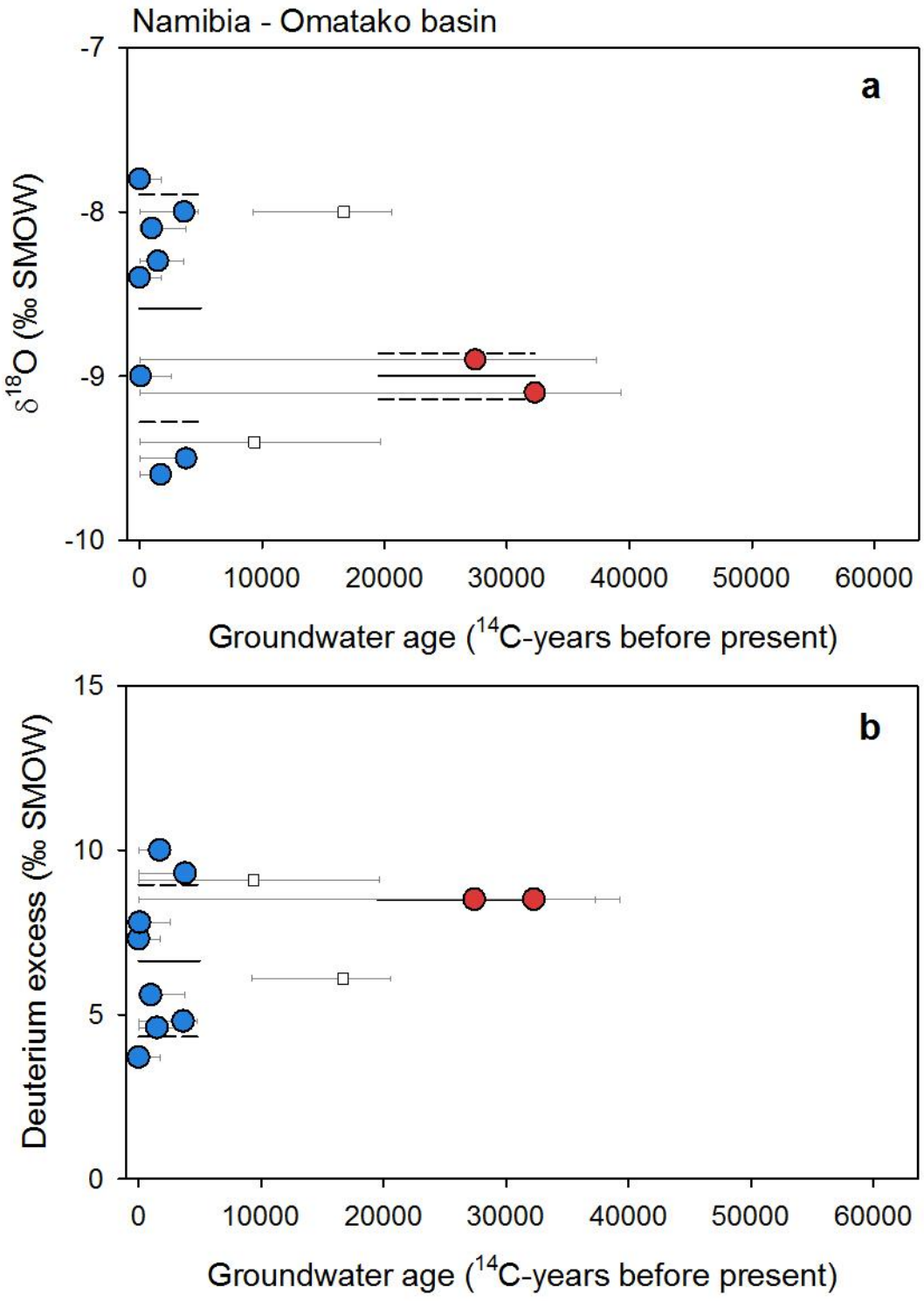

Figure S37. Groundwater isotope composition of the Omatako basin. Groundwater $\delta^{18}O$ (a) and deuterium excess (b) plotted against corrected ^{14}C ages for late-Holocene (blue circles) and ice age (red circles) groundwaters. Lines mark the average (solid line) and one standard deviation (dashed lines) for each age group (Külls, 2000).

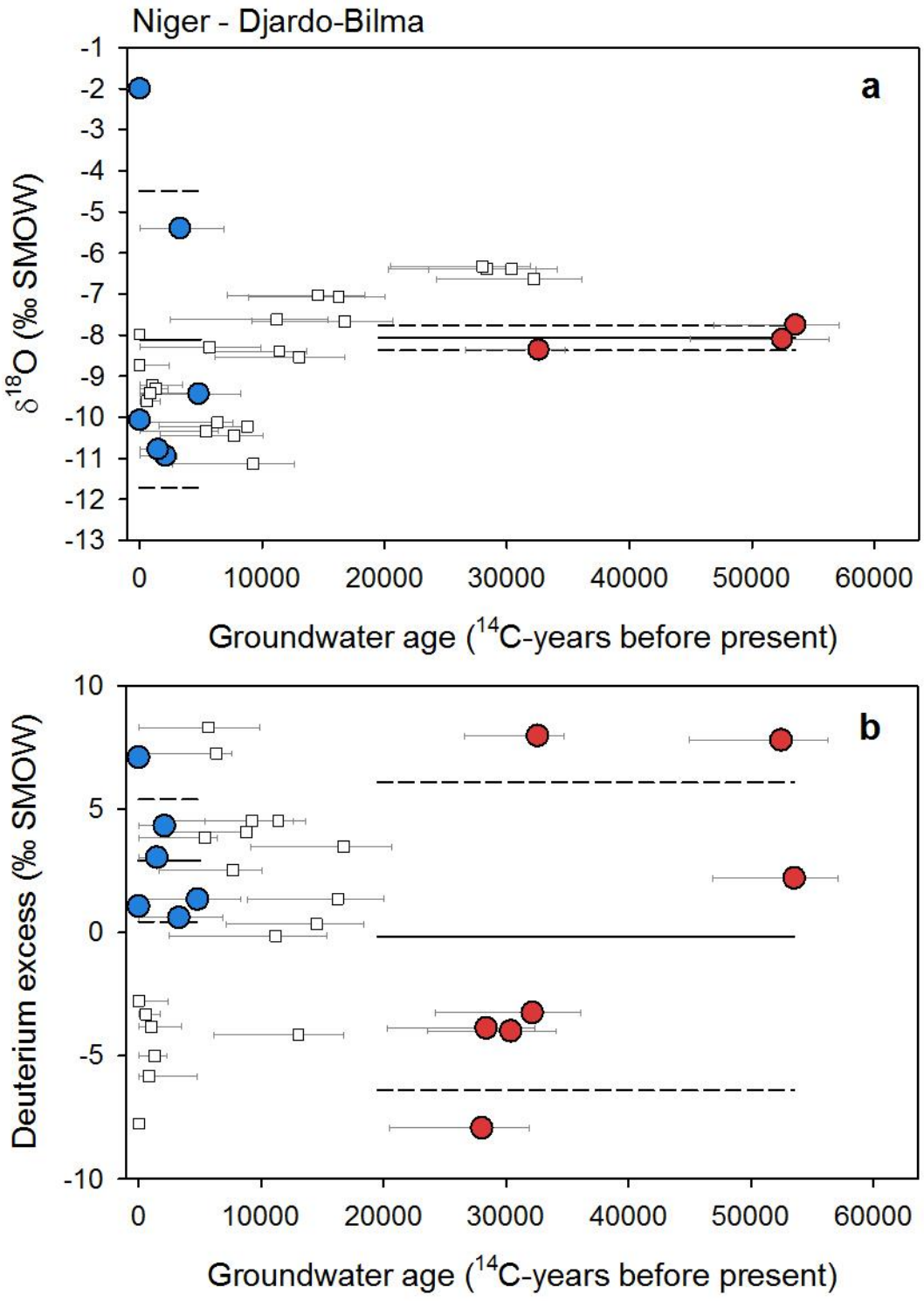

Figure S38. Groundwater isotope composition of the Djardo-Bilma basin. Groundwater $\delta^{18}O$ (a) and deuterium excess (b) plotted against corrected ^{14}C ages for late-Holocene (blue circles) and ice age (red circles) groundwaters. Lines mark the average (solid line) and one standard deviation (dashed lines) for each age group (Dodo and Zuppi, 1997; 1999).

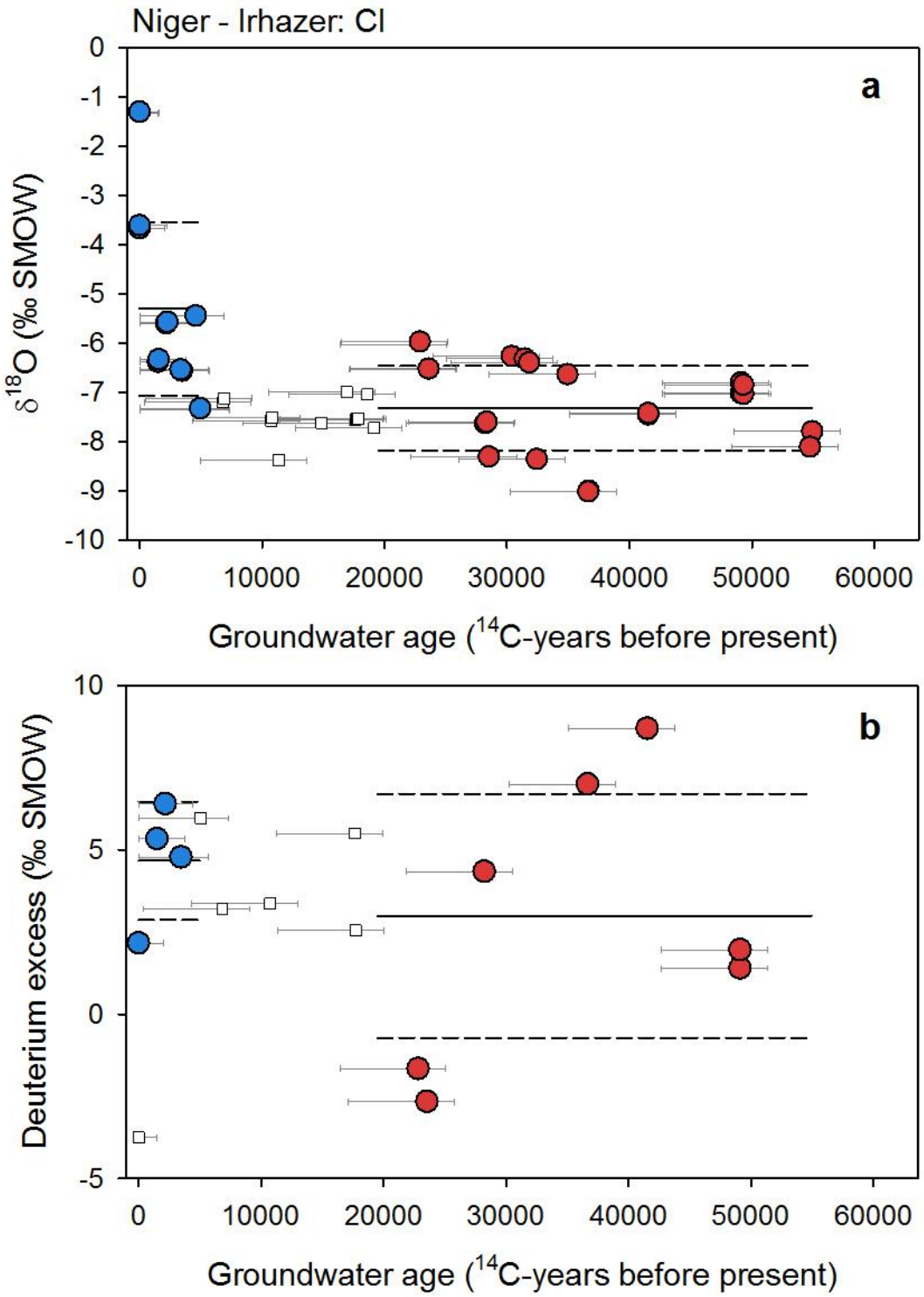

Figure S39. Groundwater isotope composition of the Irhazer aquifer (Continental Intercalaire). Groundwater $\delta^{18}O$ (a) and deuterium excess (b) plotted against corrected ^{14}C ages for late-Holocene (blue circles) and ice age (red circles) groundwaters. Lines mark the average (solid line) and one standard deviation (dashed lines) for each age group (Andrews et al., 1994; Edmunds, 2005).

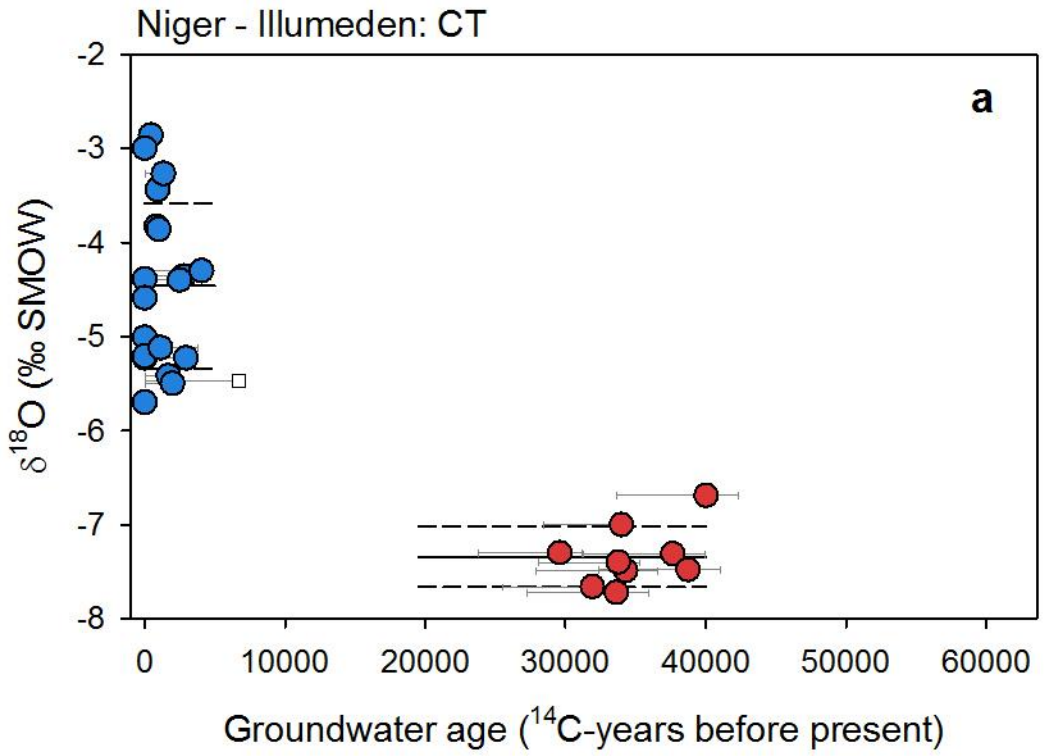

Figure S40. Groundwater isotope composition of the Illumeden aquifer (Continental Terminal). Groundwater $\delta^{18}O$ plotted against corrected ^{14}C ages for late-Holocene (blue circles) and ice age (red circles) groundwaters. Lines mark the average (solid line) and one standard deviation (dashed lines) for each age group (Le Gal La Salle et al., 2001; Beyerle et al., 2003).

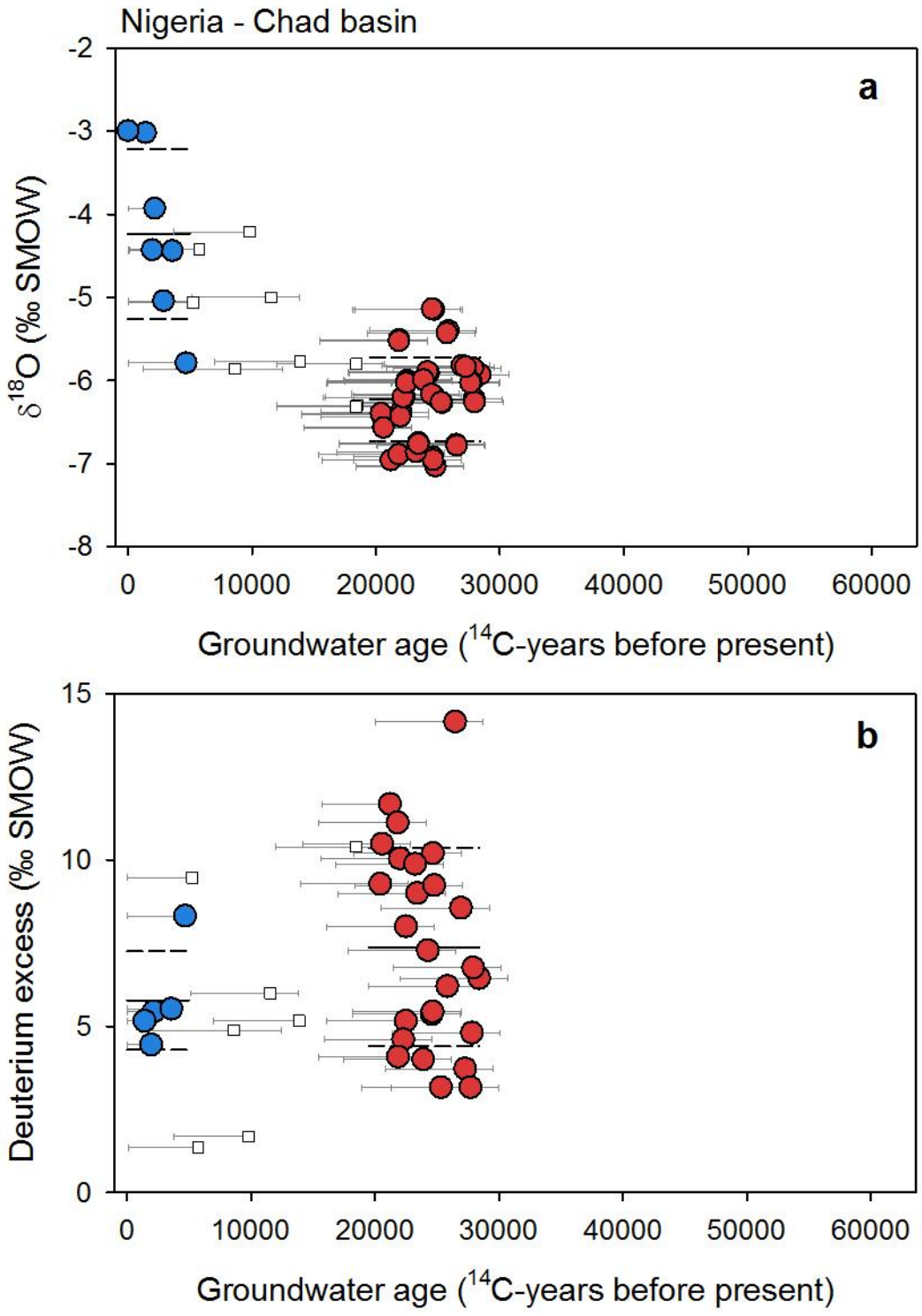

Figure S41. Groundwater isotope composition of the Chad aquifer (in Nigeria). Groundwater $\delta^{18}O$ (a) and deuterium excess (b) plotted against corrected ^{14}C ages for late-Holocene (blue circles) and ice age (red circles) groundwaters. Lines mark the average (solid line) and one standard deviation (dashed lines) for each age group (Maduabuchi et al., 2006).

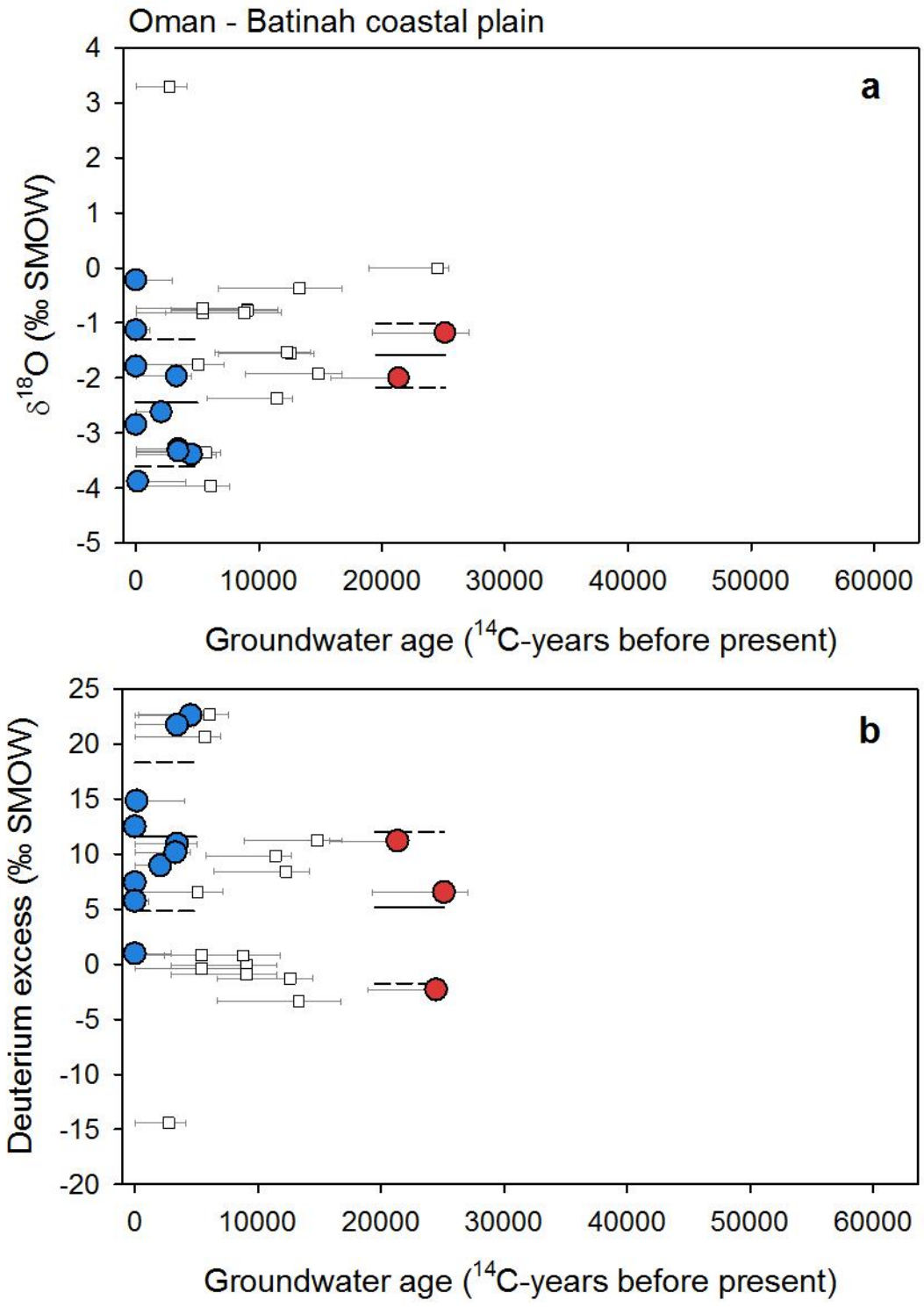

Figure S42. Groundwater isotope composition of the Batinah coastal aquifer system. Groundwater $\delta^{18}O$ (a) and deuterium excess (b) plotted against corrected ^{14}C ages for late-Holocene (blue circles) and ice age (red circles) groundwaters. Lines mark the average (solid line) and one standard deviation (dashed lines) for each age group (Weyhenmeyer et al., 2000; 2002).

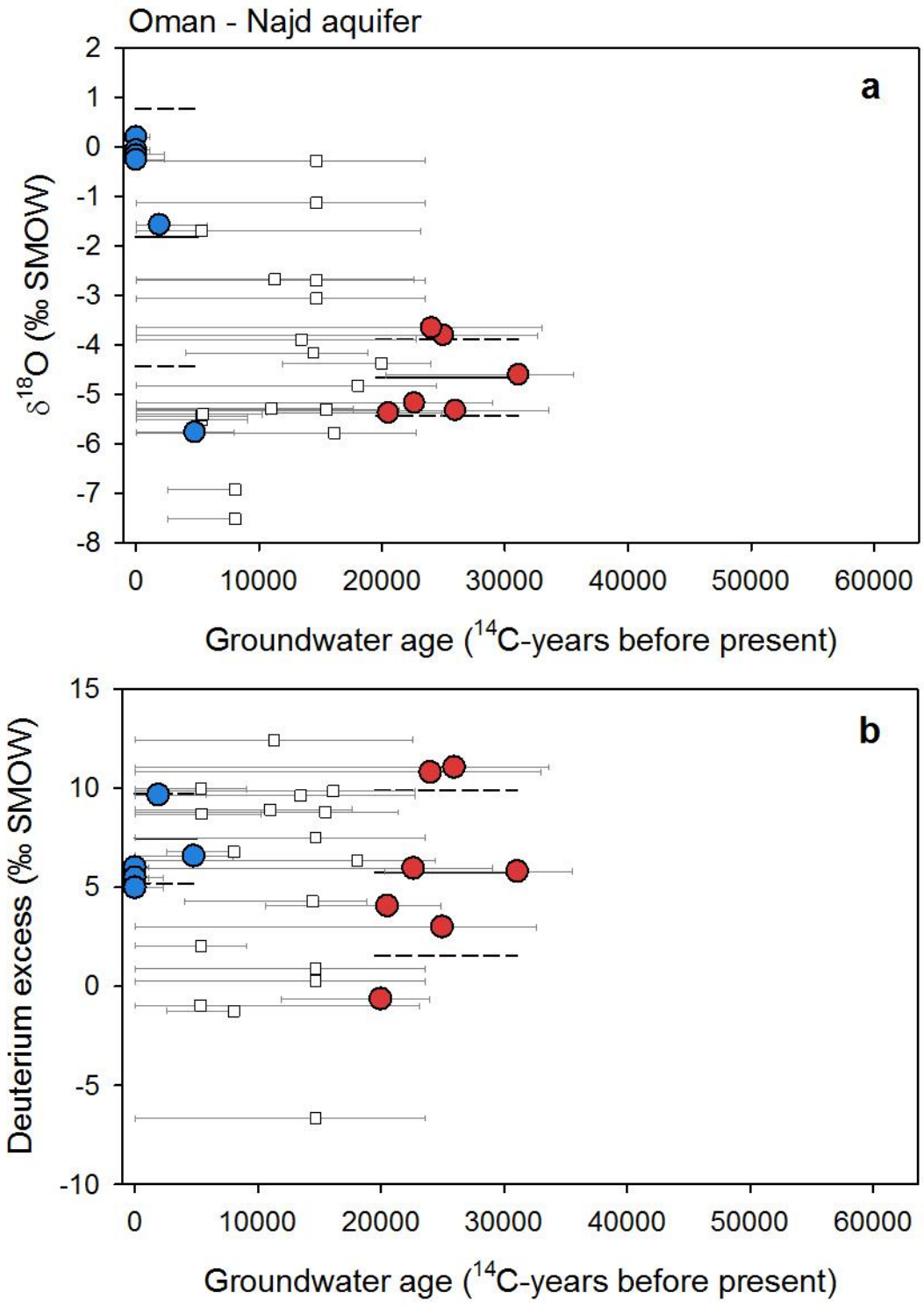

Figure S43. Groundwater isotope composition of the Najd aquifer. Groundwater $\delta^{18}O$ (a) and deuterium excess (b) plotted against corrected ^{14}C ages for late-Holocene (blue circles) and ice age (red circles) groundwaters. Lines mark the average (solid line) and one standard deviation (dashed lines) for each age group (Clark et al., 1987; Al-Mashaikhi et al., 2012).

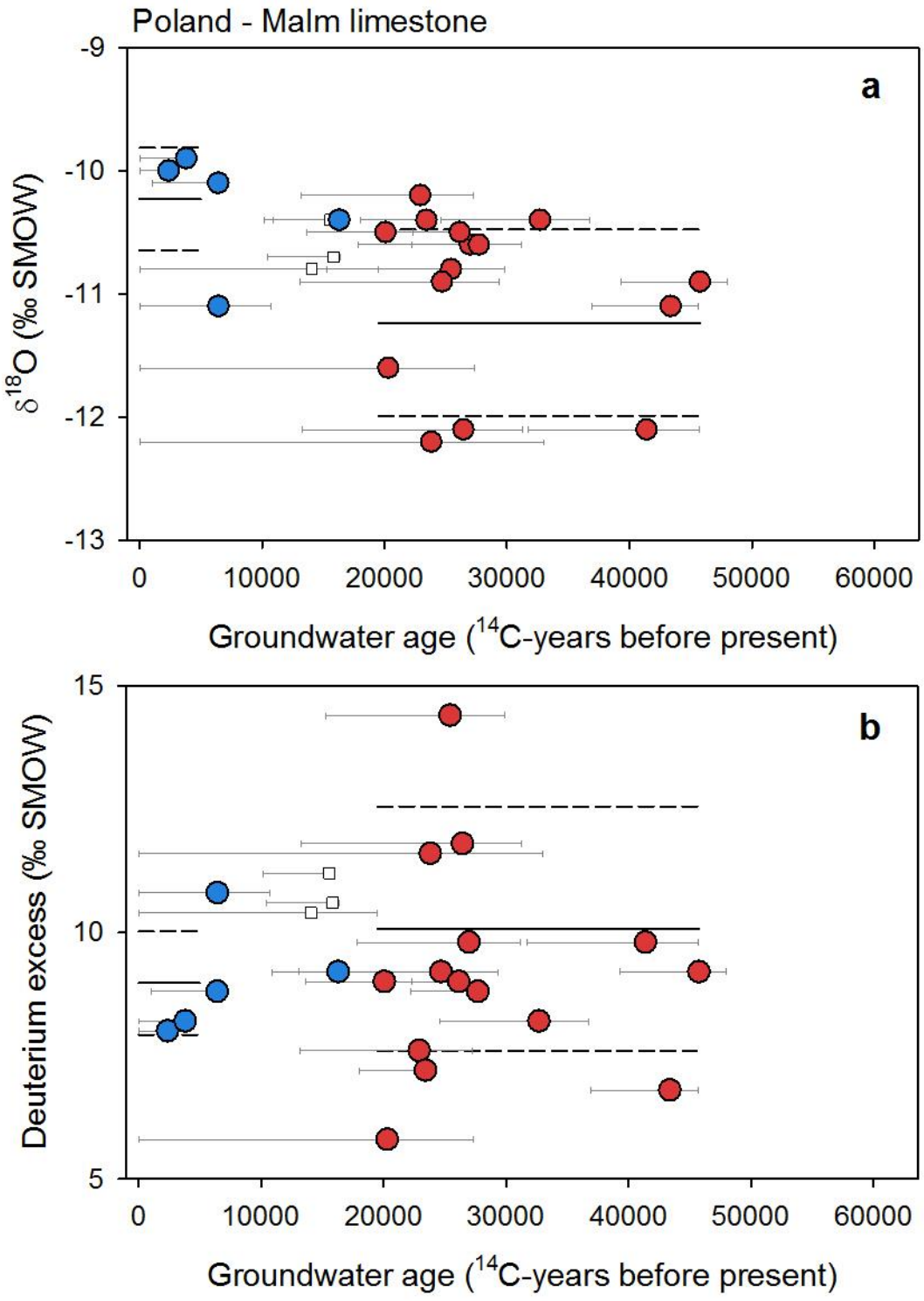

Figure S44. Groundwater isotope composition of the Malm limestone aquifer. Groundwater $\delta^{18}O$ (a) and deuterium excess (b) plotted against corrected ^{14}C ages for late-Holocene (blue circles) and ice age (red circles) groundwaters. Lines mark the average (solid line) and one standard deviation (dashed lines) for each age group (Zuber et al., 2004).

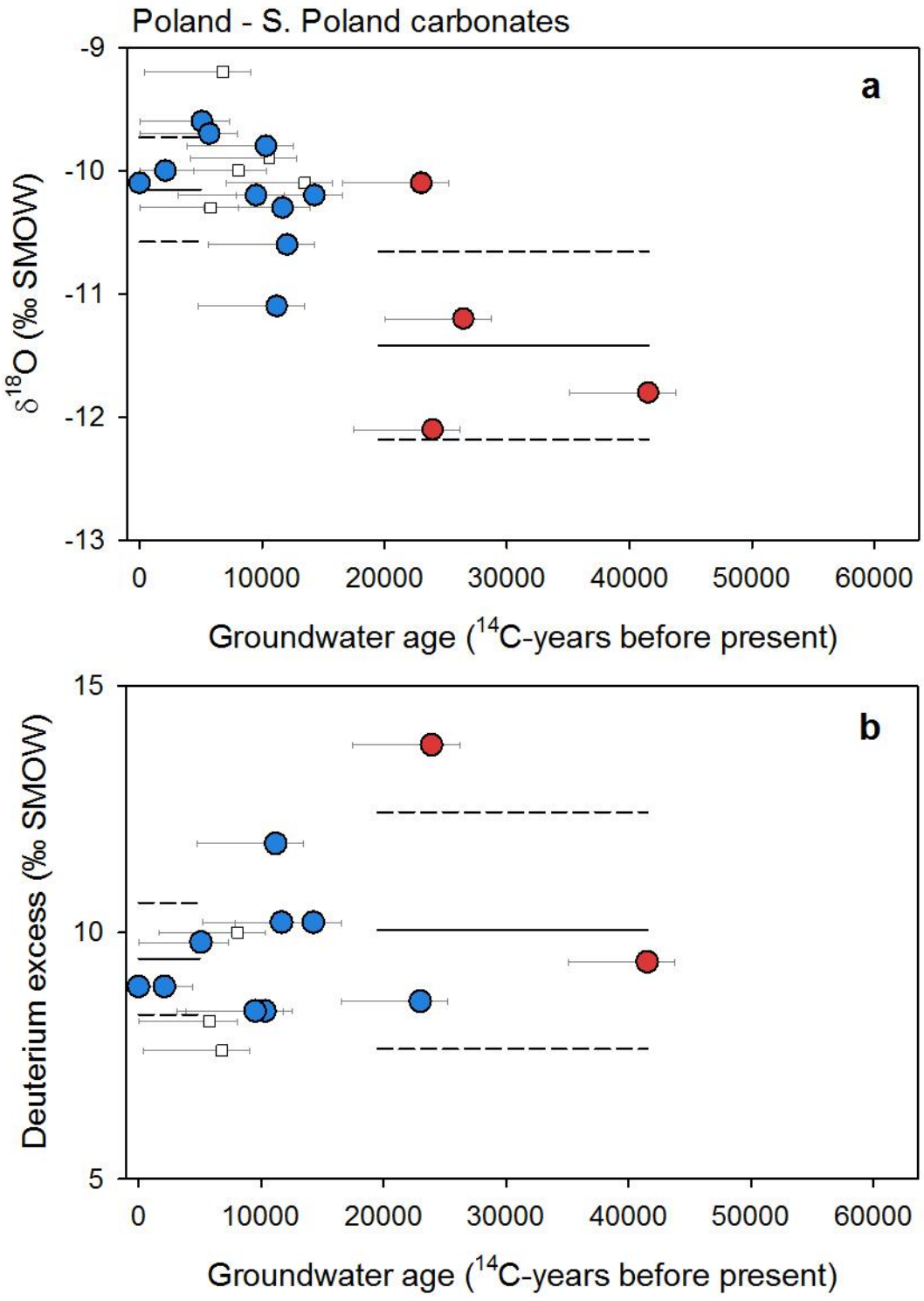

Figure S45. Groundwater isotope composition of the carbonate aquifer system of southern Poland. Groundwater $\delta^{18}O$ (a) and deuterium excess (b) plotted against corrected ^{14}C ages for late-Holocene (blue circles) and ice age (red circles) groundwaters. Lines mark the average (solid line) and one standard deviation (dashed lines) for each age group (Samborska et al., 2012).

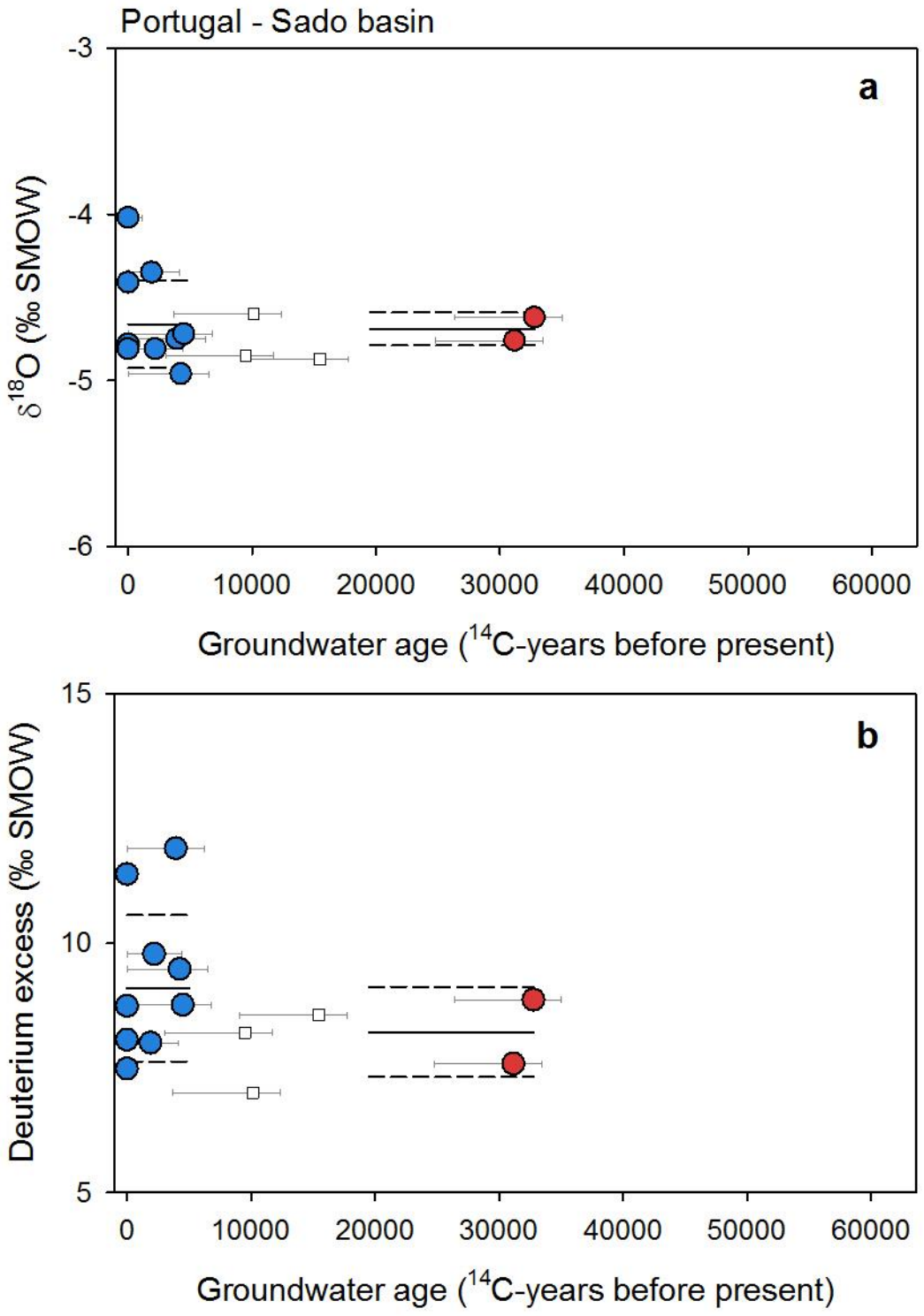

Figure S46. Groundwater isotope composition of the Sado basin. Groundwater $\delta^{18}O$ (a) and deuterium excess (b) plotted against corrected ^{14}C ages for late-Holocene (blue circles) and ice age (red circles) groundwaters. Lines mark the average (solid line) and one standard deviation (dashed lines) for each age group (Galego Fernandes and Carreira, 2008).

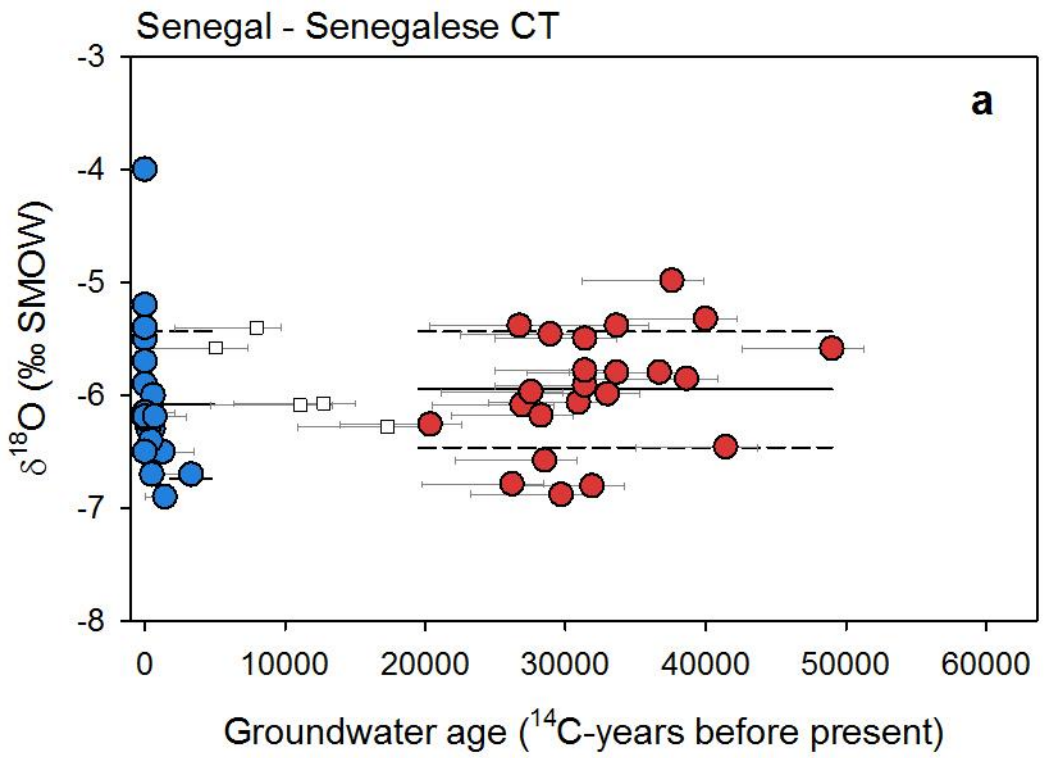

Figure S47. Groundwater isotope composition of the Senegalese Continental Terminal aquifer. Groundwater $\delta^{18}O$ plotted against corrected ^{14}C ages for late-Holocene (blue circles) and ice age (red circles) groundwaters. Lines mark the average (solid line) and one standard deviation (dashed lines) for each age group (Castany et al., 1974; Edmunds, 2009).

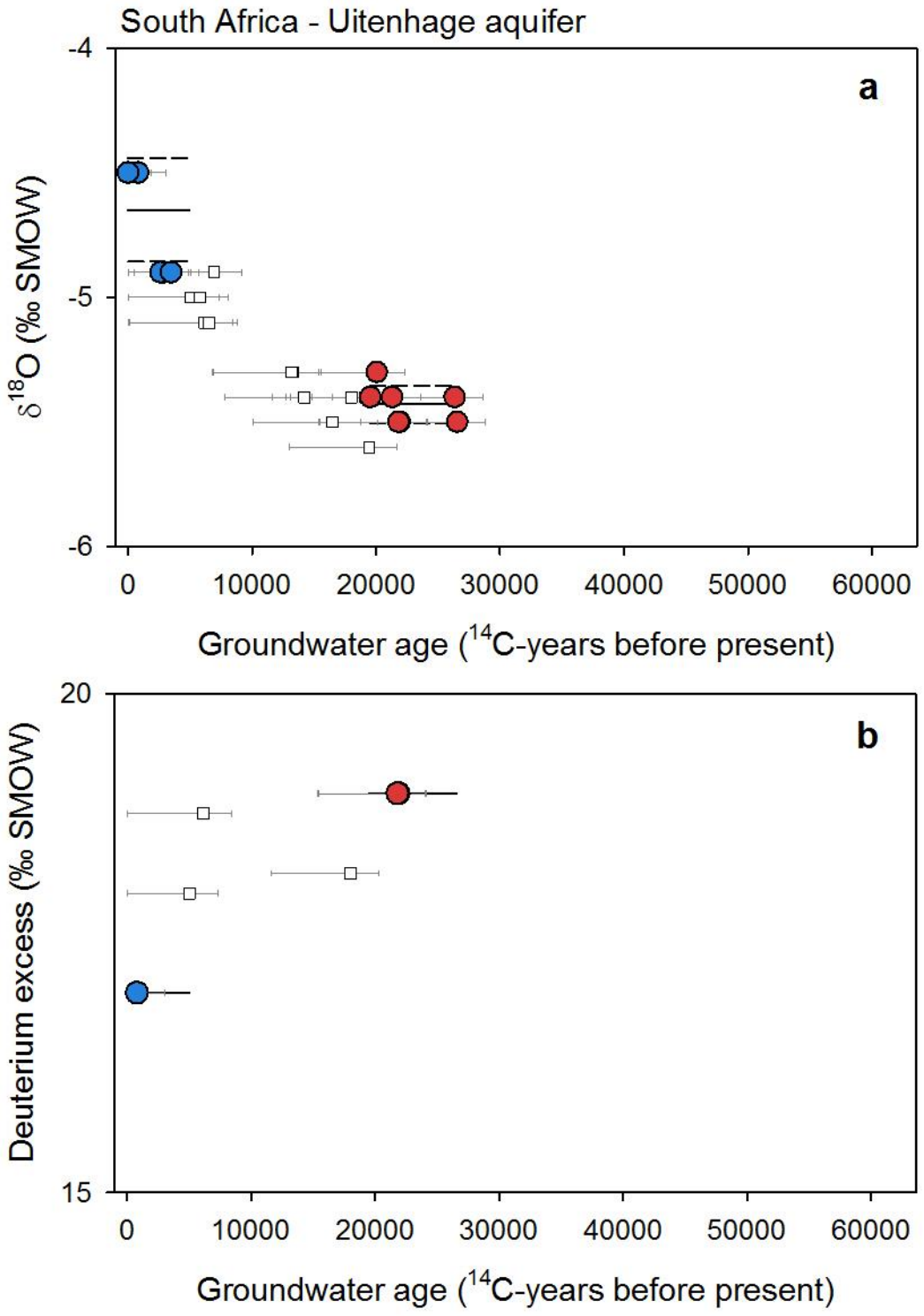

Figure S48. Groundwater isotope composition of the Uitenhage aquifer. Groundwater $\delta^{18}O$ (a) and deuterium excess (b) plotted against corrected ^{14}C ages for late-Holocene (blue circles) and ice age (red circles) groundwaters. Lines mark the average (solid line) and one standard deviation (dashed lines) for each age group (Heaton et al., 1986).

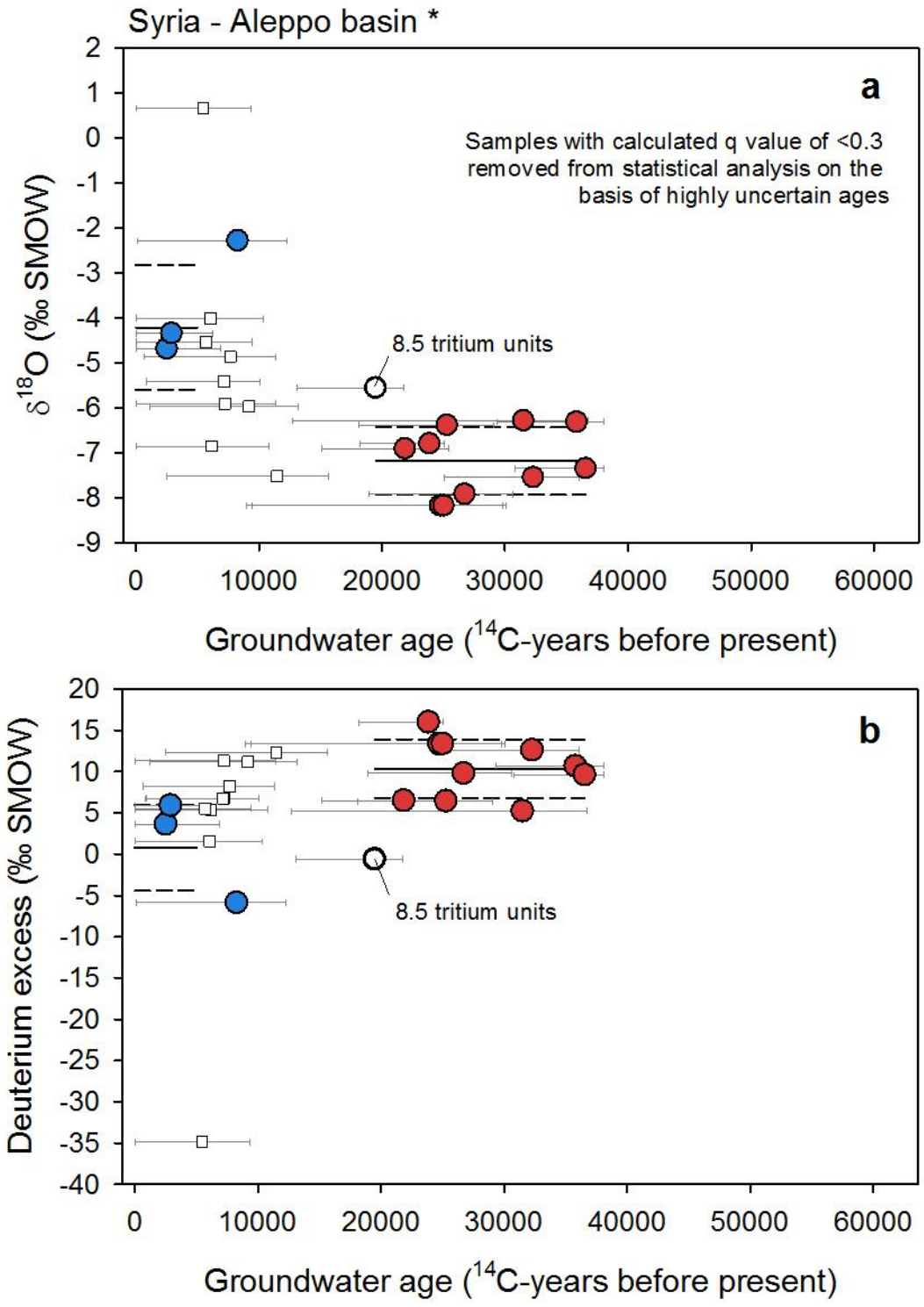

Figure S49. Groundwater isotope composition of the Aleppo basin. Groundwater $\delta^{18}O$ (a) and deuterium excess (b) plotted against corrected ^{14}C ages for late-Holocene (blue circles) and ice age (red circles) groundwaters. Lines mark the average (solid line) and one standard deviation (dashed lines) for each age group (Al-Charideh, 2012; Stadler et al., 2012).

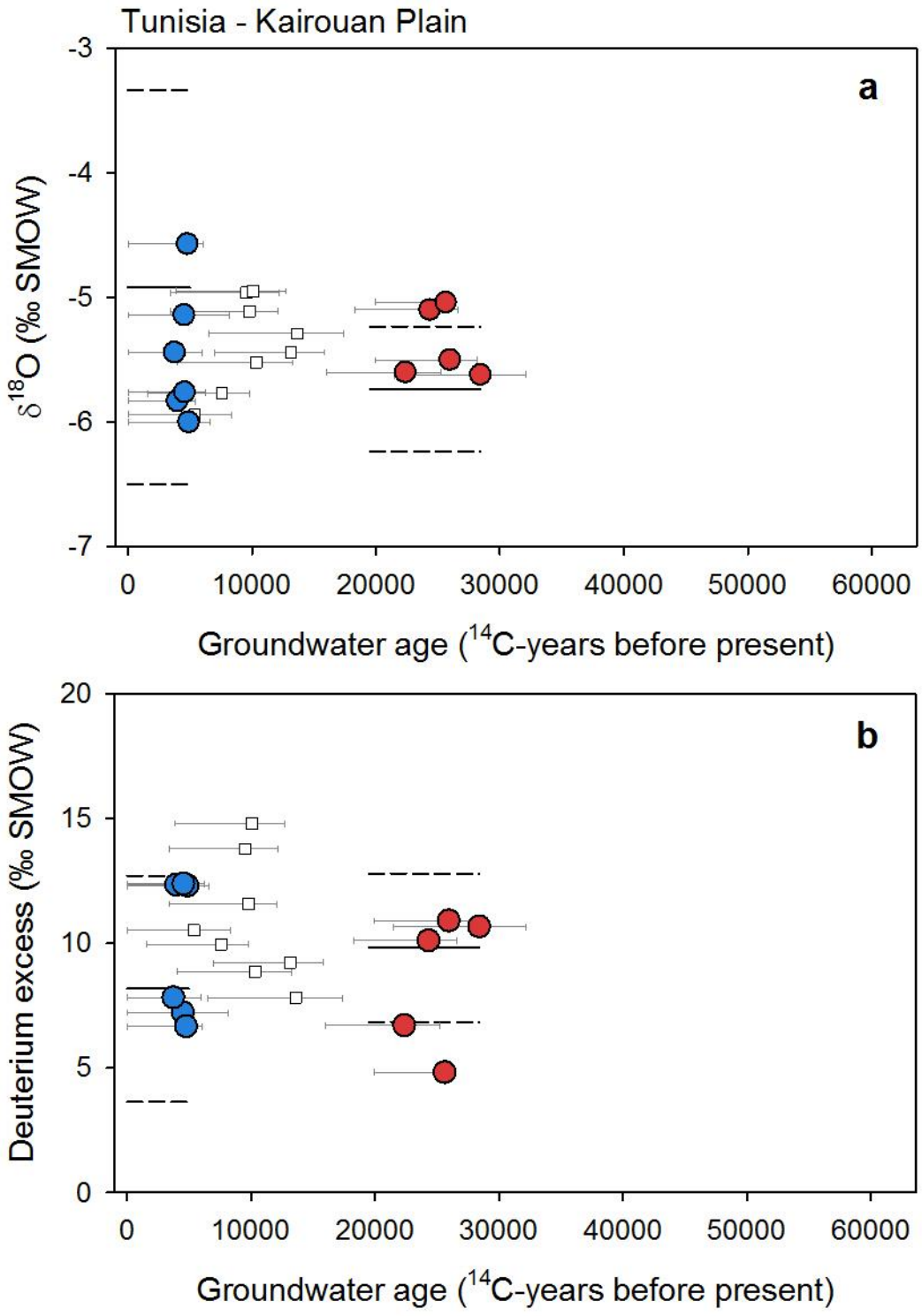

Figure S50. Groundwater isotope composition of the Kairouan Plain. Groundwater $\delta^{18}O$ (a) and deuterium excess (b) plotted against corrected ^{14}C ages for late-Holocene (blue circles) and ice age (red circles) groundwaters. Lines mark the average (solid line) and one standard deviation (dashed lines) for each age group (Derwich et al., 2012).

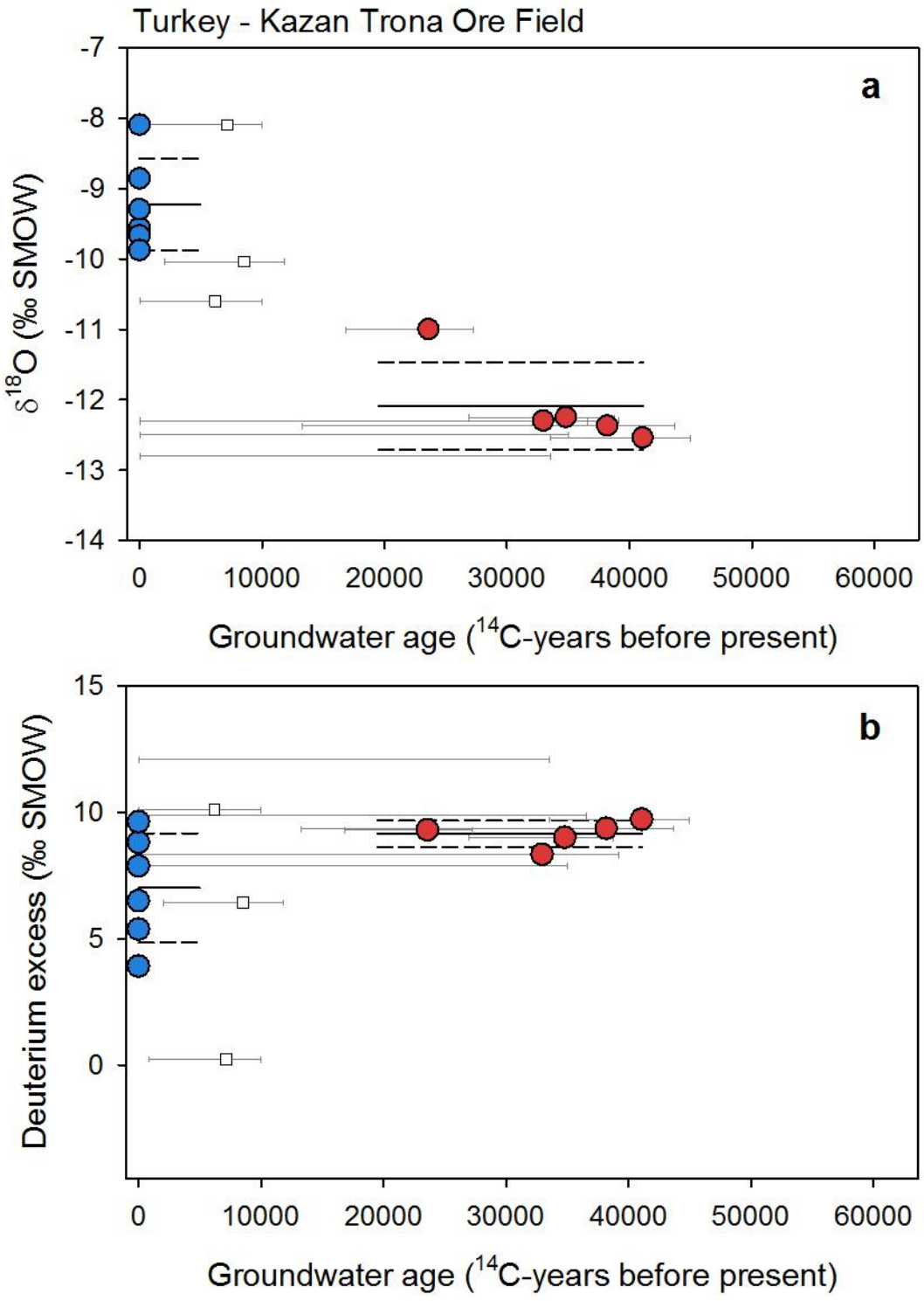

Figure S51. Groundwater isotope composition of the Kazan Trona ore field aquifer system. Groundwater $\delta^{18}O$ (a) and deuterium excess (b) plotted against corrected ^{14}C ages for late-Holocene (blue circles) and ice age (red circles) groundwaters. Lines mark the average (solid line) and one standard deviation (dashed lines) for each age group (Arslan et al., 2014).

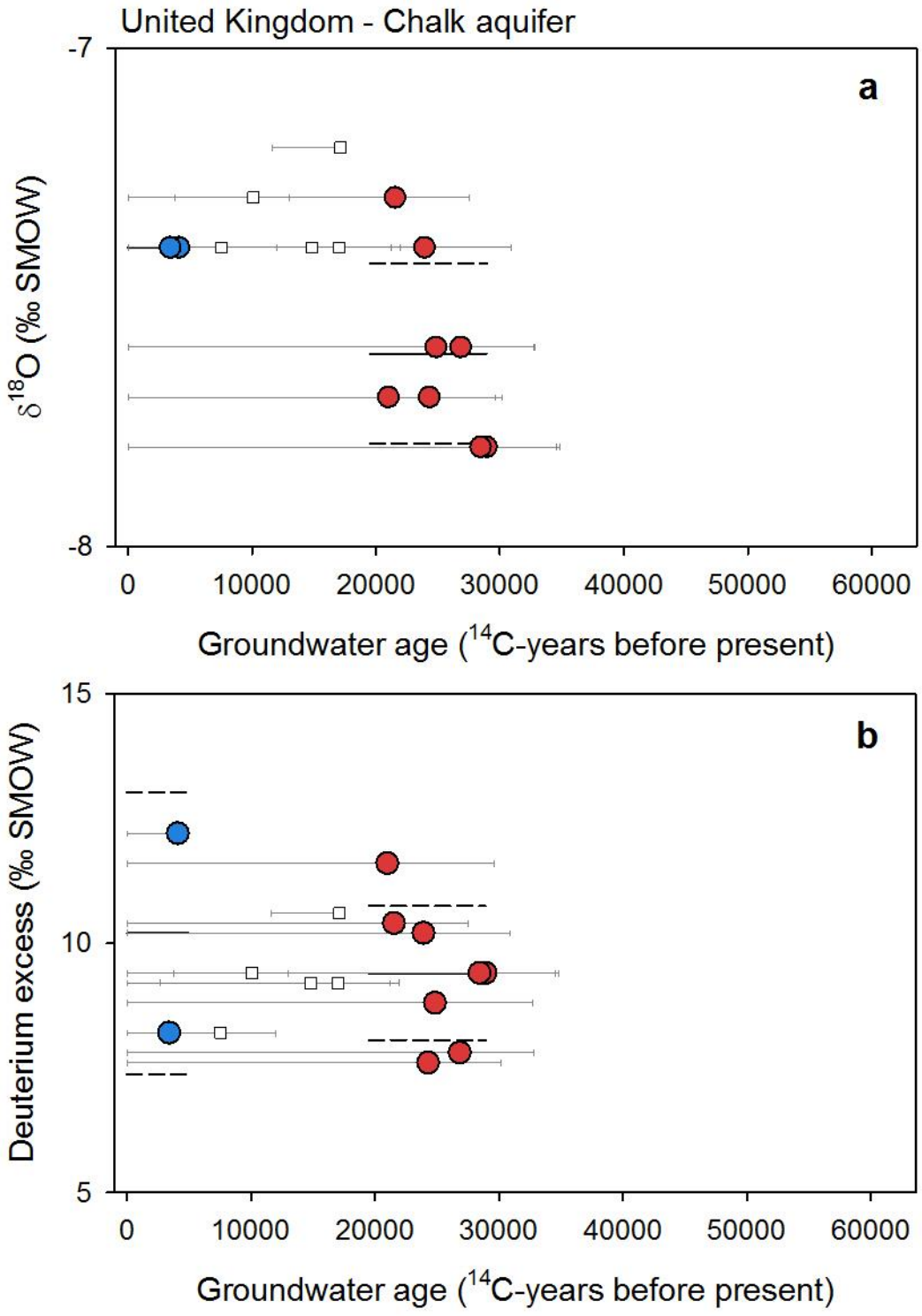

375

376 **Figure S52.** Groundwater isotope composition of the Chalk aquifer (in the United Kingdom).
377 Groundwater $\delta^{18}O$ (a) and deuterium excess (b) plotted against corrected ^{14}C ages for late-
378 Holocene (blue circles) and ice age (red circles) groundwaters. Lines mark the average (solid
379 line) and 1 s.d. (dashed lines) for each group (Darling and Bath, 1988; Dennis et al., 1997; Elliot
380 et al., 1999).

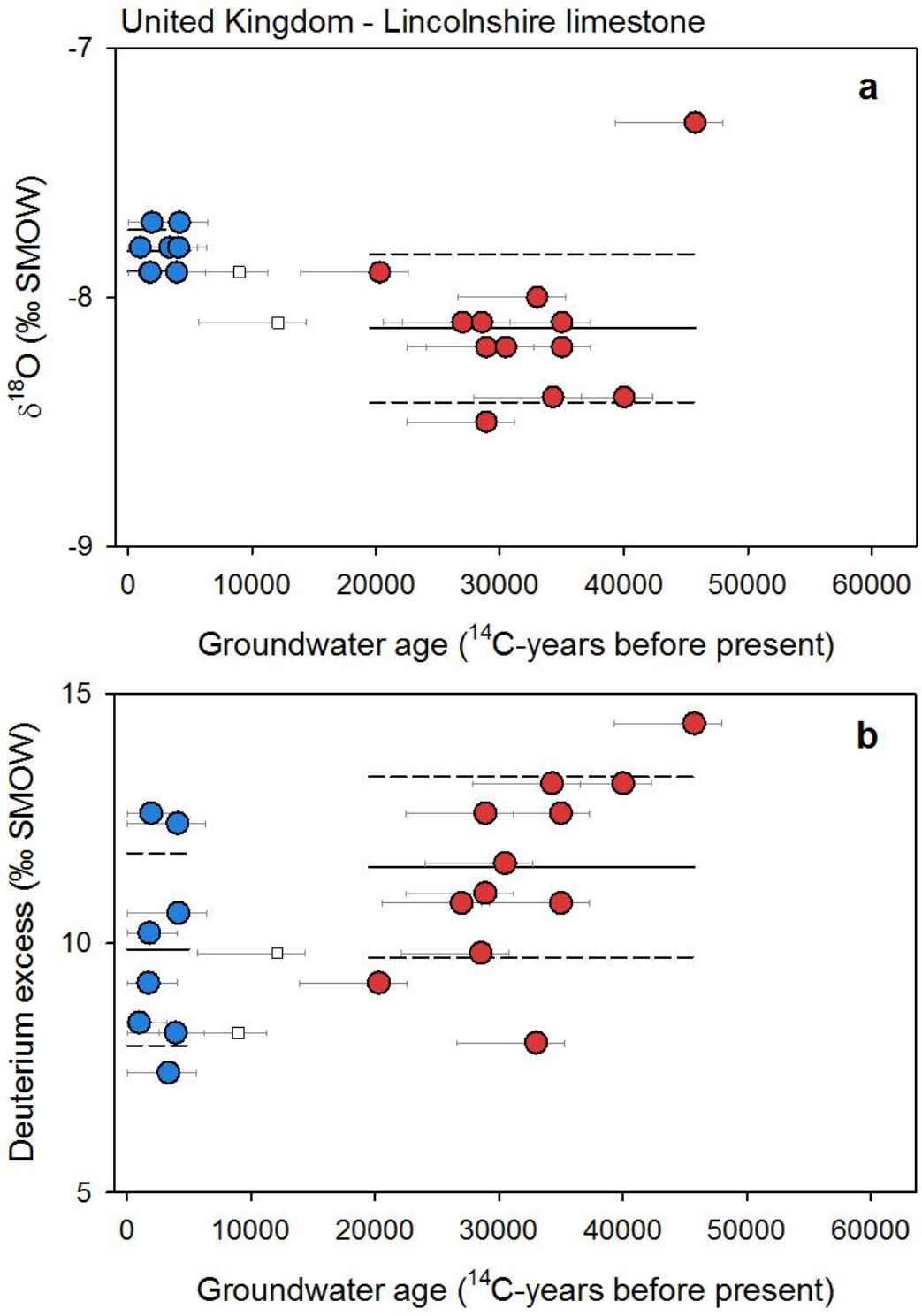

Figure S53. Groundwater isotope composition of the Lincolnshire limestone aquifer. Groundwater $\delta^{18}O$ (a) and deuterium excess (b) plotted against corrected ^{14}C ages for late-Holocene (blue circles) and ice age (red circles) groundwaters. Lines mark the average (solid line) and one standard deviation (dashed lines) for each age group (Darling et al., 1997).

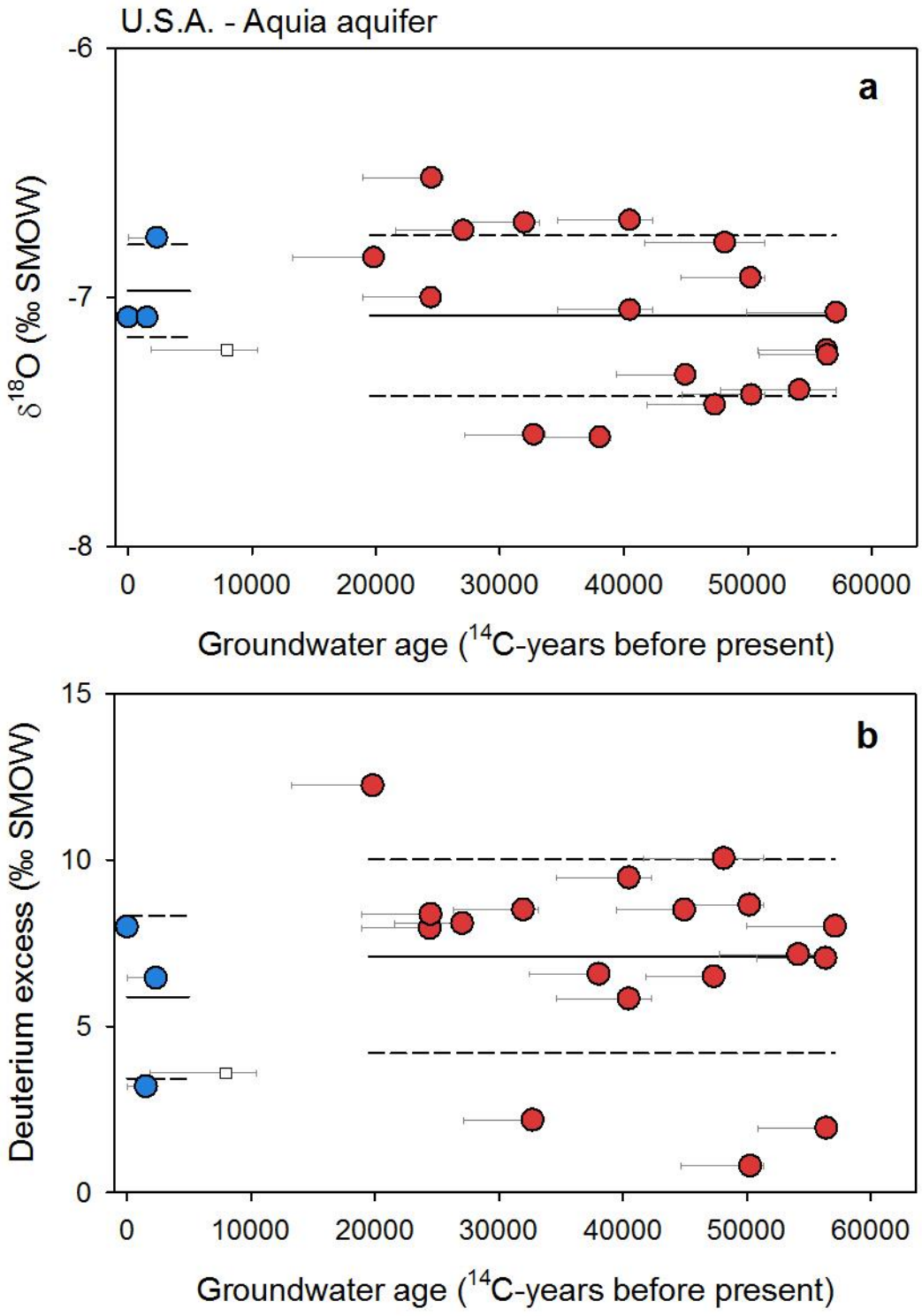

386

387 **Figure S54.** Groundwater isotope composition of the Aquia aquifer. Groundwater $\delta^{18}O$ (a) and
388 deuterium excess (b) plotted against corrected ^{14}C ages for late-Holocene (blue circles) and ice
389 age (red circles) groundwaters. Lines mark the average (solid line) and one standard deviation
390 (dashed lines) for each age group (Aeschbach-Hertig et al., 2002).

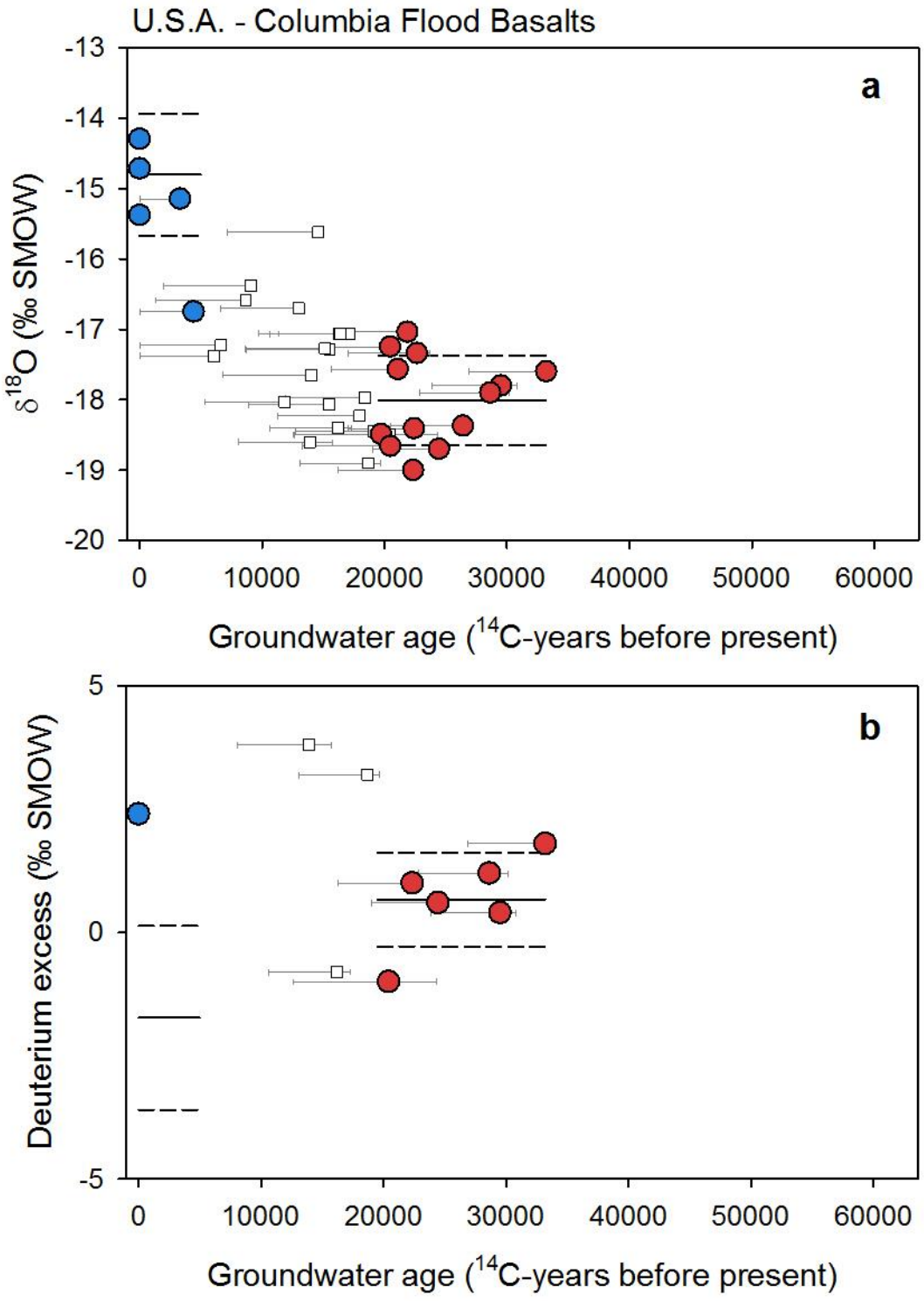

Figure S55. Groundwater isotope composition of groundwaters in the Columbia Flood Basalts. Groundwater $\delta^{18}O$ (a) and deuterium excess (b) plotted against corrected ^{14}C ages for late-Holocene (blue circles) and ice age (red circles) groundwaters. Lines mark the average (solid line) and one standard deviation (dashed lines) for each age group (Douglas et al., 2007; Brown et al., 2010).

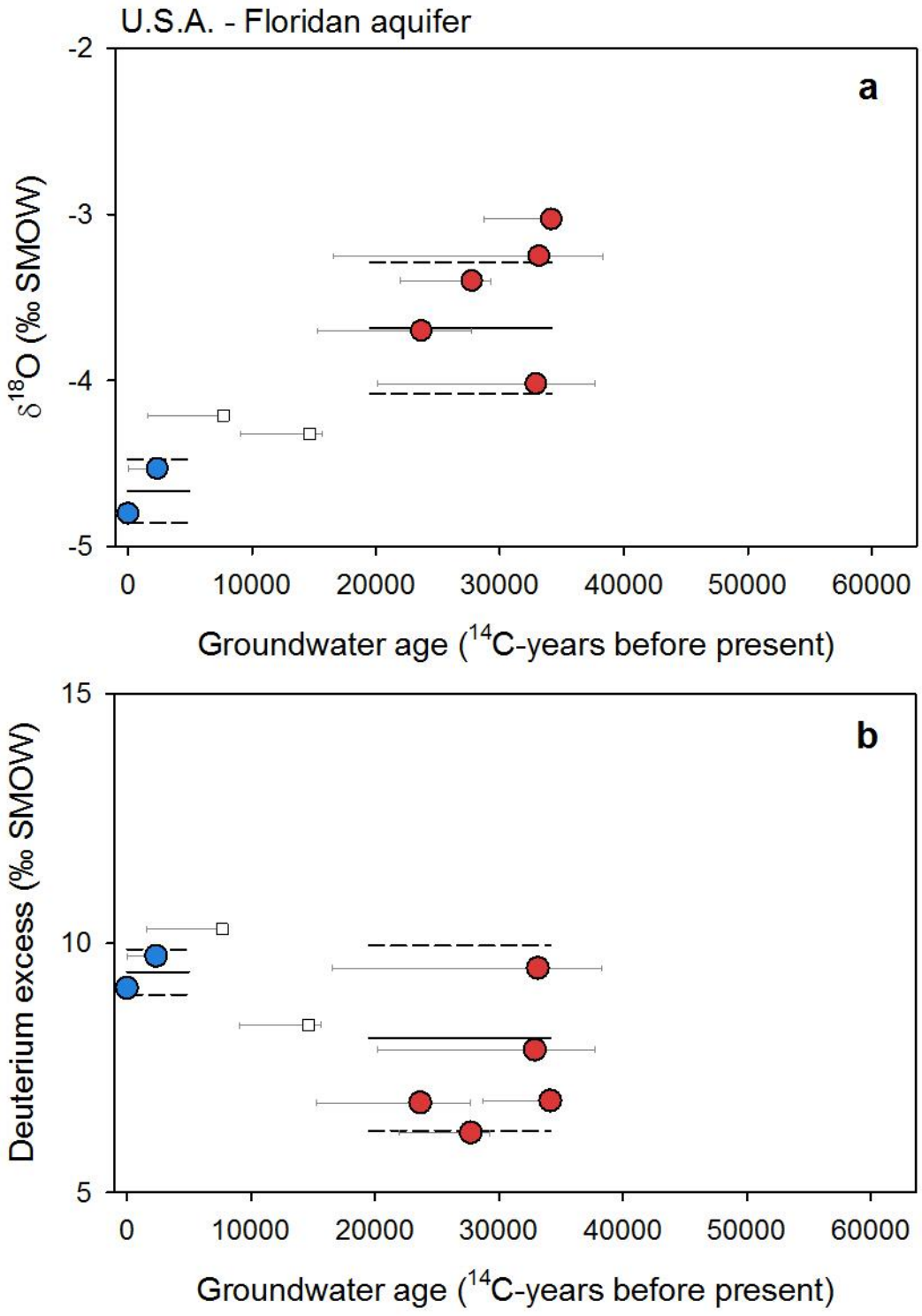

Figure S56. Groundwater isotope composition of the Floridan aquifer. Groundwater $\delta^{18}O$ (a) and deuterium excess (b) plotted against corrected ^{14}C ages for late-Holocene (blue circles) and ice age (red circles) groundwaters. Lines mark the average (solid line) and one standard deviation (dashed lines) for each age group (Clark et al., 1997).

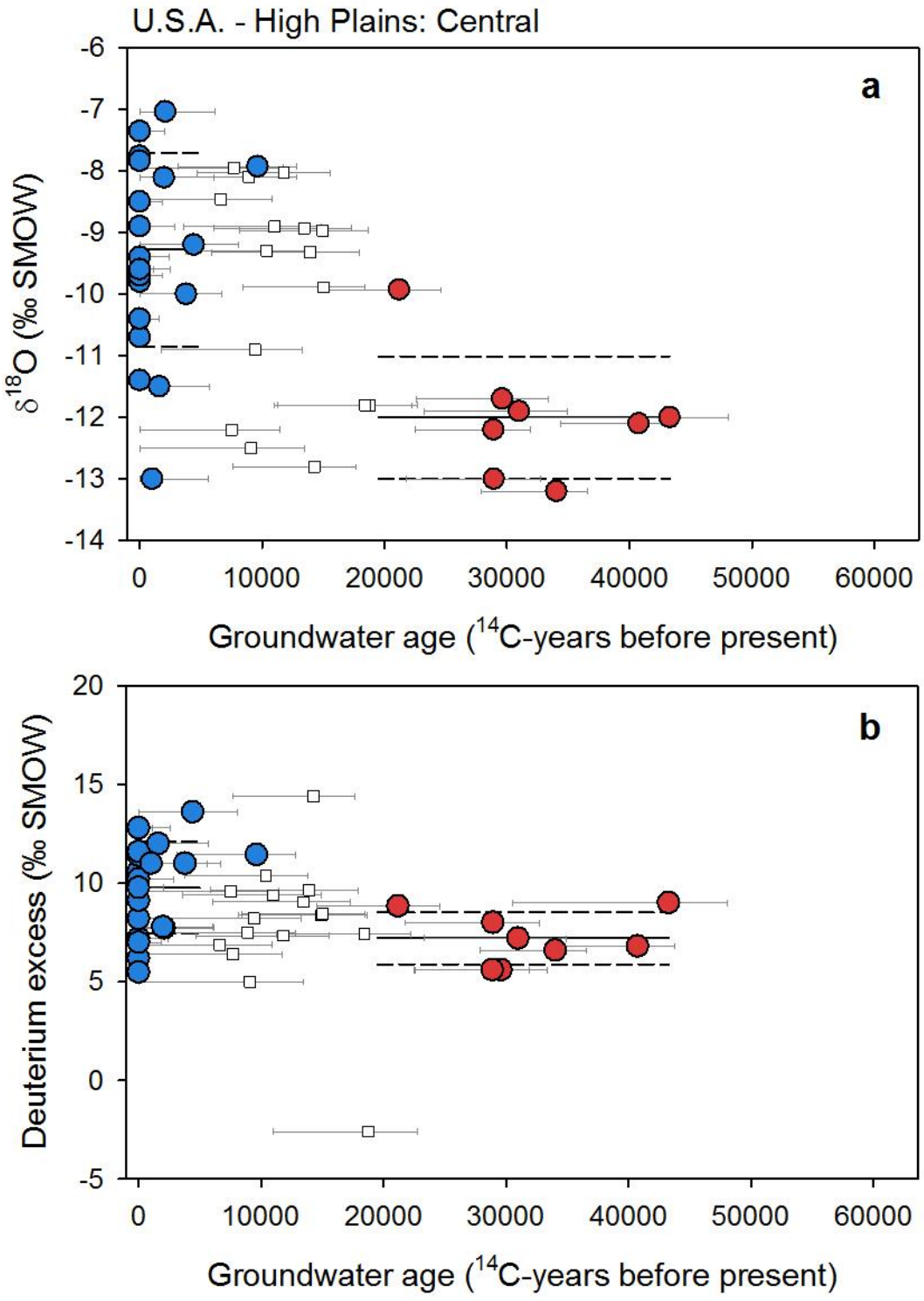

Figure S57. Groundwater isotope composition of the central High Plains aquifer. Groundwater $\delta^{18}O$ (a) and deuterium excess (b) plotted against corrected ^{14}C ages for late-Holocene (blue circles) and ice age (red circles) groundwaters. Lines mark the average (solid line) and one standard deviation (dashed lines) for each age group (Dutton, 1995; Clark et al. 1998).

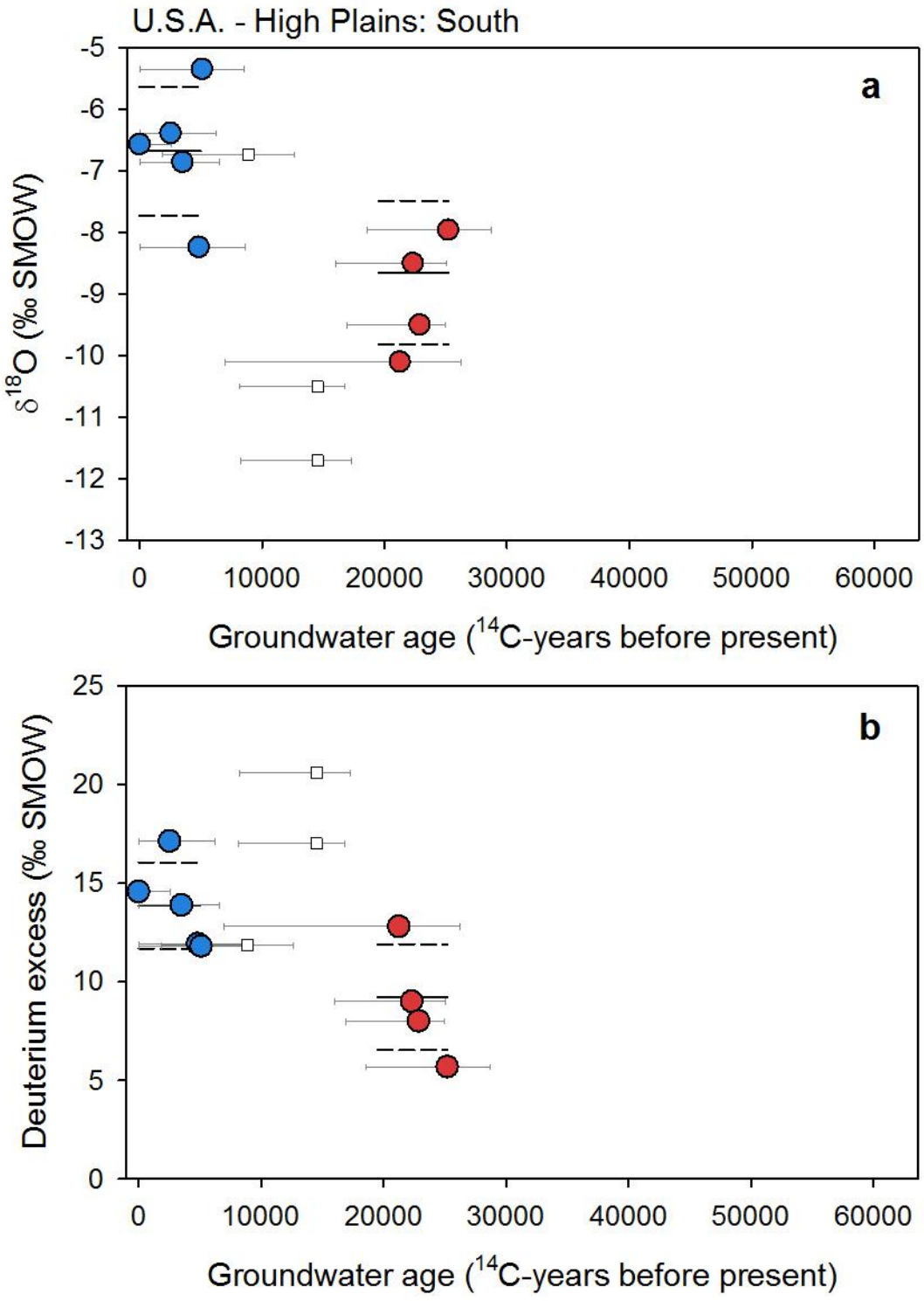

Figure S58. Groundwater isotope composition of the southern High Plains aquifer. Groundwater $\delta^{18}O$ (a) and deuterium excess (b) plotted against corrected ^{14}C ages for late-Holocene (blue circles) and ice age (red circles) groundwaters. Lines mark the average (solid line) and one standard deviation (dashed lines) for each age group (Dutton, 1995; Mehta et al., 2000).

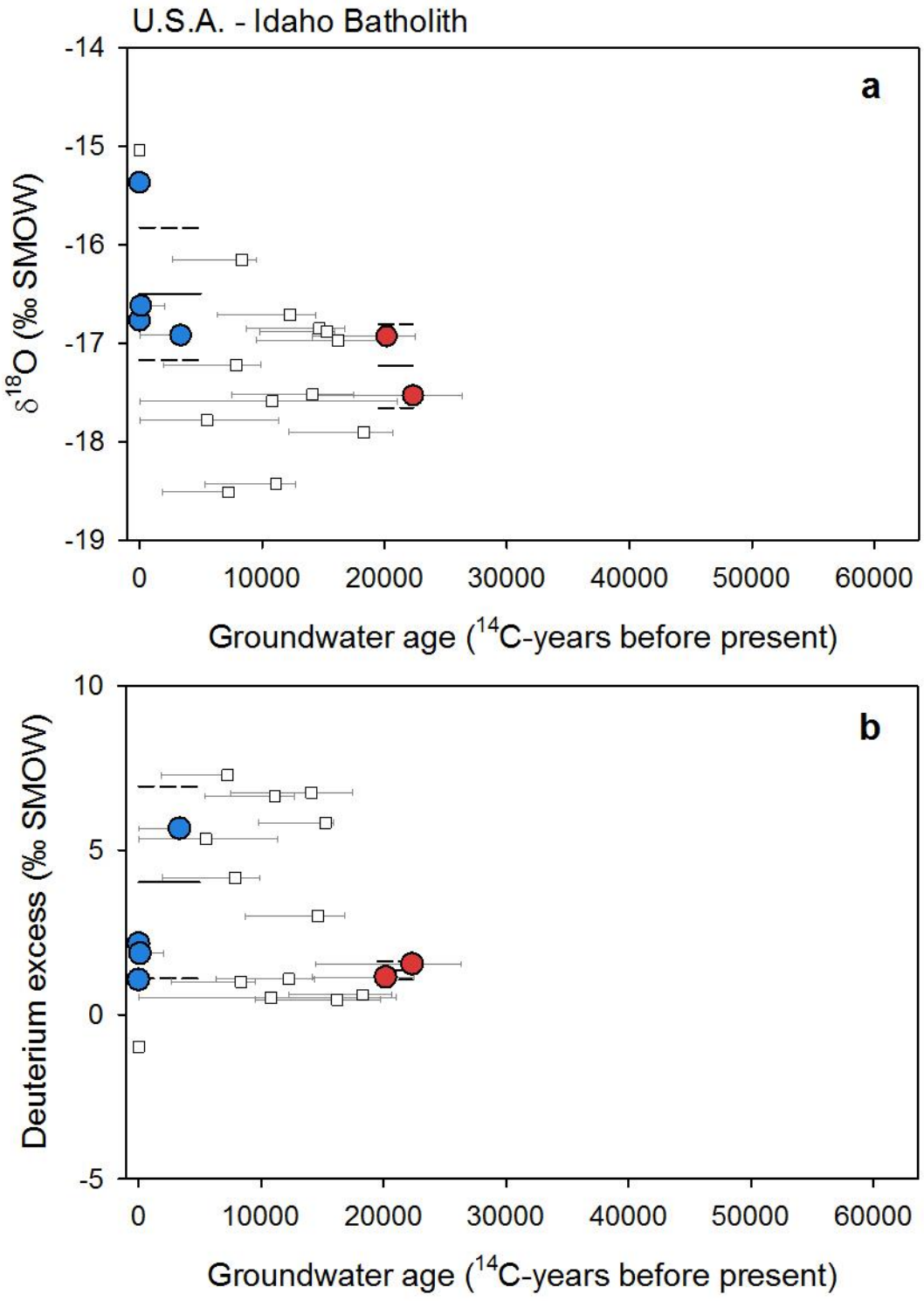

412

413 **Figure S59.** Groundwater isotope composition of the Idaho Batholith aquifer. Groundwater $\delta^{18}O$
414 (a) and deuterium excess (b) plotted against corrected ^{14}C ages for late-Holocene (blue circles)
415 and ice age (red circles) groundwaters. Lines mark the average (solid line) and one standard
416 deviation (dashed lines) for each age group (Schlegel et al., 2009).

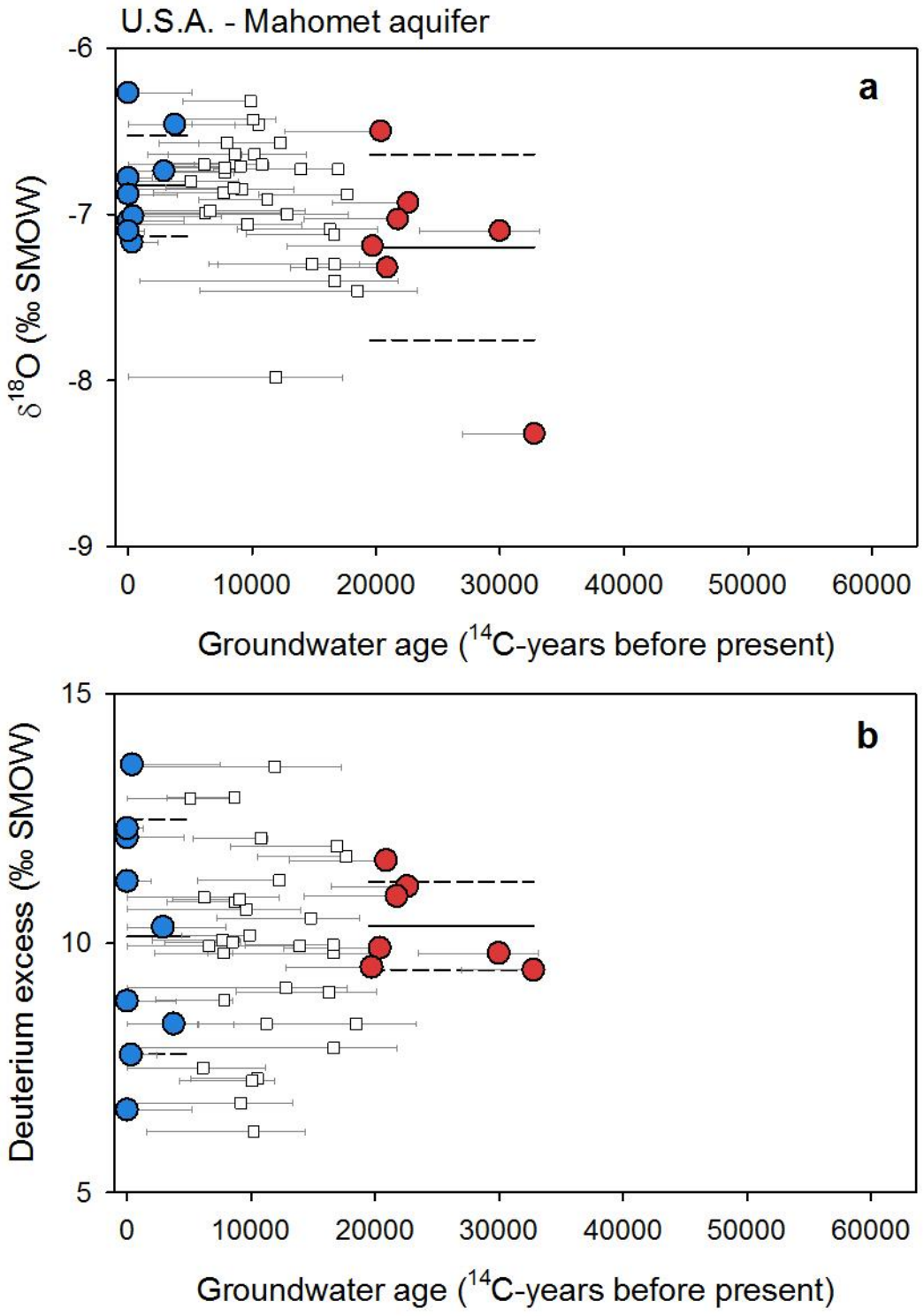

Figure S60. Groundwater isotope composition of the Mahomet aquifer. Groundwater $\delta^{18}O$ (a) and deuterium excess (b) plotted against corrected ^{14}C ages for late-Holocene (blue circles) and ice age (red circles) groundwaters. Lines mark the average (solid line) and one standard deviation (dashed lines) for each age group (Hackley et al., 2010).

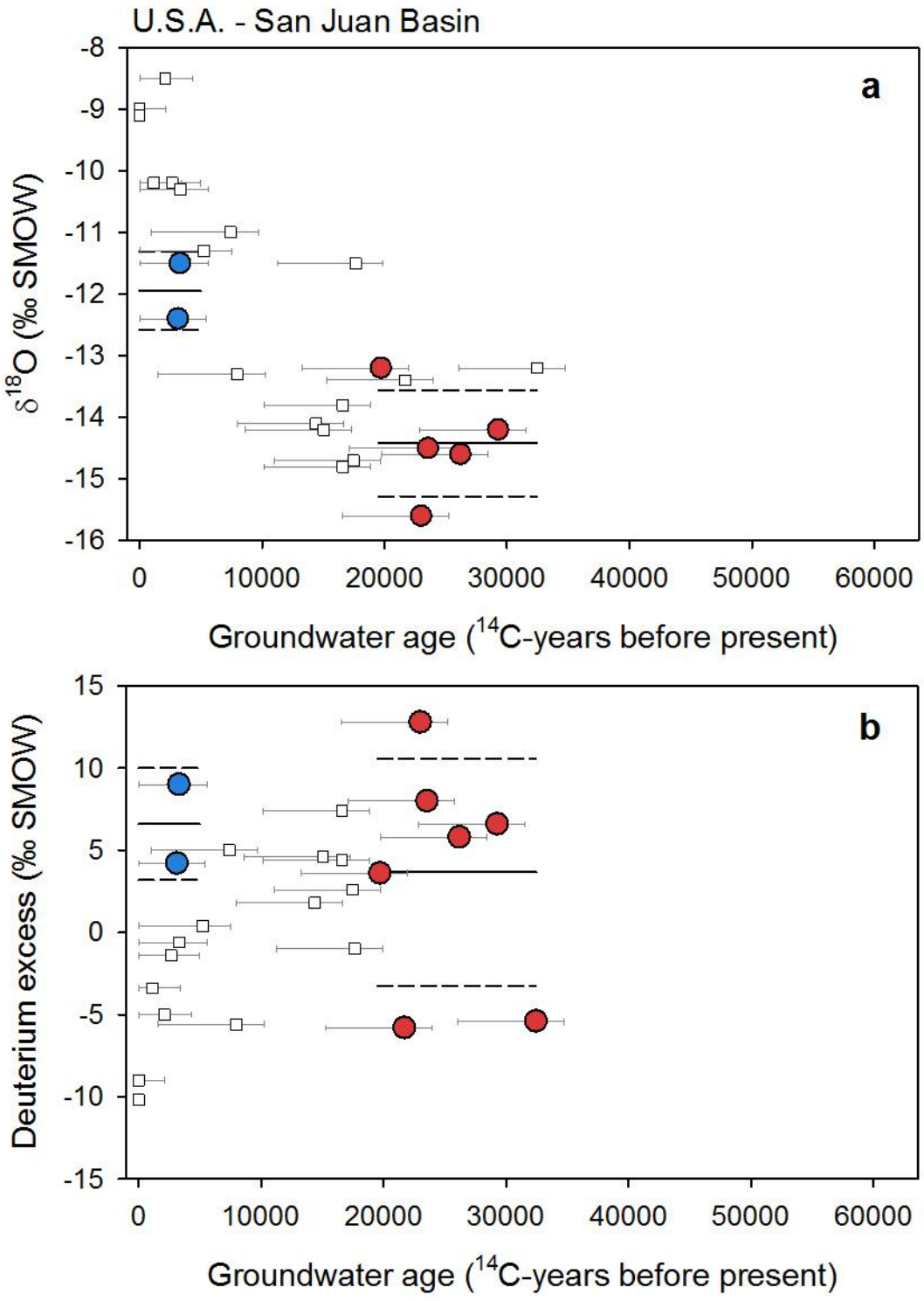

Figure S61. Groundwater isotope composition of the San Juan basin. Groundwater $\delta^{18}O$ (a) and deuterium excess (b) plotted against corrected ^{14}C ages for late-Holocene (blue circles) and ice age (red circles) groundwaters. Lines mark the average (solid line) and one standard deviation (dashed lines) for each age group (Phillips et al., 1986).

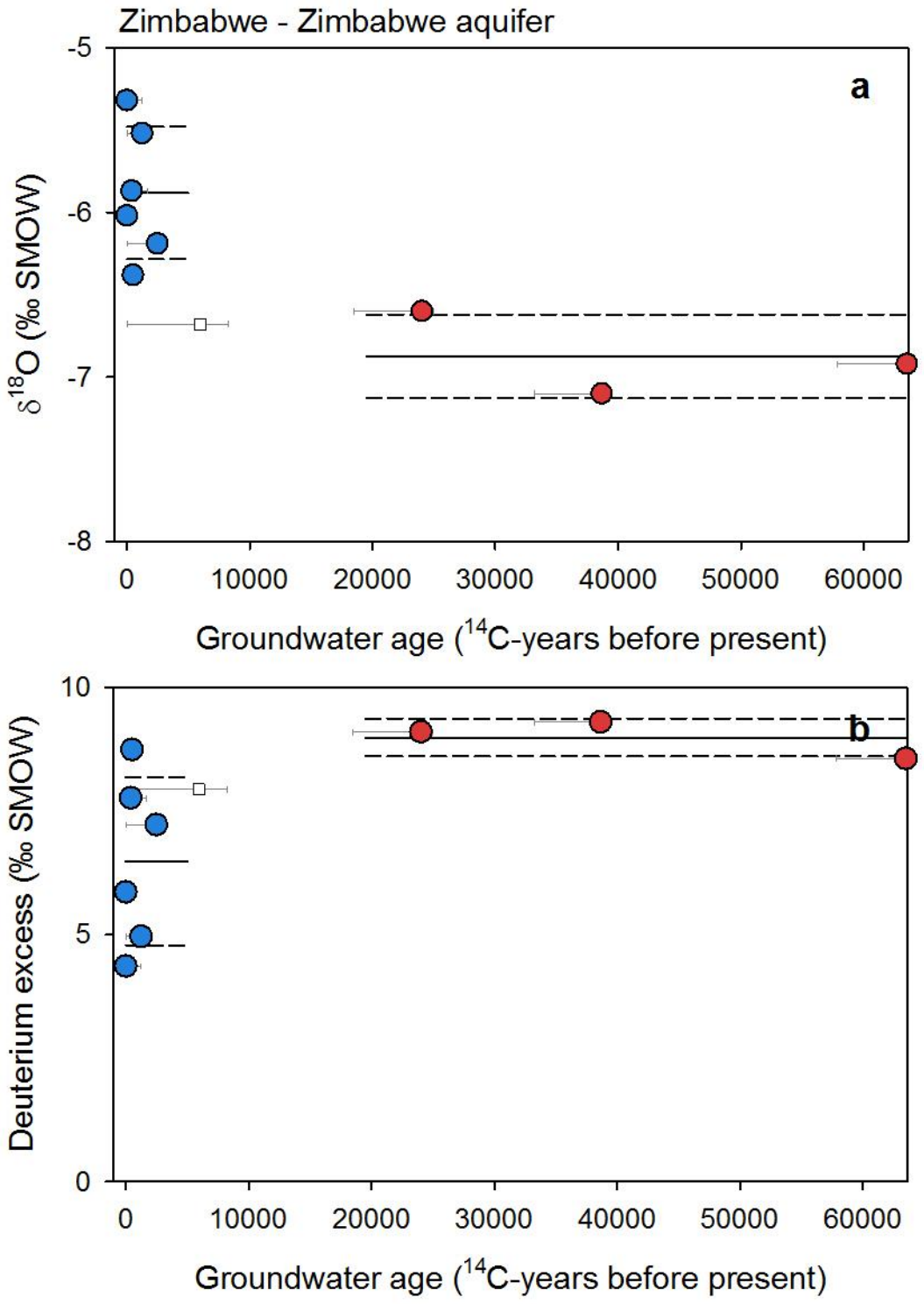

Figure S62. Groundwater isotope composition of the Zimbabwe aquifer. Groundwater $\delta^{18}O$ (a) and deuterium excess (b) plotted against corrected ^{14}C ages for late-Holocene (blue circles) and ice age (red circles) groundwaters. Lines mark the average (solid line) and one standard deviation (dashed lines) for each age group (Larsen et al., 2002).

References: Supplementary Information text

1. Annan, J. D., and Hargreaves, J. C. (2013), A new global reconstruction of temperature changes at the Last Glacial Maximum. *Climate of the Past,* **9,** 367–376.

2. Bouchaou, L., Michelot, J. L., Vengosh, A., Hsissou, Y., Qurtobi, M., Gaye, C. B., Bullen, T. D., and Zuppi, G. M. (2008), Application of multiple isotopic and geochemical tracers for investigation of recharge, salinization, and residence time of water in the Souss–Massa aquifer, southwest of Morocco, *Journal of Hydrology*, **352,** 267–287.

3. Burchuladze, A. A., Chudy, M., Eristavi, I. V., Pagava, S. V., Povinec, P., Sivo, A., and Togonidze, G. I. (1989), Anthropogenic ^{14}C variations in atmospheric CO_2 and wines, *Radiocarbon,* **31,** 771–776.

4. Clark, I. D., and Fritz, P. (1997). Environmental isotopes in hydrogeology. CRC press.

5. Fairbanks, R. G., Mortlock, R. A., Chiu, T. C., Cao, L., Kaplan, A., Guilderson, T. P. Fairbanks, T. W., Bloom, A. L., Grootes, P. M., and Nadeau, M.-J. (2005), Radiocarbon calibration curve spanning 0 to 50,000 years BP based on paired $^{230}Th/^{234}U/^{238}U$ and ^{14}C dates on pristine corals, *Quaternary Science Reviews,* **24,** 1781-1796.

6. Ferguson, G. A., Betcher, R. N., and Grasby, S. E. (2007), Hydrogeology of the Winnipeg formation in Manitoba, Canada, *Hydrogeology Journal*, **15,** 573–587.

7. Geyh, M. A., and Söfner, B. (1989), Groundwater analysis of environmental carbon and other isotopes from the Jakarta Basin Aquifer, Indonesia, *Radiocarbon*, **31,** 919–925.

8. Grasby, S. E., and Chen, Z. (2005), Subglacial recharge into the Western Canada Sedimentary Basin—Impact of Pleistocene glaciation on basin hydrodynamics, *Geological Society of America Bulletin*, **117,** 500–514.

9. Karro, E., Marandi, A., and Vaikmäe, R. (2004), The origin of increased salinity in the Cambrian-Vendian aquifer system on the Kopli Peninsula, northern Estonia, *Hydrogeology Journal*, **12,** 424–435.

10. Lisiecki, L. E., and Raymo, M. E. (2005), A Pliocene-Pleistocene stack of 57 globally distributed benthic $\delta^{18}O$ records, *Paleoceanography,* **20,** PA1003.

11. Marcott, S. A., Shakun, J. D., Clark, P. U., and Mix, A. C. (2013), A reconstruction of regional and global temperature for the past 11,300 years, *Science* **339,** 1198–1201.

12. McIntosh, J. C., Schlegel, M. E., and Person, M. (2012), Glacial impacts on hydrologic processes in sedimentary basins: evidence from natural tracer studies, *Geofluids*, **12,** 7–12.

13. New, M., Lister, D., Hulme, M., and Makin, I. (2002), A high-resolution data set of surface climate over global land areas, *Climate Research*, **21,** 1–25.

14. O'Neil, J. R., Clayton, R. N., and Mayeda, T. K. (1969), Oxygen isotope fractionation in divalent metal carbonates, *The Journal of Chemical Physics*, **51,** 5547–5558.

15. Stotler, R. L., Frape, S. K., Ruskeeniemi, T., Pitkänen, P., and Blowes, D. W. (2012), The interglacial–glacial cycle and geochemical evolution of Canadian and Fennoscandian Shield groundwaters, *Geochimica et Cosmochimica Acta,* **76,** 45–67.

16. Veizer, J., et al. (1999). $^{87}Sr/^{86}Sr$, $\delta^{13}C$ and $\delta^{18}O$ evolution of Phanerozoic seawater. *Chemical Geology*, **161,** 59–88.

References: General circulation models – additional references in Table S1

1. Argus, D. F., and Peltier, W. R. (2010), Constraining models of postglacial rebound using space geodesy: a detailed assessment of model ICE-5G (VM2) and its relatives, *Geophysical Journal International* 181, 697–723.

2. Braconnot, P. et al. (2012), Evaluation of climate models using palaeoclimatic data. *Nature Climate Change,* **2,** 417–424.

3. Collins, W. D. et al. (2006), The formulation and atmospheric simulation of the Community Atmosphere Model version 3 (CAM3), *Journal Of Climate,* **19,** 2144–2161.

4. Hansen, J., et al. (2005), Earth's energy imbalance: Confirmation and implications, *Science*, **308,** 1431–1435.

5. Hourdin, F., et al. (2006), The LMDZ4 general circulation model: Climate performance and sensitivity to parametrized physics with emphasis on tropical convection, *Climate* Dynamics, **27,** 787–813.

6. Kanamitsu, M., et al. (2002), NCEP dynamical seasonal forecast system 2000, Bulletin of the American Meteorological Society**, 83,** 1019–1037.

7. Koch, D., et al. (2011), Coupled Aerosol-Chemistry–Climate Twentieth-Century Transient Model Investigation: Trends in Short-Lived Species and Climate Responses, *Journal of Climate,* **24,** 2693–2714.

8. LeGrande, A. N., and Schmidt, G. A. (2009), Sources of Holocene variability of oxygen isotopes in paleoclimate archives, *Climate of the Past,* **5,** 441–455.

9. Licciardi, J. M., Clark, P. U., Jenson, J. W., and Macayeal, D. R. (1999), Deglaciation of a soft-bedded Laurentide Ice Sheet, *Quaternary Science Reviews,* **17,** 427–448.

10. Noone, D., and Sturm, C. (2010), Comprehensive dynamical models of global and regional water isotope distributions. In: Isoscapes: Understanding Movement, Pattern, and Process on Earth through Isotope Mapping, Springer, pp. 195–219

11. Otto-Bliesner, B. L. et al. (2006), Last Glacial Maximum and Holocene climate in CCSM3, *Journal of Climate,* **19,** 2526–2544.

12. Peltier, W. R. (1994), Ice age paleotopography, *Science,* **265,** 195¬201.

13. Roeckner, E., Brokopf, R., Esch, M., Giorgetta, M., Hagemann, S., Kornblueh, L., Manzini, E., Schlese, U., and Schulzweida, U. (2006), Sensitivity of simulated climate to horizontal and vertical resolution in the ECHAM5 atmosphere model, *Journal Of Climate,* **19,** 3771–3791.

14. Schmidt, G. A., et al. (2014), Configuration and assessment of the GISS ModelE2 contributions to the CMIP5 archive, Journal of Advances in Modeling Earth Systems, **6,** 141–184.

15. Shindell, D. T., Faluvegi, G., Miller, R. L., Schmidt, G. A., Hansen, J. E., and Sun, S. (2006), Solar and anthropogenic forcing of tropical hydrology, *Geophysical Research Letters,* **33,** L24706.

16. Sturm, C., Zhang, Q. and Noone, D. (2010), An introduction to stable water isotopes in climate models: benefits of forward proxy modelling for paleoclimatology, *Climate of the Past,* **6,** 115–129.

17. Toscano, M. A., Peltier, W. R., and Drummond, R. (2011), ICE-5G and ICE-6G models of postglacial relative sea-level history applied to the Holocene coral reef record of northeastern St Croix, USVI: investigating the influence of rotational feedback on GIA processes at tropical latitudes, *Quaternary Science Reviews*, **30,** 3032–3042.

18. Ullman, D. J., LeGrande, A. N., Carlson, A. E., Anslow, F. S., and Licciardi, J. M. (2013), Assessing the impact of Laurentide Ice-Sheet topography on glacial climate, *Climate of the Past,* **10,** 487–507

19. Werner M., Langebroek, P. M., Carlsen T., Herold M., and Lohmann G., (2011), Stable water isotopes in the ECHAM5 general circulation model: Toward high-resolution isotope modeling on a global scale, *Journal of Geophysical Research,* **116,** D15109.

20. Yoshimura, K., Kanamitsu, M., Noone, D., and Oki, T. (2008), Historical isotope simulation using Reanalysis atmospheric data, *Journal of Geophysical Research,* **113,** D19108.

References: Groundwater data

1. Aggarwal, P. K. et al. (2000), A report on isotope hydrology of groundwater in Bangladesh: implications for characterization and mitigation of arsenic in groundwater, International Atomic Energy Agency, Department of Technical Co-operation, Vienna (Austria).

2. Al-Charideh, A. (2012), Geochemical and isotopic characterization of groundwater from shallow and deep limestone aquifers system of Aleppo basin (north Syria), *Environmental Earth Sciences,* **65,** 1157–1168.

3. Al-Mashaikhi, K., Oswald, S., Attinger, S., Büchel, G., Knöller, K., and Strauch, G. (2012), Evaluation of groundwater dynamics and quality in the Najd aquifers located in the Sultanate of Oman, *Environmental Earth Sciences*, **66,** 1195–1211.

4. Al-Ruwaih, F. M., and Shehata, M. (2004), Hydrochemical processes and environmental isotopic study of groundwater in Kuwait, *Water International,* **29,** 158–166.

5. Andrews, J. N., Fontes, J. C., Aranyossy, J. F., Dodo, A., Edmunds, W. M., Joseph, A., and Travi, Y. (1994), The evolution of alkaline groundwaters in the continental intercalaire aquifer of the Irhazer Plain, Niger, *Water Resources Research*, **30,** 45–61.

6. Arslan, S., Yazicigil, H., Stute, M., Schlosser, P. (2014), Environmental isotopes and noble gases in the deep aquifer system of Kazan Trona Ore Field, central Turkey and links to paleoclimate, *Quaternary Research,* **79,** 292–303.

7. Barbecot, F., Marlin, C., Gibert, E., and Dever, L. (2000), Hydrochemical and isotopic characterisation of the Bathonian and Bajocian coastal aquifer of the Caen area (northern France), *Applied Geochemistry,* **15,** 791–805.

8. Bouchaou, L., Michelot, J. L., Vengosh, A., Hsissou, Y., Qurtobi, M., Gaye, C. B., Bullen, T. D., and Zuppi, G. M. (2008), Application of multiple isotopic and geochemical tracers for investigation of recharge, salinization, and residence time of water in the Souss–Massa aquifer, southwest of Morocco, *Journal of Hydrology,* **352,** 267–287.

9. Brown, K. B., McIntosh, J. C., Baker, V. R., and Gosch, D. (2010), Isotopically-depleted late Pleistocene groundwater in Columbia River Basalt aquifers: Evidence for recharge of glacial Lake Missoula floodwaters? *Geophysical Research Letters,* **37,** L21402.

10. Castany, G., Marce, A., Margat, J., Moussu, H., Vuillaume, Y., and Evin, J. (1974), An environmental isotope study of the groundwater regime in large aquifers, In: Isotope Techniques in Groundwater Hydrology 1974, Vol. I.

11. Celle-Jeanton, H., Huneau, F., Travi, Y., and Edmunds, W. M. (2009), Twenty years of groundwater evolution in the Triassic sandstone aquifer of Lorraine: impacts on baseline water quality, *Applied Geochemistry,* **24,** 1198–1213.

12. Chen, Z., Wei, W., Liu, J., Wang, Y., and Chen, J. (2011), Identifying the recharge sources and age of groundwater in the Songnen Plain (Northeast China) using environmental isotopes, *Hydrogeology Journal*, **19,** 163–176.

13. Clark, I. D., Fritz, P., Quinn, O. P., Rippon, P. W., Nash, H., and al Said, S. B. B. G. (1987), Modern and fossil groundwater in an arid environment: a look at the hydrogeology of southern Oman, In: Isotope Techniques in Water Resources Development.

14. Clark, J. F., Davisson, M. L., Hudson, G. B., and Macfarlane, P. A. (1998), Noble gases, stable isotopes, and radiocarbon as tracers of flow in the Dakota aquifer, Colorado and Kansas, *Journal of Hydrology,* **211,** 151–167.

15. Clark, J. F., Stute, M., Schlosser, P., Drenkard, S., and Bonani, G. (1997), A tracer study of the Floridan aquifer in southeastern Georgia: Implications for groundwater flow and paleoclimate, *Water Resources Research,* **33,** 281-289.

16. Currell, M. J., Cartwright, I., Bradley, D. C., and Han, D. (2010). Recharge history and controls on groundwater quality in the Yuncheng Basin, north China, *Journal of Hydrology,* **385,** 216–229.

17. Darling, W. G., and Bath, A. H. (1988), A stable isotope study of recharge processes in the English Chalk, *Journal of Hydrology*, **101,** 31–46.

18. Darling, W. G., Edmunds, W. M., and Smedley, P. L. (1997), Isotopic evidence for palaeowaters in the British Isles, *Applied Geochemistry,* **12,** 813–829.

19. Dennis, F., Andrews, J. N., Parker, A., Poole, J. and Wolf, M. (1997), Isotopic and noble gas study of Chalk groundwater in the London Basin, England, *Applied Geochemistry,* **12,** 763–773.

20. Derwich, L. J., Zouar, K., and Michelot, J. L. (2012), Recharge and paleorecharge of the deep groundwater aquifer system in the Zeroud Basin (Kairouan plain, Central Tunisia), *Quaternary International*, **257,** 56–63.

21. Dodo, A., and Zuppi, G. M. (1997), Groundwater flow study in the Bilma–Djado Basin (Niger) by means of environmental isotopes, *Comptes Rendus de l'Academie des Sciences. Serie 2, Sciences de la Terre et des Planetes*, **30,** 845–852.

22. Dodo, A., and Zuppi, G. M. (1999), Variabilité climatique durant le Quaternaire dans la nappe du Tarat (Arlit, Niger), *Comptes Rendus de l'Académie des Sciences–Series IIA–Earth and Planetary Science*, **328,** 371–379.

23. Douglas, A. A., Osiensky, J. L., & Keller, C. K. (2007). Carbon–14 dating of ground water in the Palouse Basin of the Columbia River basalts, *Journal of Hydrology*, **334,** 502–512.

24. Dutton, A. R. (1995), Groundwater isotopic evidence for paleorecharge in US High Plains aquifers, *Quaternary Research,* **43,** 221–231.

25. Edmunds, W. M. (2009), Palaeoclimate and groundwater evolution in Africa—implications for adaptation and management, *Hydrological Sciences Journal*, **54,** 781–792.

26. Edmunds, W. M. et al. (2003), Groundwater evolution in the Continental Intercalaire aquifer of southern Algeria and Tunisia: trace element and isotopic indicators, *Applied Geochemistry*, **18,** 805–822.

27. Elliot, T., Andrews, J. N., and Edmunds, W. M. (1999), Hydrochemical trends, palaeorecharge and groundwater ages in the fissured Chalk aquifer of the London and Berkshire Basins, UK, *Applied Geochemistry*, **14,** 333–363.

28. Fadlelmawla, A., Hadi, K., Zouari, K., and Kulkarni, K. M. (2008), Hydrogeochemical investigations of recharge and subsequent salinization processes at Al-Raudhatain depression in Kuwait, *Hydrological Sciences Journal*, **53,** 204–223.

29. Galego Fernandes, P., and Carreira, P. M. (2008), Isotopic evidence of aquifer recharge during the last ice age in Portugal, *Journal of Hydrology*, **361,** 291–308.

30. Gat, J. R., & Galai, A. (1982). Groundwaters of the Arava Valley-an isotopic study of their origin and interrelationships, *Israel Journal of Earth Sciences*, **31,** 25–38.

31. Geyh, M. A., and Söfner, B. (1989), Groundwater analysis of environmental carbon and other isotopes from the Jakarta Basin Aquifer, Indonesia, *Radiocarbon*, **31,** 919–925.

32. Gouvea da Silva, R. B. (1983), Estudo hidroquımico e isotópico das águas subterrâneas do aquıfero Botucatu no estado de Sao Paulo, Ph. D. thesis, University of Sao Paulo, Sao Paulo, Brazil.

33. Harrington, G., Stelfox, L., Gardner, W. P., Davies, P., Doble, R., and Cook, P. G. (2011), Surface water–groundwater interactions in the lower Fitzroy River, Western Australia, CSIRO Publications.

34. Heaton, T. H. E., Talma, A. S., and Vogel, J. C. (1986), Dissolved gas paleotemperatures and ^{18}O variations derived from groundwater near Uitenhage, South Africa, *Quaternary Research*, **25,** 79–88.

35. Hinsby, K., Harrar, W. G., Nyegaard, P., Konradi, P. B., Rasmussen, E. S., Bidstrup, T., Gregersen, U., Boaretto, E. (2001), The Ribe Formation in western Denmark - Holocene and Pleistocene groundwaters in a coastal Miocene sand aquifer, Geological Society of London, Special Publications, **189,** 29–48.

36. Hoque, M. A., and Burgess, W. G. (2012), ^{14}C dating of deep groundwater in the Bengal Aquifer System, Bangladesh: Implications for aquifer anisotropy, recharge sources and sustainability, *Journal of Hydrology*, **444,** 209–220.

37. Huneau, F. et al. (2011), Flow pattern and residence time of groundwater within the south–eastern Taoudeni sedimentary basin (Burkina Faso, Mali), *Journal of Hydrology*, **409,** 423–439.

38. Kotler, E., and Burn, C. R. (2000), Cryostratigraphy of the Klondike "muck" deposits, west-central Yukon Territory, *Canadian Journal of Earth Sciences*, **37,** 849–861.

39. Kreuzer, A. M., von Rohden, C., Friedrich, R., Chen, Z., Shi, J., Hajdas, I., Kipfer, R., and Aeschbach–Hertig, W. (2009), A record of temperature and monsoon intensity over the past 40 kyr from groundwater in the North China Plain, *Chemical Geology*, **259,** 168–180.

40. Külls, C. (2000), Groundwater of the North–Western Kalahari, Namibia. Ph.D. Thesis, Julius–Maximilian University of Würzburg.

41. Kulongoski, J. T., Hilton, D. R., and Selaolo, E. T. (2004), Climate variability in the Botswana Kalahari from the late Pleistocene to the present day, *Geophysical Research Letters*, **31,** L10204.

42. Kumar, S. U., Sharma, S., Navada, S. V., and Deodhar, A. S. (2009), Environmental isotopes investigation on recharge processes and hydrodynamics of the coastal sedimentary aquifers of Tiruvadanai, Tamilnadu State, India, *Journal of Hydrology*, **364,** 23–39.

43. Larsen, F., Owen, R., Dahlin, T., Mangeya, P., & Barmen, G. (2002). A preliminary analysis of the groundwater recharge to the Karoo formations, mid–Zambezi basin, Zimbabwe, *Physics and Chemistry of the Earth*, **27,** 765–772.

44. Le Gal La Salle, C., Marlin, C., Leduc, C., Taupin, J. D., Massault, M., and Favreau, G. (2001), Renewal rate estimation of groundwater based on radioactive tracers ^{3}H, ^{14}C in an unconfined aquifer in a semi-arid area, Iullemeden Basin, Niger, *Journal of Hydrology*, **254,** 145–156.

45. Le Gal La Salle, C., Marlin, C., Savoye, S., and Fontes, J. C. (1996), Geochemistry and ^{14}C dating of groundwaters from Jurassic aquifers of North Aquitaine Basin (France), *Applied Geochemistry*, **11,** 433–445.

46. Leaney, F. W., and Allison, G. B. (1986), Carbon–14 and stable isotope data for an area in the Murray Basin: its use in estimating recharge. *Journal of Hydrology*, **88,** 129–145.

47. Maduabuchi, C., Faye, S., and Maloszewski, P. (2006), Isotope evidence of palaeorecharge and palaeoclimate in the deep confined aquifers of the Chad Basin, NE Nigeria, *Science of the Total Environment*, **370,** 467–479.

48. Majumder, R. K., Halim, M. A., Saha, B. B., Ikawa, R., Nakamura, T., Kagabu, M., and Shimada, J. (2011), Groundwater flow system in Bengal Delta, Bangladesh revealed by environmental isotopes, *Environmental Earth Sciences*, **64,** 1343–1352.

49. Martinelli, G., Chahoud, A., Dadomo, A., Fava, A. (2014), Isotopic features of Emilia-Romagna region (North Italy) groundwaters: Environmental and climatological implications, *Journal of Hydrology*, **519,** 1928–1938.

50. Mazor, E., Gilad, D., and Fridman, V. (1995). Stagnant aquifer concept Part 2. Small scale artesian systems-Hazeva, Dead Sea Rift Valley, Israel, *Journal of Hydrology*, **173,** 241–261.

51. Mehta, S., Fryar, A. E., and Banner, J. L. (2000), Controls on the regional-scale salinization of the Ogallala aquifer, Southern High Plains, Texas, USA, *Applied Geochemistry*, **15,** 849–864.

52. Meyer, H., Derevyagin, A. Y., Siegert, C., and Hubberten, H. W. (2002), Paleoclimate studies on Bykovsky Peninsula, North Siberia-hydrogen and oxygen isotopes in ground ice. *Polarforschung*, **70,** 37–51.

53. Noseck, U. et al. (2009), Carbon chemistry and groundwater dynamics at natural analogue site Ruprechtov, Czech Republic: insights from environmental isotopes, *Applied Geochemistry*, **24,** 1765–1776.

54. Patterson, L. J. et al. (2005), Cosmogenic, radiogenic, and stable isotopic constraints on groundwater residence time in the Nubian Aquifer, Western Desert of Egypt, *Geochemistry, Geophysics, Geosystems*, **6,** Q01005.

55. Phillips, F. M., Peeters, L. A., Tansey, M. K., and Davis, S. N. (1986), Paleoclimatic inferences from an isotopic investigation of groundwater in the central San Juan Basin, New Mexico, *Quaternary Research,* **26,** 179–193.

56. Rahube, T. B. (2003), Recharge and groundwater resources evaluation of the Lokalane–Ncojane Basin (Botswana) using numerical modelling, MSc Thesis, *International Institute for Geoinformation Science and Earth Observation*, Enschede, Netherlands, 104.

57. Robinson, B. W., and Gunatilaka, A. (1991), Stable isotope studies and the hydrological regime of sabkhas in southern Kuwait, Arabian Gulf, *Sedimentary Geology,* **73,** 141–159.

58. Salati, E., Menezes Leal, J., and Mendes Campos, M. (1974), Environmental isotopes used in a hydrogeological study of northeastern Brazil, In: Isotope Techniques in Groundwater Hydrology 1974, Vol. I. 379–398.

59. Samborska, K., Różkowski, A., and Małoszewski, P. (2013), Estimation of groundwater residence time using environmental radioisotopes (^{14}C, T) in carbonate aquifers, southern Poland, *Isotopes in Environmental and Health Studies,* **49,** 73-97.

60. Schlegel, M. E., Mayo, A. L., Nelson, S., Tingey, D., Henderson, R., and Eggett, D. (2009), Paleo-climate of the Boise area, Idaho from the last glacial maximum to the present based on groundwater δ^2H and δ^{18}O compositions, *Quaternary Research,* **71,** 172–180.

61. Shehata, M., and Al-Ruwaih, F. (1999), Major ions geochemistry and environmental isotope study of the Nubian Aquifer system, Dakhla Oasis, Western Desert, Egypt, *Arabian Journal for Science and Engineering,* **24,** 43–58.

62. Sikdar, P. K., and Sahu, P. (2009), Understanding wetland sub-surface hydrology using geologic and isotopic signatures, *Hydrology and Earth System Sciences Discussions,* **6,** 3143–3173.

63. Stadler, S., Geyh, M. A., Ploethner, D., and Koeniger, P. (2012), The deep Cretaceous aquifer in the Aleppo and Steppe basins of Syria: assessment of the meteoric origin and geographic source of the groundwater, *Hydrogeology Journal*, **20,** 1007–1026.

64. Stute, M., and Deak, J. (1989), Environmental isotope study ^{14}C, ^{13}C, ^{18}O, D, noble gases on deep groundwater circulation systems in Hungary with reference to paleoclimate, *Radiocarbon,* **31,** 902–918.

65. Stute, M., Clark, J. F., Schlosser, P., Broecker, W. S., and Bonani, G. (1995a), A 30,000 yr continental paleotemperature record derived from noble gases dissolved in groundwater from the San Juan Basin, New Mexico, *Quaternary Research,* **43,** 209–220.

66. Sukhija, B. S., Reddy, D. V., and Nagabhushanam, P. (1998), Isotopic fingerprints of paleoclimates during the last 30,000 years in deep confined groundwaters of Southern India, *Quaternary Research,* **50,** 252–260.

67. van Geldern, R., Baier, A., Subert, H. L., Kowol, S., Balk, L., Barth, J. A. C. (2014), Pleistocene paleo-groundwater as a pristine fresh water resource in southern Germany – evidence from stable and radiogenic isotopes, *Science of the Total Environment,* **496**, 107–115.

68. Varsányi, I., Palcsu, L., and Kovács, L. Ó. (2011), Groundwater flow system as an archive of palaeotemperature: Noble gas, radiocarbon, stable isotope and geochemical study in the Pannonian Basin, Hungary, *Applied Geochemistry,* **26,** 91–104.

69. Walraevens, K. (1990), Natural-isotope research on groundwater from the semi-confined Ledo-Paniselian aquifer in Belgium: application of ^{14}C-correction methods. Natuurwetenschappelijk Tijdschrift, **72,** 79–89.

70. Walraevens, K., Van Camp, M., Lermytte, J., Van Der Kemp, W. J. M., and Loosli, H. H. (2001), Pleistocene and Holocene groundwaters in the freshening Ledo-Paniselian aquifer in Flanders, Belgium, *Geological Society, London, Special Publications,* **189,** 49–70.

71. Weyhenmeyer, C. E., Burns, S. J., Waber, H. N., Aeschbach-Hertig, W., Kipfer, R., Loosli, H. H., and Matter, A. (2000), Cool glacial temperatures and changes in moisture source recorded in Oman groundwaters, *Science,* **287,** 842–845.

72. Weyhenmeyer, C. E., Burns, S. J., Waber, H. N., Macumber, P. G., and Matter, A. (2002), Isotope study of moisture sources, recharge areas, and groundwater flow paths within the eastern Batinah coastal plain, Sultanate of Oman, *Water Resources Research*, **38,** 1184.

73. Yechieli, Y., Kafri, U., and Sivan, O. (2009), The inter–relationship between coastal sub–aquifers and the Mediterranean Sea, deduced from radioactive isotopes analysis, *Hydrogeology Journal*, **17,** 265–274.

74. Zongyu, C., Jixiang, Q., Jianming, X., Jiaming, X., Hao, Y., and Yunju, N. (2003), Paleoclimatic interpretation of the past 30 ka from isotopic studies of the deep confined aquifer of the North China plain, *Applied Geochemistry*, **18,** 997–1009.

75. Zuber, A., Weise, S. M., Motyka, J., Osenbrück, K., and Różański, K. (2004), Age and flow pattern of groundwater in a Jurassic limestone aquifer and related Tertiary sands derived from combined isotope, noble gas and chemical data, *Journal of Hydrology*, **286,** 87–112.

References: Speleothem data

1. Asmerom, Y., Polyak, V. J., and Burns, S. J. (2010), Variable winter moisture in the southwestern United States linked to rapid glacial climate shifts, *Nature Geoscience,* **3,** 114–117.

2. Bar-Matthews, M., Ayalon, A., Gilmour, M., Matthews, A., and Hawkesworth, C. (2003), Sea-land oxygen isotopic relationships from planktonic foraminifera and speleothems in the Eastern Mediterranean region and their implication for paleorainfall during interglacial intervals, *Geochimica et Cosmochimica Acta,* **67,** 3181–3199.

3. Cai, Y., Tan, L., Cheng, H., An, Z., Edwards, R. L., Kelly, M. J., Kong, X., and Wang, X. (2010), The variation of summer monsoon precipitation in central China since the last deglaciation, *Earth and Planetary Science Letters,* **291,** 21–31.

4. Cruz, F. W., Burns, S. J., Karmann, I., Sharp, W. D., Vuille, M., Cardoso, A. O., Ferrari, J. A., Dias, P. L. S., and Viana, O. (2005), Insolation-driven changes in atmospheric circulation over the past 116,000 years in subtropical Brazil, *Nature,* **434,** 63–66.

5. Dykoski, C. A., Edwards, R. L., Cheng, H., Yuan, D., Cai, Y., Zhang, M., Lin, Y., Qing, J., An, Z., and Revenaugh, J. (2005), A high-resolution, absolute-dated Holocene and deglacial Asian monsoon record from Dongge Cave, China, *Earth and Planetary Science Letters*, **233,** 71–86.

6. Fleitmann, D. *et al. (*2009*),* Timing and climatic impact of Greenland interstadials recorded in stalagmites from northern Turkey, *Geophysical Research Letters*, **36,** *L19707.*

7. Frumkin, A., Ford, D. C., and Schwarcz, H. P. (1999), Continental oxygen isotopic record of the last 170,000 years in Jerusalem, *Quaternary Research,* **51,** 317–327.

8. Holmgren, K., Lee-Thorp, J. A., Cooper, G. R., Lundblad, K., Partridge, T. C., Scott, L., Sithaldeen, R., Talma, A. S., and Tyson, P. D. (2003), Persistent millennial-scale climatic variability over the past 25,000 years in Southern Africa, *Quaternary Science Reviews,* **22,** 2311–2326.

9. Partin, J. W., Cobb, K. M., Adkins, J. F., Clark, B., and D. P. Fernandez (2007), Millennial-scale trends in west Pacific warm pool hydrology since the Last Glacial Maximum, *Nature,* **449,** 452–455.

10. Shakun, J. D., Burns, S. J., Fleitmann, D., Kramers, J., Matter, A., and Al-Subary, A. (2007), A high-resolution, absolute-dated deglacial speleothem record of Indian Ocean climate from Socotra Island, Yemen, *Earth and Planetary Science Letters*, **259,** 442–456.

11. Wagner, J. D. M., Cole, J. E., Beck, J. W., Patchett, P. J., Henderson, G. M., and Barnett, H. R. (2010), Moisture variability in the southwestern United States linked to abrupt glacial climate change, *Nature Geoscience* **3,** 110–113.

12. Wang, X. F. et al. (2007), Millennial-scale precipitation changes in southern Brazil over the past 90,000 years, *Geophysical Research Letters*, **34,** L23701.

13. Wang, Y. J., Cheng, H., Edwards, R. L., An, Z. S., Wu, J. Y., Shen, C-C., and Dorale, J. A. (2001), A high-resolution absolute-dated late pleistocene monsoon record from Hulu Cave, China, *Science,* **294,** 2345–2348.

14. Williams, P. W., Neil, H. L., and Zhao, J. X. (2010), Age frequency distribution and revised stable isotope curves for New Zealand speleothems: palaeoclimatic implications, *International Journal of Speleology,* **39,** 99–112.

15. Yang, Y., Yuan, D., Cheng, H., Zhang, M., Qin, J., Lin, Y., XiaoYan, Z. and Edwards, R. L. (2010), Precise dating of abrupt shifts in the Asian Monsoon during the last deglaciation based

on stalagmite data from Yamen Cave, Guizhou Province, China, *Science China Earth Sciences,* **53,** 633–641.

16. Yuan, D. et al. (2004), Timing, Duration, and Transitions of the Last Interglacial Asian Monsoon, *Science*, **23,** 575–578.

References: Ice core data

1. Blunier, T., and Brook, E. J. (2001), Timing of millennial-scale climate change in Antarctica and Greenland during the last glacial period, *Science*, **291,** 109–112.

2. Buiron, D. et al. (2011), TALDICE-1 age scale of the Talos Dome deep ice core, East Antarctica, *Climate of the Past*, **7,** 1–16.

3. EPICA community members (2006), One-to-one coupling of glacial climate variability in Greenland and Antarctica. *Nature*, **444,** 195–198.

4. Kawamura, K., et al. (2007), Northern Hemisphere forcing of climatic cycles in Antarctica over the past 360,000 years, *Nature*, **448,** 912–916.

5. Paterson, W. S. B., Koerner, R. M., Fisher, D., Johnsen, S. J., Clausen, H. B., Dansgaard, W., Bucher, P., and Oeschger, H. (1977), An oxygen-isotope climatic record from the Devon Island ice cap, arctic Canada, *Nature*, **266,** 508–511.

6. Pedro, J. B., Van Ommen, T. D., Rasmussen, S. O., Morgan, V. I., Chappellaz, J., Moy, A. D., Masson-Delmotte, V. and Delmotte, M. (2011), The last deglaciation: timing the bipolar seesaw, *Climate of the Past*, **7,** 671–683.

7. Thompson, L. G. et al. (1998), A 25,000-year tropical climate history from Bolivian ice cores. *Science*, **282,** 1858–1864.

8. Thompson, L. G., Mosley-Thompson, E., Davis, M. E., Lin, P. N., Henderson, K. A., Cole-Dai, J., Bolzan, J. F., and Liu, K. B. (1995), Late glacial stage and Holocene tropical ice core records from Huascaran, Peru, *Science*, **269,** 46–50.

9. Thompson, L. O., Yao, T., Davis, M. E., Henderson, K. A., Mosley-Thompson, E., Lin, P. N., Beer, J., Synal, H.-A., Cole-Dai, J., and Bolzan, J. F. (1997), Tropical climate instability: The last glacial cycle from a Qinghai-Tibetan ice core, *Science,* **276,** 1821–1825.

10. Vinther, B. M. et al. (2006), A synchronized dating of three Greenland ice cores throughout the Holocene, *Journal of Geophysical Research,* **111,** D13102.

11. Vinther, B. M., Clausen, H. B., Fisher, D. A., Koerner, R. M., Johnsen, S. J., Andersen, K. K., Dahl-Jensen, D., Rasmussen, S. O., Steffensen, J. P., and Svensson, A. M. (2008), Synchronizing ice cores from the Renland and Agassiz ice caps to the Greenland Ice Core Chronology, *Journal of Geophysical Research: Atmospheres,* **113,** D08115.